STRUCTURAL AND MECHANISTIC INSIGHTS INTO THE YEAST DISAGGREGASE HSP104

Elizabeth A Sweeny

A DISSERTATION

in

Biochemistry and Molecular Biophysics

Presented to the Faculties of the University of Pennsylvania

in

Partial Fulfillment of the Requirements for the

Degree of Doctor of Philosophy

2014

Supervisor of Dissertation

_____

James Shorter, Ph.D., Associate Professor

Graduate Group Chairperson

_____

Kathryn M. Ferguson, Ph.D., Associate Professor

Dissertation Committee

Mark Lemmon, Ph.D., Professor

Walter Englander, Ph.D., Professor

Gregory D. Van Duyne, Ph.D., Professor

Kim A. Sharp, Ph.D., Associate Professor

Ben E. Black, Ph.D., Associate Professor

Aaron Gitler, Ph.D., Associate Professor (Stanford)

STRUCTURAL AND MECHANISTIC INSIGHTS INTO THE YEAST DISAGGREGASE HSP104

For my grandmother Corinne

Acknowledgements

I'd like to thank everyone, past and present in the Shorter lab, especially Drs James Shorter, Morgan DeSantis and Mimi Cushman Nick and everyone in the Van Duyne and Englander labs especially Drs Kushol Gupta and Zhong-yuan Kan. Finally, I would like to thank my family for supporting me and most especially my husband (life and science partner) Dr. Matt Sochor and our wonderful son Iggy.

ABSTRACT

STRUCTURAL AND MECHANISTIC INSIGHTS INTO THE YEAST DISAGGREGASE HSP104

Elizabeth A Sweeny

Dr. James Shorter

Hsp104 is a hexameric, AAA+ disaggregase from yeast, which couples ATP hydrolysis to remodeling diverse substrates ranging from amorphous aggregates to amyloid fibers. A mechanistic understanding of Hsp104's substrate remodeling activities remains poorly defined. The hexamer undergoes large conformational changes upon ATP hydrolysis, but the details of these changes and how they are coupled to substrate remodeling are unresolved. The goals of this thesis were to elucidate low and high-resolution structural information about the Hsp104 hexamer and to discover new details of the mechanism of substrate remodeling.

We used the in solution structural techniques small angle x-ray scattering and synchrotron x-ray footprinting, complemented by several biochemical assays, to elucidate novel roles for several Hsp104 domains, and to develop a comprehensive model for how the Hsp104 hexamer engages substrate and unleashes its remodeling capabilities. We discovered that the N-terminal domain (NTD) is involved in substrate binding, productive interactions with Hsp70, and an interface with nucleotide binding domain 1 (NBD1) and the middle domain (MD). We discovered a loop in NBD1 that may engage substrate in the ADP bound state to prevent premature substrate release, identified the region of the MD (helix 2) responsible and the mechanism of signal transmission between NBD1 and NBD2, and confirmed the validity of a hexameric model of the NBD2 domain.

Hsp104 engages substrate in the ATP-bound state. We have found that in this state Hsp104 displays an increase in rigidity, which we propose as a pre-payment of the entropic cost of substrate binding. Initial substrate engagement in the NTD and NBD1, as well as Hsp70 interactions at the NTD:NBD1:MD interface, serve to 'prime the pump'. These interactions result in large conformational changes of the MD, specifically in helix 2, which spans the entirety of the

domain. These conformational changes increase MD dynamics, partially releasing MD:NBD2 contacts, and allow signal transmission between NBD1 and NBD2. As NBD2 responds to these signals, a positive feedback loop is created. Further nucleotide binding in NBD2 stimulates ATP hydrolysis in NBD1, and substrate is remodeled by iterative binding events and peristaltic motions of the Hsp104 hexamer channel.

Table of Contents

List of Tables

List of Illustrations

Chapter 1: Background and significance

1.1 Protein folding

Proper cellular function and viability is dependent upon proteins being able to efficiently fold into their functional, native states [1]. Not only does an inability to correctly fold prevent proteins from performing their cellular functions [2-4], but unfolding and misfolding of proteins can lead to protein aggregation, a state associated with numerous human diseases [1, 2, 4-7]. Anfinsen's seminal work showed that a protein's amino acid sequence contains all of the information necessary for it to adopt its functional, three-dimensional shape[8] – but it turns out that this is only part of an even more interesting story. More recent work has shown that proteins are capable of accessing a number of different folds and oligomeric states, and emerging work indicates that this is unlikely to be an evolutionary error [9, 10]. Not only do these different states represent intermediates along multiple parallel folding pathways, but also the conformational diversity of natively folded proteins [11, 12]. Small changes in energy can result in large conformational changes [12] and these fluctuations allow proteins to sample a huge variety of states, resulting in a dynamic ensemble of protein conformations at any given time [11, 12].

In addition to thermal fluctuations, which allow proteins to explore small changes in conformation, some proteins can access a number of different conformational states based on chemical and protein partners, and environmental conditions [13-18]. Indeed, a growing number of proteins have been found to contain regions or domains that do not even fold into three-dimensional structures under normal physiological conditions [15, 19]. These intrinsically disordered proteins may adopt structure upon posttranslational modifications [13-15], ligand binding [14-16] (often DNA or RNA), protein-protein interactions [15, 16], chaperone binding [17, 20], or environmental changes within the cell [18]. Many of these proteins are involved in crucial cell regulatory pathways [15, 19], and control over their temporal and spatial activity along with targeted degradation is critical for cell health [6]. The realization that there are ongoing protein transitions between partially and fully folded states, monomeric and oligomeric states, and even

the assembly and disassembly of large heterologous protein complexes, reveals that nature has exploited the ability to control protein folding to regulate cellular functions.

The conformational state of proteins in the cell is, by necessity, tightly regulated. Controlling the conformational state of the proteome in the crowded environment of the cell, 300-400mg/mL [21], is not trivial. To minimize the presence of incorrectly folded proteins, the cell contains chemical and molecular chaperones to help nascent and denatured polypeptides fold [22, 23], protein-remodeling factors to rescue aggregated proteins [24, 25], and protein degradation systems to clear the cell of proteins resistant to re-folding efforts [26, 27]. In addition to these safeguards there are a number of factors that regulate controlled conformational shifts, into stress granules [28, 29], functional amyloids and prions [20, 30-34], and other protein complexes [9, 10] that may either activate, inactivate, or modify the activity of a given protein [9, 10, 20, 28-34]. When these transitions are improperly controlled, pathogenesis may occur [1].

1.2 Aggregation, amyloids and prions

There are two types of protein aggregates, disordered and ordered. Which type of aggregation occurs is a function of protein sequence and environment, and a vast number of proteins appear capable of accessing either aggregated state [35, 36]. Amorphous aggregates are largely unstructured with little long-range order [35]. These aggregates can be induced *in vitro* by exposure to heat and high protein concentrations and are soluble in chemical denaturants such as SDS [35]. Amorphous aggregates have been found associated with human diseases such as ALS [37, 38], multisystem proteinopathy [37], cancer [39], and cystic fibrosis [40].

Amyloid aggregates display stable long-range order comprised of characteristic cross-β fibrils, in which the β-strands run perpendicular to the fiber axis [41-44]. The ends of the fibers act as templates seeding the conformational change of natively folded versions of the protein into the amyloid form [45]. Amyloid displays a number of physical characteristics such as a unique x-ray

diffraction pattern resulting from the uniform, repeating fiber structure [41, 42], an ability to bind certain dyes and change their spectroscopic qualities [46-48] (termed 'amyloid binding dyes' such as Thioflavin T and congo red), a fibrillar morphology when viewed using electron microscopy [48], and a resistance to solubilization by denaturants such as SDS [49, 50], heat [51] and even proteases [52]. The term prion simply refers to infectious amyloid [7], meaning that the conformational state can be passed to different individuals – such as mother to daughter inheritance of yeast prions [53] – or between species – such as cow to human transmission in bovine spongiform encephalopathy [54], or mad cow disease. Amyloids and prions are often associated with human disease; cardiac amyloids, cardiomyopathy, cerebral amyloid angiopathy, Alzheimer's disease, Parkinson's disease, type II diabetes, prion diseases and more [55, 56]. These diseases can stem from a number of factors including genetic mutation, environmental stresses, or simply age [55, 56]. However, more recent work has revealed that amyloids and prions are not always detrimental; in a growing number of cases they have been found to play important roles in a number of organisms from bacteria to humans [20, 30-34]. Once again we find that transitions from one conformational state to another are an important facet of natural protein function, it is only when control over these transitions is lost that severe, sometime lethal, complications develop [7].

The formation of amyloid occurs through a series of oligomeric species and eventual nucleation of fibril growth [57] (Figure 1). A growing number of proteins have been found to be capable of accessing the amyloid form and it has even been suggested that under the right circumstances all proteins could adopt the amyloid conformation [36]. Generally, there is either a region, or domain, which is largely unstructured [58], or there is an environmental shift that causes some form of unfolding [59]. Sampling of conformational space by the unfolded regions leads to the build-up of oligomeric species [57]. Initially, these oligomeric species are soluble, but at some point there is a transition to insoluble oligomers with amyloid characteristics [57, 58]. There is evidence that in human disease some of these oligomers are responsible for cellular toxicity [60-62] and therefore there has been an interest in characterizing the structure and other

properties of these oligomers and understanding what controls the transition from one to another. The ability to develop antibodies that recognize oligomeric, but not monomeric or fibrillar conformations of a variety of amyloid forming proteins indicates that there are common structural elements within the amyloidogenic oligomers [63]. When spontaneous amyloid formation is tracked over time (i.e. in the absence of preformed amyloid), the result is a sigmoidal curve (Figure 1); the interplay between different oligomeric species represents a lag phase, during which time there is little to no amyloid characteristic [57]. During this slow, thermodynamically unfavorable phase there is a diverse range of oligomeric structures sampled [57]. Details such as temperature, buffer conditions and the presence of mutated proteins can have dramatic influence over the nature of these oligomeric species [57]. The next phase of amyloid formation progresses once nucleation occurs, i.e., amyloidogenic oligomers capable of seeding fiber formation have evolved. During this polymerization, or exponential phase, the curve displays a rapid increase of amyloid structure as the nucleated fibers grow from each end (Figure 1). These fiber ends act as templates, converting soluble versions of the protein into the amyloid state [64]. The lag phase can be shortened or even skipped altogether if amyloidogenic seed is added to the soluble species [64]. Interestingly, there is evidence showing that under certain circumstances, cross-seeding may even be possible [65-68], i.e., seeding amyloid formation of protein X by amyloidogenic versions of protein Y. This behavior may have important implications for the progression of a number of human diseases [65]. Eventually, fiber growth slows and the curve plateaus; at this point an equilibrium has been reached between the amyloid and soluble species [57]. Monomeric versions of the protein come off and onto the fiber ends, but as a whole the large, fibrous structure remains highly stable [57].

Though the amyloid, or prion state of proteins has been largely associated with devastating human diseases, it is not always an aberrant state [20, 30-34]. In yeast, prions act as self-propagating, protein-based heritable elements; they display non-Mendelian segregation in crosses [69, 70], can be cytoduced [71, 72], and reversibly cured [71, 73]. Yeast prions confer diverse and often beneficial phenotypes to the cells that harbor them [74]. These changes can be

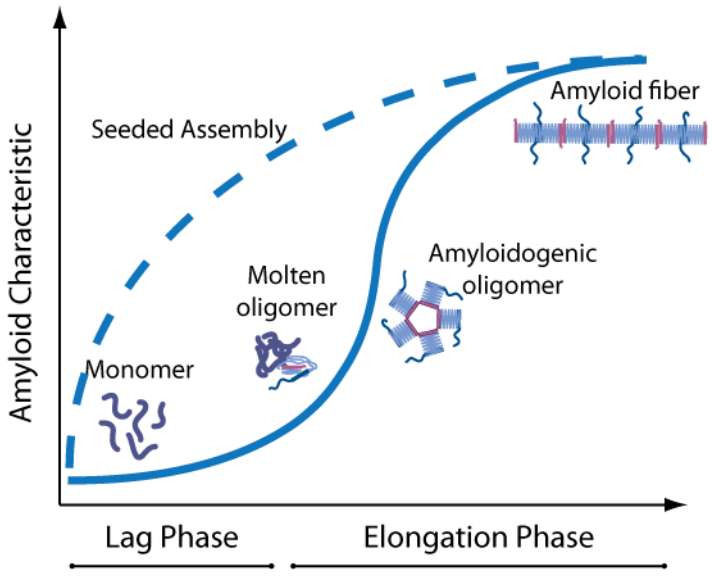

Figure 1. Amyloid formation. Spontaneous (solid blue line) assembly of amyloid over time. During the lag phase, soluble monomers sample molten oligomeric states. Formation of an amyloidogenic oligomer nucleates fiber growth and fibers then recruit soluble monomers to the growing fiber ends. By adding small amounts of fragmented fibers (seeding) the lag phase can be bypassed (dashed blue line).

due to partial loss of function, such as seen with [*PSI*$^{+}$] [70, 75] and [*URE3*] [71], or the gain of a novel function such as with [*PIN*$^{+}$] [68], [*ISP*$^{+}$] [76] and [*MOD*$^{+}$] [77]. One of the best characterized yeast prions, [*PSI*$^{+}$], is comprised of the translation termination factor, Sup35 [78, 79]. The depletion of soluble Sup35 upon prionogenesis results in the partial read-through of stop codons, suppression of nonsense mutations [75] and access to novel gene products, some of which are advantageous [53, 80].

Initially there were a limited number of yeast prions described, namely [*PSI*$^{+}$] [20, 81, 82], [*URE3*] [71, 83] and [*RNQ*$^{+}$] [30, 84], and it was proposed that they may have been a by-product of the yeast being cultivated in a laboratory environment [85]. However, more recently prions have been found in a variety of wild-yeast strains, indicating that it is not a laboratory artifact [85]. Further, the discovery of at least 24 additional yeast proteins that appear to have a prion-forming domain [86] indicates that use of the prion conformation may be a common mechanism in yeast.

Prion-forming domains (PrDs) have been identified as necessary and sufficient to facilitate the transition between the soluble and prion form [84, 87-89]. PrDs are largely unfolded and are often rich in polar uncharged residues [90]. They are independent of functional domains, and can be transferred to other proteins to induce the prion state [84, 88], while deletion of the PrD leads to an inability to form prions [84, 88]. Interestingly, when an algorithm designed to identify novel prion domains was applied to the human genome, a number of the identified proteins have been found associated with devastating neurodegenerative diseases [91]. Many of the identified domains are found in RNA-binding proteins, which are involved in the development and dynamics of beneficial, aggregation-like structures such as stress granules [92]. This then returns us to the theme of controlled protein aggregation playing a crucial role in normal cellular function. Tight regulation over conformational transitions is essential, indeed, even in the case of [*PSI*$^{+}$], a potentially beneficial prion state, excessive amounts of aggregated Sup35 results in toxicity [93].

Understanding how yeast regulate their well-characterized prion states has broad implications for understanding how higher eukaryotes may regulate the aggregation state of their proteomes, as well as allow for the targeted design of novel therapeutics to use against aberrant protein aggregation in human disease. Yeast employ both environmental signals and modulation of chaperones expression levels to control the prion state of its proteins [77, 94, 95]. Certain environmental stresses such as the presence of antifungals for [*MOD*$^{+}$] [77], or ethanol for [*MOT3*$^{+}$] [94], can induce the prion state of the Mod5 and Mot3 proteins respectively. The network of chaperones that play a role in prionogenesis and curing is more complex, and is best understood for the canonical prion protein, Sup35. Central to the regulation of prion state is the AAA+ protein Hsp104, however, a number of other chaperones have been found to play important roles *in vivo*, namely the Hsp70 system, which includes Hsp40 chaperones as well as Hsp70 nucleotide exchange factors (NEFs) [95].

1.3 Hsp104 function in yeast

Hsp104 is a hexameric, Hsp100 AAA+ (ATPases Associated with various cellular Activities) [96, 97] disaggregase [98]. AAA+ proteins have been described as molecular machines [99], coupling ATP hydrolysis to protein degradation [99, 100], remodeling and dismantling of macromolecular complexes [97], translocation of proteins and nucleic acids [99, 101], as well as resolubilization of aggregates [96, 102]. Hsp104 appears to be involved in all things aggregate in the yeast cell; from amorphous aggregates formed after heat shock, to the regulation of prion proteins, to control over the segregation of carbonylated, aggregated proteins in order to control aging and cell death [103-105].

Hsp104 was originally discovered as a gene required for induced thermotolerance in *Saccharomyces cerevisiae* [106]. When yeast cells were pre-incubated at 37°C for 30 minutes prior to heat shock at 50°C for 20 minutes, the cells containing a wild-type version of the Hsp104 gene displayed a 100- to 1000-fold increase in survival compared to yeast lacking the Hsp104 gene[106]. After the initial discovery of its critical role in thermotolerance Hsp104 was found to confer tolerance to ethanol, arsenite, and prolonged exposure to the cold as well [107]. Hsp104 is a member of the ClpA/ClpB protein family [108]. Unlike Hsp70 chaperones, which can prevent aggregation of unfolded polypeptides [22], or ClpA, which promotes proteolysis of proteins [109], it was shown that Hsp104 protects cells from stress, including heat shock, through the resolubilization and reactivation of insoluble protein aggregates [110, 111], generally once the stress was removed.

It was subsequently discovered that Hsp104 plays a central role in the regulation of yeast prions [112]. Hsp104 is necessary for the propagation of all known naturally occurring amyloid-based yeast prions including [*PSI*$^{+}$] [20, 81, 82], [*URE3*] [83] and [*RNQ*$^{+}$] [30, 84], and demonstrates concentration dependent effects on the yeast prions [*PSI*$^{+}$] [82] and [*MOD*$^{+}$] [77]. Prionogenesis of Sup35 and resulting mother-to-daughter transmission results in the [*PSI*$^{+}$] [20, 81, 82] phenotype. Prionogenesis can either be promoted, and inheritance maintained, or it can

be inhibited and even cured, i.e., the prion phenotype lost [82]. *In vivo,* Hsp104 deletion or over-expression eliminates [*PSI*$^{+}$] [82]. Pure protein biochemistry has revealed that low concentrations of Hsp104 catalyze Sup35 prionogenesis by nucleating fiber assembly[20, 81], and by severing fibers to increase the number of growing fiber ends[20, 81]. By contrast, at high concentrations Hsp104 couples ATP hydrolysis to the disassembly of both Sup35 fibers and oligomers into non-infectious conformers[20, 81, 113]. *In vivo*, and *in vitro*, the concentration dependent activity is tuned by the presence of Hsp70:Hsp40 pairs as well as NEFs [114].

A number of papers have dissected the role of various Hsp70:Hsp40 pairs as well as NEFs in the prionogenesis of Sup35 [95]. Hsp70 chaperones are ATPases that bind and release substrates that contain large regions of unfolded and non-natively folded polypeptide [22]. In the ADP bound state Hsp70 has a high affinity for substrate, and in the ATP bound state the affinity is much lower [22]. This difference in affinity results in rounds of substrate binding and release, which prevents interactions with other unfolded proteins that could lead to aggregation, as well as giving the substrates the chance to re-fold into the native state upon their release [22]. However, the basal rate of ATP hydrolysis for Hsp70 is very low, and therefore they require the activity of Hsp40 proteins, which contains ATPase stimulating J-domains [22]. In addition to Hsp40, there are a number of NEFs, which stimulate the exchange of ADP for ATP [22]. There are two Hsp70 subfamilies that have been shown to affect [*PSI*$^{+}$], Ssa, whose four members are found throughout the cytoplasm [115] and Ssb, whose two members are mostly associated with the ribosome [116]. While Ssb is always a [*PSI*$^{+}$] antagonist [117-119], Ssa has been shown to either promote [117, 120-123] or antagonize [118, 121, 124] [*PSI*$^{+}$] based on protein partners and environmental factors (Figure 2).

Ssa1 mainly collaborates with the Hsp40 proteins Ydj1 and Sis1 [125] while Ssb1 requires a heterodimer of Zuo1, an Hsp40, and Ssz1, an atypical Hsp70 [126]. Fes1 and Sse1 are NEFs that are able to facilitate nucleotide exchange for both Ssa1 and Ssb1 [127-130]. The Ssb1:Zuo1:Ssz1 complex, generally associated with the ribosome, is a potent antagonist of

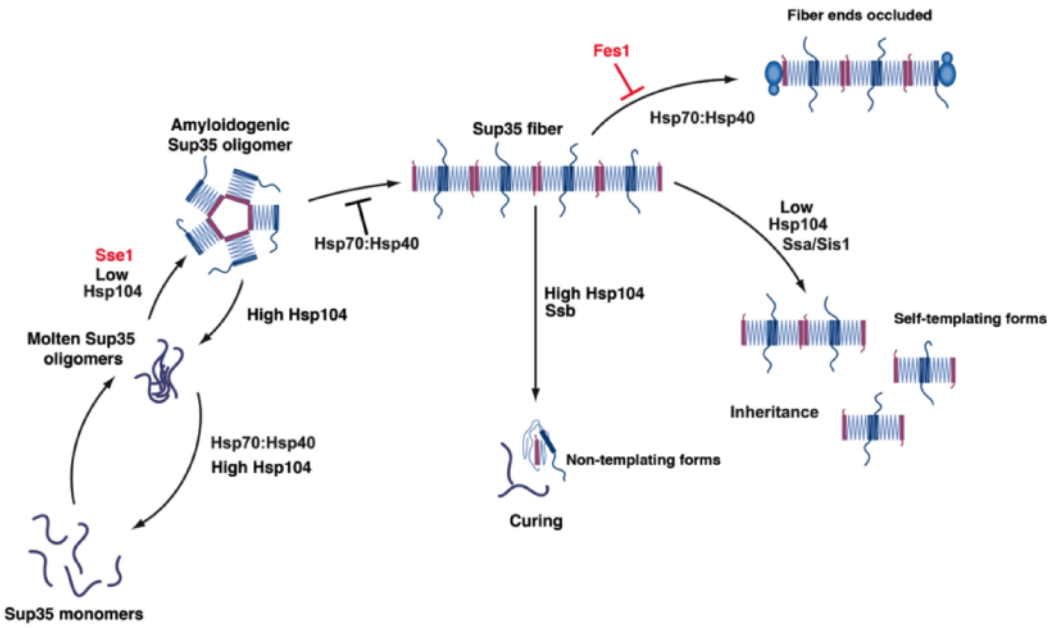

Figure 2. The role of Hsp104, Hsp70, Hsp40 and NEFs in Sup35 prionogenesis (From Sweeny and Shorter 2008). A) Sup35 prions assemble after a lag phase during which a dynamic ensemble of monomeric and molten oligomeric species form. The intermolecular contacts that nucleate prion assembly are likely established within amyloidogenic oligomers. Once formed, fibers stimulate their own assembly by recruiting and converting monomers at their ends. Various steps are promoted or antagonized by Hsp104, Hsp70, Hsp40 and the NEFs Fes1 and Sse1 as indicated. At high concentrations, Hsp70 and Hsp40 can bind Sup35 prions and occlude prion recognition elements. The C-terminal domain of Sup35 is not depicted for clarity.

Sup35 prionogenesis [114]. Although unable to rapidly disassemble preformed Sup35 prions [114], a number of Hsp70:Hsp40 pairs appear to bind both Sup35 oligomers and fibers, disassembling soluble oligomers [114] and blocking nucleation and seeding events [114]. These activities allow for overexpression of Hsp70:Hsp40 to cure certain [*PSI*$^{+}$] phenotypes [118, 124]. The Hsp40 proteins Sis1 and Ydj1 preferentially interact with the Sup35 oligomers and fibers rather than the monomers and promote Ssa1 and Ssb1 binding [114]. The NEF Sse1 was found to directly stimulate prionogenesis of the prion domain of Sup35 [123], while Fes1 had no effect [114]. Though Fes1 had no direct effect on Sup35 prionogenesis, it was found to diminish the inhibitory effects of Hsp70:Hsp40 [114]. Fundamental to the balance of this complex chaperone

network is the protein Hsp104 [95]. Based on its expression levels and collaboration with the previously described Hsp70 system, it is the main determinant of prion state (Figure 2).

The prion stimulating activity at low Hsp104 concentrations was found to be capable of overriding the inhibitory activities of Hsp70:Sis1 pairs, but not Hsp70:Ydj1 pairs [114]. Additionally, ex vivo Sup35 fibers contain a large amount of Ssa1/2; ~one Ssa1 for every two Sup35 molecules, as well as smaller amounts of Ssb1, Ydj1 and Sis1 [131]. Incorporation of Hsp70 and Hsp40 into the Sup35 fibers makes them better substrates for remodeling by high concentrations of Hsp104 [114]. Though *in vivo* there appears to be a delicately balanced interplay between Hsp104, Hsp70, Hsp40 and NEFs, *in vitro* experiments have demonstrated that Hsp104 displays robust activity promoting, inhibiting or remodeling Sup35 fibers on its own in a concentration dependent manner [20, 81, 114]. Indeed, it has even been shown that Hsp104 has the ability to remodel amyloid forms of a number of human proteins involved in disease [132], a feat that its bacterial homologue, ClpB, is unable to achieve [132].

More recently Hsp104's role in aging was revealed [104, 105]. In the budding yeast *Saccharomyces cerevisiae,* oxidatively damaged, aggregated proteins are retained in the mother cell in an Hsp104-dependent manner [104, 105]. Disruption of this asymmetric inheritance of aggregates results in accelerated aging of the progeny [104]. Interestingly, in the fission yeast *Schizosaccharomyces pombe* aging does not occur under normal conditions, however, after the yeast is subjected to stress some of the cells begin to age and become more likely to die [133]. This increased chance of death is due to the asymmetric inheritance of large, Hsp104-associated aggregates formed in response to stress [133]. By forming one large aggregate which segregates asymmetrically to only one cell, the yeast are able to sacrifice one cell in return for the health of the others.

Overall, the activity of Hsp104 appears to be focused on the control of the aggregation state of a number of proteins as well as the spatial localization of aggregates [103, 134]. The questions then become almost endless: How does Hsp104 carry out these activities? Does it

employ the same mechanism for all of its diverse substrates? Can it sense differences in stability between a disordered and amyloid aggregate? When does its function shift from remodeling, to sequestration of aggregates? Is remodeling coupled to sequestration? To understand and begin to answer these questions we need to examine details about the structure and possible mechanisms of the Hsp104 hexamer.

1.4 Hsp104 mechanism and structure

1.4.1 Overview

A mechanistic understanding of Hsp104's substrate remodeling activities remains poorly defined [135]. An Hsp104 monomer is 908 residues and 102kD; the fully assembled hexamer is a large, hollow, barrel shaped molecule [102, 136] with 12 sites capable of ATP binding and hydrolysis. The hexamer undergoes large conformational changes upon ATP hydrolysis [137, 138], but the details of these changes as well as how they are coupled to substrate remodeling is unclear. There are no high-resolution structures, and most mutagenesis analyses have relied on random mutagenesis, or focused on a few highly conserved residues such as those found in the nucleotide binding pockets [138]. Hsp104 is comprised of five domains, the N-terminal domain (NTD), two nucleotide-binding domains (NBD1 and NBD2), a coiled-coil middle domain (MD) inserted within NBD1, and a unique C-terminal extension [138]. The hexameric structure of Hsp104 remains unresolved. In fact, two radically distinct models have been advanced [135]. Both are based on cryo-EM reconstructions with rigid body fit domains from the crystal structure of the *Thermus thermophilus* homolog, tClpB [102]. Unfortunately, tClpB was resolved as a spiral of 3 ClpB monomers with distinct conformations, rather than the functional, hexameric state [102]. Using assumptions based on other AAA+ proteins and poorly documented cryo-EM reconstructions of chemically fixed tClpB, an initial hexameric structure with an external placement of the coiled-coil was proposed [102]. However, this structure was incompatible with the dimensions of Hsp104 hexamers observed by another cryo-EM study [136]. This led to a

second model with the coiled-coil domain intercalated between the two nucleotide-binding domains [136]. However, this new model did not preserve the typical AAA+ nucleotide binding sites, and the debate over the hexameric structure continues [135]. The stability of the hexamer is affected by the presence of nucleotide [139] and salt concentration [140]. Nucleotide binding stabilizes the hexamer, while high salt concentrations favor the monomer and smaller oligomers such as dimers and trimers. The domains appear to cooperate in a highly tuned manner in order to remodel diverse substrates and substrate structures [132]. Each domain plays specific roles, and allosterically communicates with adjacent domains and subunits [138]. However, the details of intra- and inter-protomer communication, and precisely what role(s) the individual domains play in substrate remodeling are not fully resolved.

1.4.2 The N-terminal Domain (NTD)

Crystal structures of the N-terminal domains of the bacterial Hsp100 proteins ClpA [141], ClpB [102, 142], and ClpC [143] have been solved. The NTDs are highly structurally conserved; they are very stable globular domains [141-144] made up of two imperfect repeats of four helical bundles [141-143] and are connected to the adjacent nucleotide-binding domain by a highly mobile linker [102, 145-147]. In the bacterial disaggregase ClpB, Hsp104's orthologue, the NTD appears to be involved in substrate binding [102, 142, 148-151], casein-stimulated ATPase activity [148], and its mobility via the NTD-NBD1 linker is necessary for efficient translocation and disaggregation of substrate [152, 153].

In contrast to the bacterial Hsp100 proteins, the function of the Hsp104 N-terminal domain has been poorly explored. *In vivo,* deletion or specific point mutations (e.g. T160M) within the N-terminal domain has little effect on thermotolerance or prion propagation [154]. Therefore, Hsp104 can still dissolve heat-denatured aggregates and fragment prions. Yet, over-expression of these mutants fails to cure [*PSI*$^{+}$] [154]. This suggests that Hsp104's ability to eliminate amyloid conformers is selectively perturbed and that there may be a fundamental difference in how

amorphous and amyloid substrates are remodeled. Indeed, a recent paper found that cooperativity of the subunits was dispensable for reactivation of amorphous aggregates, while global cooperativity was needed for remodeling of amyloid substrates [132]. This indicates that the NTD may be essential for global cooperativity. In addition to this possibility, the NTD of Hsp104 may participate in substrate binding and interactions with adapter proteins such as Hsp70, although the role(s) of the Hsp104 NTD remains unknown.

1.4.3 Nucleotide Binding Domains (NBD1 and NBD2)

Hsp104 contains two canonical AAA+ domains, designated NBD1 and NBD2. Each NBD contains highly conserved AAA+ motifs but belong to different AAA+ clades (subgroups) [155]. These clades are defined by the insertion of specific secondary structure elements within the core AAA+ fold, and have specific functional consequences [155, 156]. Since the NBDs belong to different clades, (clade 3 for NBD1 and clade 5 for NBD2) it has been proposed that the protein arose from a gene fusion event rather than a gene duplication event [155]. Each domain is able to bind and hydrolyze ATP, but they have very different catalytic properties [140]. By fitting the steady-state kinetics of ATP hydrolysis to two independent allosteric sites, and following up with mutational analyses, the general properties of the two NBDs were determined [140]. NBD1 contains a low affinity, high turnover site and NBD2 a high affinity, low turnover site [140]. Both domains display positive cooperativity, and a high degree of allosteric communication between the two, e.g., hydrolysis in NBD1 depends upon the nucleotide state of NBD2 [140].

The nucleotide binding domains of AAA+ proteins are highly structurally conserved, consisting of a large, α/β subdomain and a small α-helical subdomain [156]. Features that define these domains include regions involved in ATP binding and hydrolysis, namely the Walker A and Walker B motifs, the arginine finger, sensor-1 and sensor-2 residues (Figure 3), as well as pore loops that couple conformational changes of the AAA+ protein due to ATP hydrolysis to substrate

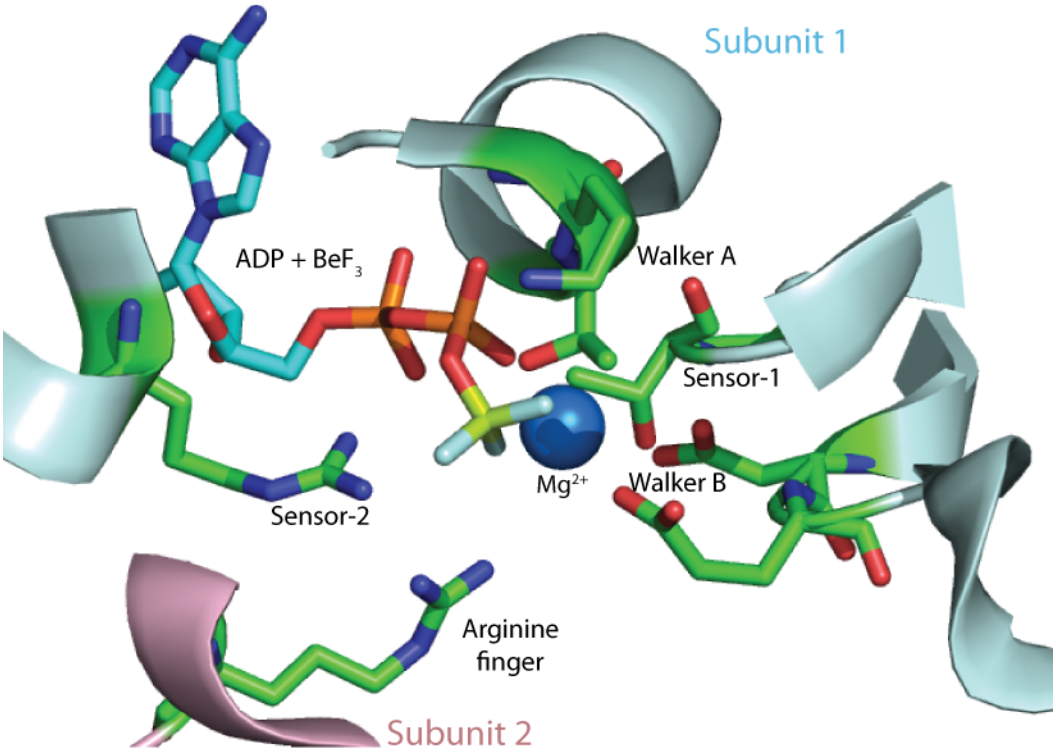

Figure 3. Schematic of a typical AAA+ catalytic site. The AAA+ site of ATP binding is located between two subunits (subunit 1 in blue, subunit 2 in pink). Important residues are labeled as well as ADP + BeF_3 and the Mg^{2+} ion. The Walker A lysine interacts with the phosphates of the bound nucleotide while the Walker B residues coordinate the Mg^{2+} ion and activate the attacking water (not pictured). Sensor-1 and sensor-2 residues participate in various activities such as ATP binding, hydrolysis, nucleotide-state sensing, and propagtion of conformational changes upon ATP hydrolysis. The arginine finger, which is essential for hydrolysis, reaches from one subunit into the next and contacts the bound ATP. Figure is based on the pdb 3glf, a AAA+ clamp loader (Simonetta 2009).

remodeling [155]. In addition to the conserved AAA+ motifs, NBD2 was discovered to contain a nuclear localization signal (NLS) [157].

The P-loop, or Walker A motif, is common in a number of ATPases and GTPases and has the consensus sequence GXXXXGKT/S [158, 159]. The Walker A residues, particularly the highly conserved lysine, are involved in interactions with the phosphates of the bound nucleotide

[155] (Figure 3). Indeed, the lysine residues K218 in NBD1 and K620 in NBD2 of Hsp104 are essential for nucleotide binding [160]. By separately mutating conserved Walker A residues in either NBD1 (G217V or K218T) or NBD2 (G619V or K620T), it was revealed that NBD1 contributes the majority of the ATPase activity, while NBD2 is responsible for nucleotide-induced hexamerization [160]. The Walker B motif has the consensus sequence *hhhh*DE [158], where *h* represents a hydrophobic residue. The aspartate residue can coordinate Mg^{2+} while the glutamate is thought to activate the attacking water in order to facilitate ATP hydrolysis [156]. In Hsp104, as well as many other Hsp100 proteins, mutation of the Walker B glutamate residues, E285 in NBD1 and E687 in NBD2, does not disrupt nucleotide binding but does inhibit hydrolysis (Figure 3). An interesting consequence of this is that since most AAA+ proteins, including Hsp104, engage substrate in the ATP-bound state, double Walker B mutants (E285Q/A:E687Q/A in Hsp104) can be used as substrate 'traps' [161]. This allows for a number of interesting biochemical investigations.

The sensor-1 and sensor-2 motifs can participate in various activities including ATP binding, hydrolysis, discriminating between ADP and ATP, and the propagation of conformational changes upon hydrolysis [162]. The sensor-1 residue is found in a structurally conserved region called the secondary region of homology (SRH) [163]. It is a polar residue, generally Asn or Thr, which interacts with regions of the Walker B motif as well as the γ-phosphate of the bound ATP molecule [156]. Mutation of these conserved residues in Hsp104, T317 in NBD1 and N728 in NBD2, reduces the ATPase rate but does not affect nucleotide binding [140]. Although both sensor-1 mutants display a loss-of-function phenotype *in vivo,* the NBD2 mutant N728A is active *in vitro* in the presence of ATP and the absence of Hsp70:Hsp40, a condition in which the wild-type protein is not active [113]. Why exactly this would be is unclear and underscores how hard it is to get a comprehensive picture of mechanism in a protein as large and complex as Hsp104. The sensor-2 motif, GAR, is located in the small α-helical subdomain and the conserved Arg interacts with the γ-phosphate of the bound ATP [163]. In Hsp104 NBD1 does not appear to have

a sensor-2 motif [102]. In NBD2 mutation of the conserved Arg, R826, results in an equal decrease in binding to both ADP and ATP, as well as a decrease in ATP hydrolysis in NBD1 [164]. At the far end of the SRH from sensor-1 is the arginine finger, which completes the ATP-binding pocket (Figure 3). AAA+ proteins are oligomeric and the nucleotide-binding pocket is located at the subunit:subunit interface [155]. An essential component of the catalytic site is the arginine finger, which reaches from one protomer into the active site of its neighbor, contacting the nucleotide [165]. In Hsp104 the arginine fingers are R334 in NBD1 and R765 in NBD2 and mutation of these conserved arginines results in a loss of ATPase activity. A schematic of a typical AAA+ catalytic site is shown in Figure 3 with AAA+ features based on the pdb 3glf [166].

The pore loops, or substrate binding loops, have the general consensus sequence YVG, and couple the large conformational changes that take place during ATP hydrolysis to the remodeling of substrate [167-169]. These conserved loops are on the interior of the axial channel, which runs the length of the hexamer N-to C-terminally [102, 136] and facilitate partial and/or full translocation of substrate through the channel [109, 167, 168, 170]. In Hsp104 the NBD1 substrate-binding loop is 256-KYKG-259, and in NBD2 the more typical 661-GYVG-664; the highly conserved tyrosine residues, Y257 and Y662 are the most essential for substrate binding [167]. *In vivo,* Y257A displays a reduction in survival after heat shock of only ~10-fold, while Y662A fared only slightly better than having no Hsp104 at all [167]. This implies that Y662 is the more crucial residue, and that there may be additional substrate binding motifs in NBD1 and the NTD. Fluorescence studies showed that nucleotide binding in NBD2 determines the position of residue 662 [167], which supports the idea that conformational changes due to ATP hydrolysis are transmitted through the pore loop to the substrate.

1.4.4 Middle domain (MD)

Hsp104 and its bacterial homologue ClpB contain a ~85Å long coiled-coil middle domain (MD) inserted into the small α-helical subdomain of NBD1 [102]. In the two hexameric models

proposed for Hsp104 and ClpB, the position of the middle domain is the most highly contested. In one model, the domain is intercalated between NBD1 and NBD2 [136, 137] while in the other it projects out into solution [171]. The MD consists of four helices that make up an anti-parallel, broken coiled-coil [102]. Helix 1 and half of helix two are designated motif 1, with the second half of helix 2 along with helices 3 and 4 designated motif 2 (Figure 4). Helix 3 appears to undergo conformational changes in response to nucleotide, possibly transitioning between loop and helix [102, 172].

The MD is essential for disaggregation activity [145, 173] and is the site of interaction with Hsp70 [172-175]. The MD has been shown to interact with NBD1 in an auto-inhibitory fashion, repressing activity of the hexamer [172, 175-177]. Hsp70 binds directly to the MD, specifically in the region of helix 2 in motif 2 [174, 175, 178]. This interaction appears to relieve the autoinhibitory interactions between the MD and NBD1 [174, 175, 178]. Thus, it appears that the MD is a highly dynamic domain involved in regulation of the hexamer activity. Indeed, point mutations in the MD can lead to inactive variants with stabilized MD-NBD1 interactions [176], or hyperactive variants with enhanced unfolding power [176, 179]. Recent findings have begun to uncover the role and characteristics of the MD, however, many of the details of the placement, dynamics and the mechanism of MD-mediated regulation remain unresolved.

1.4.5 C-terminal Domain (CTD)

Hsp104 contains a unique C-terminal extension of ~50 residues. The region is enriched in acidic residues, and the last four residues are a conserved DDLD motif that allows binding to the chaperone Cpr7 [180], although the importance of this interaction remains unknown as deletion of the motif does not affect thermotolerance [180]. The CTD was initially thought to be a main site of substrate interaction [181], and CTD binding to lysine rich polypeptides stimulates ATPase activity in NBD1 via the MD [181]. However, subsequent work supported a model in which substrates are translocated N- to C-terminally [111, 161], which leaves poly-Lys binding at

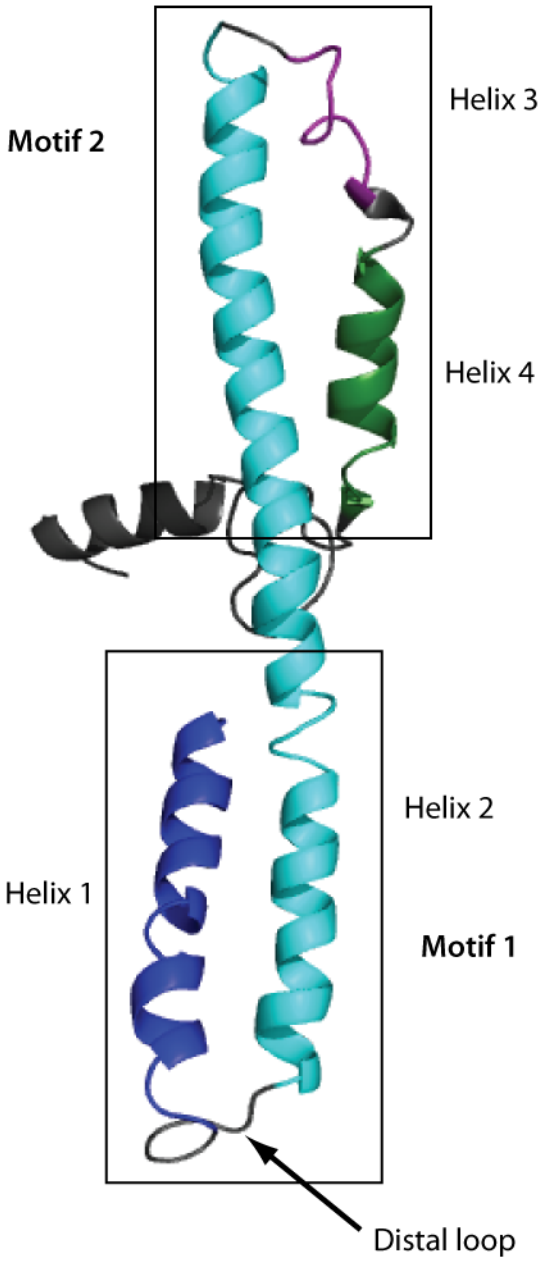

Figure 4. Hsp104 Middle Domain (MD). The MD consists of four helices that make up an anti-parallel, broken coiled-coil. Helices 1 and half of helix 2 are designated motif 1, with the second half of helix 2 along with helices 3 and 4 designated motif 2. Helix 3, as well as the middle of helix 2, undergo changes in secondary structure, transitioning between loop and helix (Lee 2003).

the CTD of mysterious function. More recently, the CTD was shown to be essential for hexamerization [180, 182], and though the sequence indicates that it is highly disordered, this role implies that may not necessarily be the case.

1.5 Research aims

Hsp104 is a large, dynamic, multi-domain hexamer that couples large conformational changes due to ATP hydrolysis to applying mechanical force to myriad substrates [138]. A better understanding of the structure and mechanism of Hsp104 will not only allow insight into its natural function, but open the door for directed evolution and protein design to tailor Hsp104 to specifically remodel disease associated aggregates, as well as other therapeutic and research purposes.

The goals of this thesis were to elucidate low and high-resolution details about the structure and substrate remodeling mechanism of Hsp104. First, I set out to determine the role of the Hsp104 NTD and to visualize large conformational changes of the hexamer using SAXS/WAXS in order to make and test predictions about the structure and mechanism of Hsp104. Specifically, we first aimed to understand why deletion of the NTD (ΔN-Hsp104) resulted in an inability to remodel amyloid substrates and to use our findings to understand mechanistic details of the wild-type hexamer. Secondly, we used an in solution technique, x-ray footprinting (XF), that directly probes the solvation state of the Hsp104 hexamer in the presence of different nucleotides. The changes in solvation allowed us to make predictions about what these conformational changes mean for the individual domains, the Hsp104 hexamer as a whole, and the mechanism of substrate remodeling. Using a variety of biochemical techniques, we tested these predictions and were able to elucidate novel insights into substrate binding and processing, interaction with Hsp70, movements of the coiled-coil middle domain, and the subunit:subunit interface.

Chapter 2: The role of the N-terminal domain (NTD) of Hsp104

2.1 NTD introduction

The bacterial Hsp100 proteins ClpA [183] and ClpB [148] have internal start sites which allow for the production of truncated protein products missing the N-terminal domain (NTD). These natural Hsp100 truncations as well as other N-terminal truncations have been examined in the literature for ClpA and ClpB as well as other AAA+ proteins. The activity of these truncated products varies depending upon the identity and structure of the substrate [141, 144, 145, 148, 149, 183], and the location of the truncation [141, 144, 145, 148, 183, 184]. The crystal structures of the NTDs of the bacterial Hsp100 proteins ClpA [141], ClpB [102, 142], and ClpC [143] have been solved. The NTDs are structurally conserved; they are very stable globular domains [141-144] made up of two imperfect repeats of four helical bundles [141-143] and are connected to the NBD1 domain by a highly mobile linker [102, 145-147]. Strikingly, though the structure of the repeats differs in content, other AAA+ proteins such as mammalian p97 and NSF also have NTDs that contain two subdomains [185] connected to the NBD1 domain via mobile linkers [186, 187], and the NTDs may play similar roles in activity [187-190].

For the bacterial Hsp100s, though the effects vary with the details of substrate and the location of the N terminal truncation, the NTD as well as the linker between the NTD and NBD1 domains have been shown to play a role in a number of functions. These include regulation of binding and hydrolysis of ATP in the nucleotide binding domain(s) [144, 148, 183, 187], substrate interaction [102, 141, 142, 144, 148-151], binding to adaptor proteins [141, 143, 188-192] and controlling access to the central channel [136, 146, 184].

The NTD is not directly involved in ATP hydrolysis, however, the deletion of the NTD has been shown to affect the behavior of the ATP-binding domains [144, 148, 183, 187]. These effects are not always the same and vary depending on whether the NTD to NBD1 linker is also removed [144, 148, 183, 187]. In ClpA, NTD deletion has been shown to decrease the ATPase

rate [144, 183], in ClpB, eliminate the stimulation of ATPase rate by substrate [148], and in p97 the linker, along with the NTD-NBD1 interface has been shown to control the number of ATP molecules that the NBD1 domain can bind at a given time [187]. Mutations in these regions in p97 have been linked with inclusion body myopathy with early-onset Paget disease and frontotemporal dementia (IBMPFD), a devastating autosomal dominant degenerative disease [187].

The region of the NTD that binds substrate is a highly-conserved hydrophobic patch that is exposed to solvent and lies between the two subdomain repeats [102, 141, 142, 144, 150]. Even p97, with its divergent NTD structure retains a hydrophobic pocket between its NTD subdomains [188], though it binds an adaptor protein p47 rather than substrate [188]. Near the hydrophobic patch are two acidic residues that have been implicated in substrate binding in ClpB [150], specifically involved in processing large aggregates [150]. In ClpA the corresponding residues are arginine and alanine, and it has been proposed that the sequence variation is related to differences in substrate specificity [150].

Several AAA+ proteins require binding of adaptor proteins for proper hexamer formation [143, 193], determining substrate specificity [141, 191], or for stimulation of activity [24, 141, 188-190, 193-195]. Many of these adaptor proteins interact with the NTD [141, 143, 188-190]. In the case of ClpC and its adaptor protein MecA and ClpA with its adaptor protein ClpS, the exact site of interaction is conserved [141, 143]. In fact, the only examples of non-NTD sites of adaptor protein interaction occur in the MD, a unique coiled-coil domain inserted within the first nucleotide-binding domain in Hsp104 and ClpB [172-175, 196]. ClpC has a truncated version of a coiled-coil middle domain [143]. Interestingly, the ClpC-MecA interaction occurs at both the NTD and the MD [143].

Despite the plethora of data on bacterial Hsp100 NTDs, there is very little published information on the NTD of the AAA+ yeast protein Hsp104, which, like ClpA [109] and ClpB [170], is able to unfold and translocate substrates through its central channel [167]. Curiously, Hsp104

does not have a corresponding internal start site, which could imply that the NTD of Hsp104 plays a more crucial role in activity than NTDs of its bacterial homologues. This may be due to Hsp104's unique *in vivo* role in regulating various yeast prions including [*PSI*$^{+}$] [20, 81, 82], [*URE3*] [83] and [*RNQ*$^{+}$] [30, 84]. In yeast, prions act as nonchromosomal heritable elements [30, 53, 80], which can confer selective advantages in times of stress [53, 80]. From *in vivo* yeast studies, it has been shown that the N terminal domain of Hsp104 is not necessary for thermotolerance or yeast prion propagation, but is essential for curing of the yeast prion phenotype [*PSI+*] caused by Sup35 prions [154, 197]. This finding led to the hypothesis that the Hsp104 NTD may play an essential role in the unique ability of Hsp104 to remodel amyloid substrates, specifically, the ability to eliminate the infectious cross-beta structure, as opposed to simple fragmentation without altering the cross-beta structure [198].

In this chapter I present data from structural and biochemical techniques to understand the role of the Hsp104 NTD. We wanted to understand how the NTD contributes to Hsp104 function, and therefore illuminate new details of how Hsp104 remodels amyloid aggregates into non-infectious forms. This work elucidates, for the first time, the essential role of the NTD in cooperativity of the hexamer. Recent work in our lab revealed that the ability of the Hsp104 hexamer to remodel amyloid substrates depends upon a high degree of plasticity and the ability to operate in a fully cooperative manner [132]. The following work details how deletion of the NTD results in a stable Hsp104 hexamer with a diminished ability to undergo productive conformational changes, specifically in the channel running the length of the hexamer. This profound alteration in conformational changes leads to defects in hexamer cooperativity. These defects in cooperativity then lead to deregulation of the ATPase cycle and various functional defects. These findings establish that the Hsp104 NTD is crucial for robust Hsp104 activity, necessary for the global cooperativity needed for amyloid remodeling, and explain why an internal start site is not found in the Hsp104 gene. The NTDs of Hsp100 proteins are often removed for ease of *in vitro* biochemical characterization. Our work implicates that this practice, at least for

Hsp104, could lead to drastic changes in how the hexameric assemblies function, even if activity remains.

2.2 Results

2.2.1 The NTD is required for inhibition of Sup35 amyloid formation in vitro

Yeast studies have shown that the NTD of Hsp104 is required for curing the yeast prion phenotype [*PSI*$^{+}$] through Hsp104 overexpression [154, 197]. The [*PSI*$^{+}$] prion phenotype is caused by the translation termination factor, Sup35, forming infectious amyloid conformations [78, 79]. Pure protein biochemistry using Sup35 has been shown to recapitulate the *in vivo* concentration dependent activity of Hsp104 on prions [20, 81]. At low concentrations Hsp104 promotes amyloidogenesis by nucleating fiber formation as well as severing the fibers to increase the number of growing ends [20, 81]. Conversely, at high concentrations, Hsp104 is able to completely remodel the Sup35 amyloid fibers into non-infectious, soluble conformations [20, 81, 113, 114]. We decided to test whether deletion of the NTD resulted in defects in prion remodeling *in vitro*.

Using Sup35 as our model substrate we monitored amyloid formation over time using an amyloid binding dye, Thioflavin T (ThT), which increases in fluorescence when bound to amyloid [47]. We also used negative stain electron microscopy (EM) to visualize the reaction products. By adding either WT Hsp104 or a NTD truncation mutant (ΔN Hsp104), we could monitor how deletion of the NTD affected the ability of Hsp104 to alter the conformational state of Sup35. We began by testing the effect on Sup35 amyloid assembly at a concentration shown to be inhibitory, a ratio of Sup35 monomer to Hsp104 hexamer of 15:1 [20]. We found that while the WT Hsp104 inhibited amyloid assembly as expected, ΔN Hsp104 enhanced fibrilization (Figure 1A). Since this behavior resembled what occurs at low concentrations of WT Hsp104 [20, 81], we next tested whether we would see inhibition of Sup35 fibrilization at higher ΔN Hsp104 concentrations. We found that even up to a ratio of Sup35 monomer to ΔN Hsp104 hexamer of 3:1, Sup35 amyloid

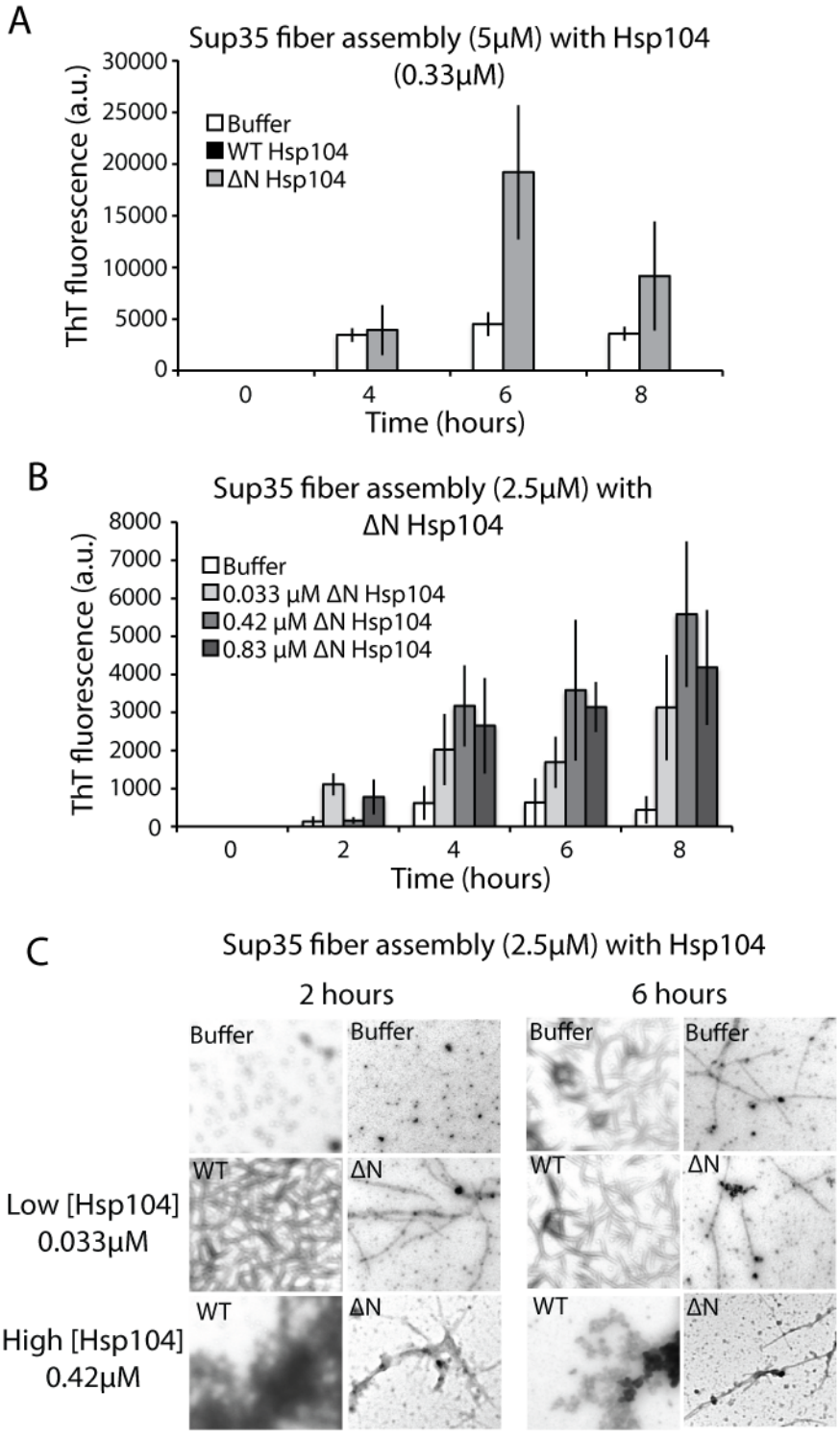
A
Sup35 fiber assembly (5μM) with Hsp104 (0.33μM)
ThT fluorescence (a.u.)
30000
25000
20000
15000
10000
5000
0
Buffer
WT Hsp104
ΔN Hsp104
0
4
6
8
Time (hours)
B
Sup35 fiber assembly (2.5μM) with ΔN Hsp104
ThT fluorescence (a.u.)
8000
7000
6000
5000
4000
3000
2000
1000
0
Buffer
0.033 μM ΔN Hsp104
0.42 μM ΔN Hsp104
0.83 μM ΔN Hsp104
0
2
4
6
8
Time (hours)
C
Sup35 fiber assembly (2.5μM) with Hsp104
2 hours
6 hours
Buffer
Buffer
Buffer
Buffer
WT
ΔN
WT
ΔN
Low [Hsp104]
0.033μM
WT
ΔN
WT
ΔN
High [Hsp104]
0.42μM

Figure 1. The N-terminal domain of Hsp104 is necessary for inhibition of Sup35 fiber formation. A) Sup35 fiber formation (5 μM) was monitored over time using the amyloid binding dye Thioflavin T (ThT) in the presence of buffer, WT Hsp104 (0.33 μM) or ΔN Hsp104 (0.33 μM) and an ATP regenerating system (1 mM creatine phosphate, 0.25 μM creatine kinase). Values represent mean ± S.E. (n=3). B) Sup35 fiber formation (2.5 μM) was monitored over time using the amyloid binding dye Thioflavin T (ThT) in the presence of buffer, 0.033 μM, 0.42 μM, or 0.83 μM ΔN Hsp104 and an ATP regenerating system (1 mM creatine phosphate, 0.25 μM creatine kinase). Values represent mean ± S.E. (n=3). C) Sup35 (2.5 μM) fiber formation products with buffer, WT Hsp104 (0.033 or 0.42 μM) or ΔN Hsp104 (0.033 or 0.42 μM) were imaged using negative stain electron microscopy at 2 and 6 hours.

formation was enhanced by the ΔN Hsp104 variant (Figure 1B). Our ThT findings were confirmed by negative stain EM. Low concentrations of both WT and ΔN Hsp104 (75:1 Sup35 monomer to Hsp104 hexamer) promoted Sup35 amyloid fiber formation (Figure 1C). At high concentrations, WT Hsp104 inhibits the formation of amyloid fibers (instead shifting the species toward amorphous, ThT negative Sup35 aggregates), while ΔN Hsp104 continues to promote amyloid fiber formation (Figure 1C).

2.2.2 Deletion of the NTD results in an increase in ATPase rate

Since we found the NTD to be essential, *in vitro*, for the inhibition of Sup35 amyloid formation, we sought to determine what role the domain plays in hexamer function. Since ATP hydrolysis is required for the successful remodeling of Sup35 amyloid fibers [20], we wanted to test whether the ATPase rate of the ΔN Hsp104 variant was altered. The NTD is not directly involved in ATP binding or hydrolysis, however, the NTD of homologous proteins have been shown to play a role in regulating these events in neighboring domains [144, 148, 183, 187]. Surprisingly, the ATPase rate of ΔN Hsp104 was approximately 2-fold higher than the WT Hsp104 (Figure 2A). This shows that while ΔN Hsp104 is unable to inhibit Sup35 amyloid formation, it is not a functionally inactive hexamer. Further, this finding supports a role for the NTD of Hsp104 in regulating the ATPase rate of the hexamer.

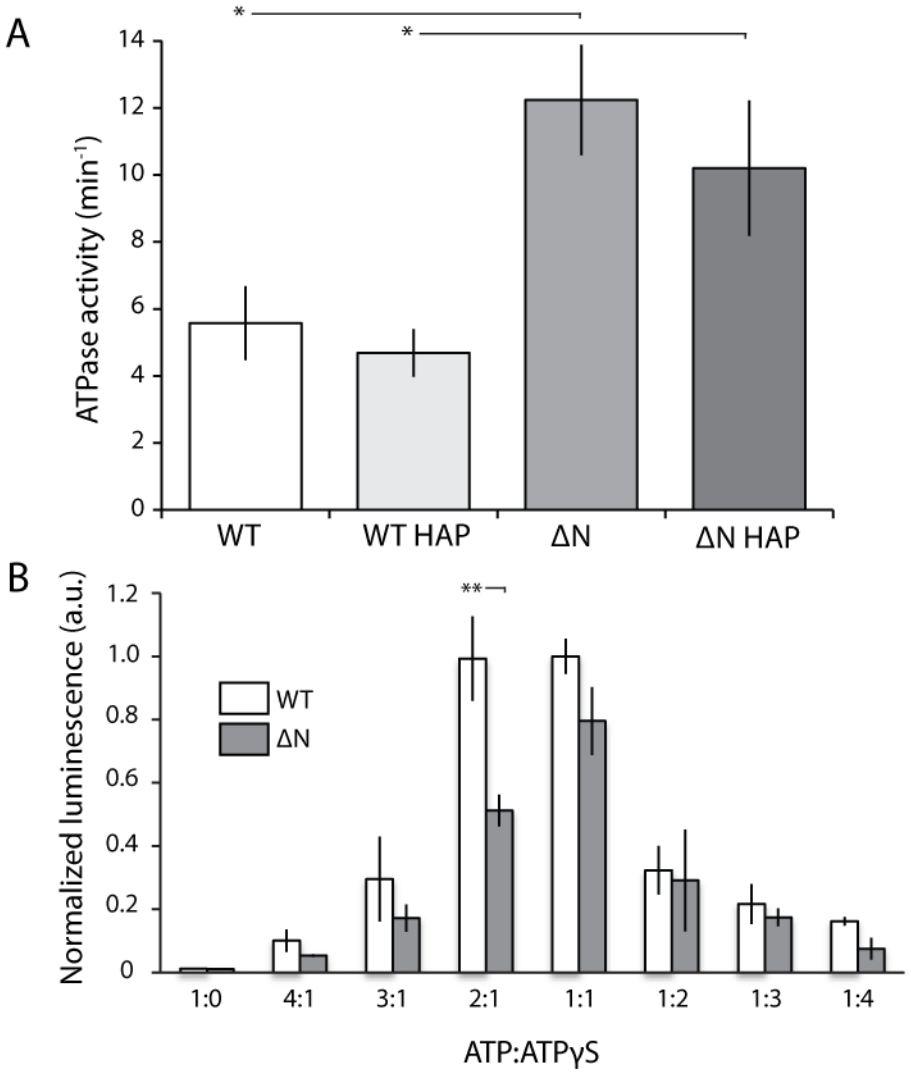

Figure 2. Deletion of the Hsp104 N-terminal domain leads to disregulation of the ATPase rate and increased sensitivity to ATP:ATPγS ratios in luciferase reactivation. A) After a 5 minute incubation with ATP (1 mM) at 25°C, ATPase activity of WT and ΔN, as well as the ClpP interacting variants HAP and ΔNHAP Hsp104 (0.25 μM monomer) were assessed using a malachite green phosphate detection kit. Values represent mean ± S.E. (n=3-4), * denotes $p < 0.05$. B) Urea-denatured firefly luciferase was incubated with either WT or ΔN Hsp104 (1 μM) for 90 min at 25˚C in the presence of 5.1 mM total nucleotide with varying ratios of ATP:ATPγS, 1:0, 4:1, 3:1, 2:1, 1:1, 1:2, 1:3, 1:4 and an ATP regenerating system (1 mM creatine phosphate, 0.25 μM creatine kinase). Reactivation of luciferase was then determined by measuring luminescence and converted to fraction WT disassembly at a 1:1 ratio of ATP:ATPγS. Values represent mean ± S.E. (n=3), ** denotes $p < 0.02$.

2.2.3 Deletion of the NTD does not affect maximal inherent disaggregase activity, but does increase sensitivity to ATP:ATPγS ratios

We next wanted to assess whether the truncated hexamer was effective at *in vitro* amorphous aggregate remodeling, for which we used a luciferase reactivation assay, which assesses disaggregation and reactivation of chemically denatured firefly luciferase [132]. By supplementing reaction conditions with different ratios of ATP:ATPγS, Hsp104 is able to disaggregate amorphous aggregates in the absence of the Hsp70 system [113]. Since ΔN Hsp104 displayed an elevated ATPase activity we were curious to find out if the ideal ATP:ATPγS ratio would differ from that of WT Hsp104. Our findings were surprising. Although both the WT and ΔN Hsp104 hexamers reached a peak activity at a ratio of 1:1 ATP:ATPγS, the ΔN hexamer was much more sensitive to changes in nucleotide ratios than the WT protein (Figure 2B). At a ratio of 2:1 ATP:ATPγS, WT Hsp104 shows statistically insignificant differences in activity to the WT protein at a ratio of 1:1 ATP:ATPγS. However, ΔN Hsp104, which shows no statistically significant difference in activity compared to WT Hsp104 at a ratio of 1:1 ATP:ATPγS is only about 50% ($p < 0.02$) as active as WT Hsp104 at a ratio of 2:1 (Figure 2B). This finding indicated that while the ΔN Hsp104 retained activity under specific conditions, it had lacked the robustness needed for activity at a broad range of ATP:ATPγS ratios.

2.2.4 Deletion of the NTD leads to changes in conformation of the Hsp104 hexamer

To determine the basis for the specific defects of ΔN Hsp104, and to use these findings to enhance our understanding of the WT protein, we wanted to visualize changes in the shape of the hexamer through the ATPase cycle for WT Hsp104 as well as ΔN Hsp104. For this we used the in solution structural technique Small (and Wide) Angle X-ray Scattering (SAXS/WAXS). To simulate the steps of the ATP hydrolysis cycle, in solution scattering experiments were carried out on the full-length protein (WT) and ΔN Hsp104 in six different states: in the presence of AMP-PNP, ATPγS, ATP, ADP-AlF_x (an ATP hydrolysis transition state mimic), ADP, and no nucleotide.

Monodispersity of both the WT and ΔN Hsp104 constructs was assessed using size exclusion chromatography coupled to multi-angle light scattering (SEC-MALS). A single peak elutes as expected for a hexameric assembly, and using the inline multi-angle scattering and refractive interferometer, an exact molecular weight can be calculated which corresponds to the theoretical weight of the hexameric particle (Figure 3A). The molecular weights obtained by SEC-MALS compare favorably to the theoretical molecular weights of the two hexamers (Figure 3A). Both WT and ΔN Hsp104 particles also have linear Guinier regions (Figure 3B) in all nucleotide states, indicating that there are no interparticle interactions such as aggregation [199]. We measured scattering for each sample at multiple concentrations as well as different beamlines (SSRL 4-2 and NSLS X9) and obtained similar results in each case (Table 1). None of the samples showed signs of aggregation or any other concentration-dependent effects.

Examples of raw scattering profiles (I(Q) vs. Q, where $Q=4\pi(\sin\theta)/\lambda$) and a representative GNOM [200] fit to the experimental data are shown for WT and ΔN Hsp104 in the presence of ADP in Figure 4A. Distinctive features in the low Q region that are present in all of the WT Hsp104 samples but not the ΔN Hsp104 samples are highlighted by the inset in Figure 4A. A summary of R_g and D_{max} values is reported in Table 2, as calculated by the program GNOM [200] which uses an indirect Fourier transform to convert reciprocal space information into real space information. The values reflect the average (including standard error) of measurements at varying concentrations and two beamlines. The reproducibility of the measurement is evidence that the samples are well behaved and ideally suited for SAXS analysis. The change in R_g is displayed as a bar graph in Figure 4B, with the nucleotide states ordered to represent a round of ATP hydrolysis (AMP-PNP, a non-hydrolysable ATP analog, ATPγS, a slowly hydrolysable ATP analog, ATP, which in our WT Hsp104 may be partially hydrolyzed, ADP-AlF_x, an ATP hydrolysis transition state mimic, ADP, and the no nucleotide state). These values represent the average dimensions of the Hsp104 hexamer in the presence of the various nucleotides.

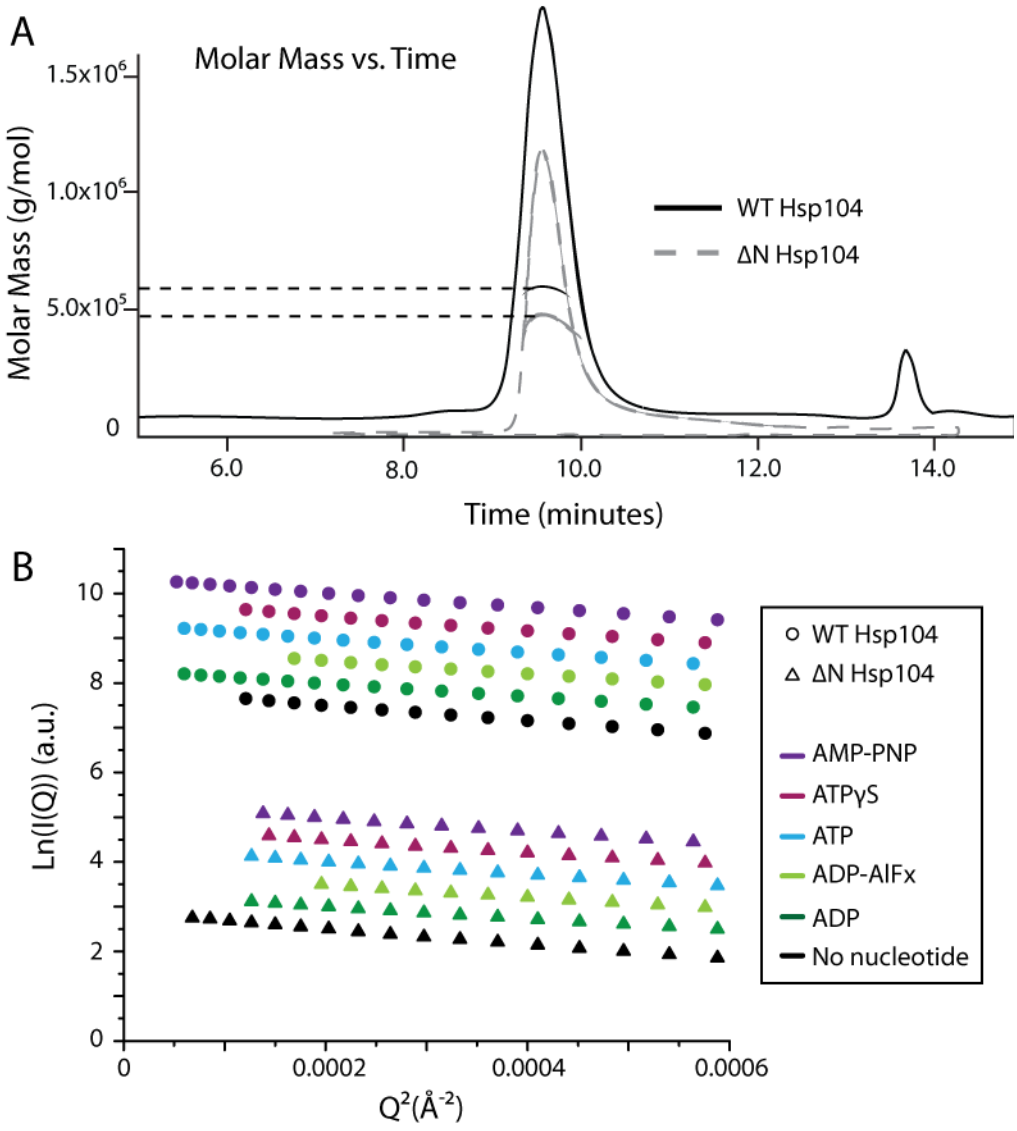

Figure 3. WT and ΔN Hsp104 for SAXS experiments are hexameric, mondisperse and aggregation free. A) UV profiles of molar mass versus time from size exclusion chromatography coupled to multi-angle light scattering (SEC-MALS) experiments for WT and ΔN Hsp104. Before use in SAXS experiments, SEC-MALS was used to assess monodispersity and oligomeric state. Both WT-Hsp104 and ΔN-Hsp104 samples are monodisperse hexamers. B) Guinier plots of the raw scattering for both WT and ΔN Hsp104 in the presence of AMP-PNP, ATPγS, ATP, ADP-AlFx, ADP and no nucleotide. Linearity of the Guinier plot indicates that there were no interparticle interactions such as aggregation.

Table 1. Parameters derived from SAXS/WAXS of WT and ΔN Hsp104. Rg values from the Guinier region of the scattering curves were determined using the program PRIMUS (Konarev 2003). Distance distribution functions P(r) were calculated by the program GNOM using an indirect Fourier transform (Svergun 1992). The maximum dimension of the particle (Dmax) was determined by examining the quality of fit to the experimental data for a Dmax range of 180 to 280 Å varied in 5-Å increments. Values for Rg were computed from the second moment of the P(r). The Porod volume and p value were calculated by the java-based program ScÅtter (www.bioisis.net/tutorial/9). The mass of the particle was calculated from Qr as described (Rambo 2013). GASBOR (Svergun 2001) was run on the raw scattering data and DAMAVER (Volkov 2003) used to avergae the envelopes and calculate normalized spatial discrepancy (NSD). Damaver and damfilt pdb files were converted using the prgram pdb2vol from the SITUS suite of programs (Wriggers 2011). Channel dimensions of the reconstructed volumes were determined using MATLAB. See also Experimental Procedures.

	Hsp104 WT		Guinier				GNOM				
	Location	Conc.	q_{min}	qRg range	Rg	I(0)	Angle range	Dmax	Rg	I(0)	Porod total estimate
AMP-PNP	NSLS	2.5 mg/mL	0.01100	0.748-1.50	68.0 +- 0.0811	522.49 +- 0.644	0.0092-0.8290	255	69.2	526	0.774
	NSLS	5.0 mg/mL	0.01098	0.755-1.51	68.7 +- 0.0547	1011.5 +- 0.811	0.0073-0.8300	230	68.6	1010	0.671
	NSLS	2.9 mg/mL	0.01201	0.817-1.50	68.1 +- 0.0980	570.01 +- 0.835	0.0120-0.7950	235	68.2	567	0.652
ATPγS	NSLS	2.5 mg/mL	0.01101	0.754-1.51	68.5 +- 0.0739	530.51 +- 0.592	0.0097-0.7290	235	69.2	530	0.603
	NSLS	5.0 mg/mL	0.01100	0.756-1.51	68.7 +- 0.0518	1085.4 +- 0.824	0.0103-0.7290	235	69	1080	0.606
	SSRL	2.9 mg/mL	0.01497	1.04-1.53	69.4 +- 0.264	18.144 +- 0.0786	0.0140-0.4435	235	70.2	18	0.675
	SSRL	5.9 mg/mL	0.01506	1.04-1.53	69.5 +- 0.209	35.650 +- 0.124	0.0140-0.4435	235	69.4	35	0.667
	NSLS	1.5 mg/mL	0.01300	0.893-1.51	68.7 +- 0.108	318.88 +- 0.521	0.0110-0.7950	225	69	317	0.661
	NSLS	2.9 mg/mL	0.01300	0.909-1.54	69.9 +- 0.0832	616.75 +- 0.800	0.0110-0.7950	240	71.5	620	0.623
ATP	NSLS	2.5 mg/mL	0.01000	0.677-1.49	67.7 +- 0.0701	450.12 +- 0.458	0.0103-0.8290	220	67.1	445	0.684
	NSLS	5.0 mg/mL	0.01100	0.749-1.50	68.1 +- 0.0507	936.03 +- 0.685	0.0078-0.8100	230	68.2	935	0.599
	SSRL	2.9 mg/mL	0.01499	1.01-1.55	67.1 +- 0.241	17.190 +- 0.0683	0.0140-0.3171	230	67.1	17.1	0.657
	SSRL	5.9 mg/mL	0.01493	1.01-1.56	67.5 +- 0.185	32.498 +- 0.100	0.0140-0.4435	230	67.1	32	0.662
	NSLS	1.5 mg/mL	0.01000	0.670-1.54	67.0 +- 0.0871	242.38 +- 0.331					
	NSLS	2.9 mg/mL	0.01099	0.736-1.54	66.9 +- 0.0862	444.53 +- 0.592	0.0110-0.7900	230	67.2	443	0.55

Table 1 continued. Parameters derived from SAXS/WAXS of WT and ΔN Hsp104.

Hsp104 WT			Guinier				GNOM				
	Location	Conc.	q_{min}	qRg range	Rg	I(0)	Angle range	Dmax	Rg	I(0)	Porod total estimate
ADP-AlFx	SSRL	2.9 mg/mL	0.01498	0.981-1.51	65.4 +- 0.234	17.404 +- 0.0672	0.0140-0.4435	220	65	17.2	0.713
	SSRL	5.9 mg/mL	0.01500	0.990-1.52	66.1 +- 0.188	33.300 +- 0.100	0.0140-0.4435	220	65.1	32.7	0.67
	NSLS	1.5 mg/mL	0.02108	1.39-1.73	66.3 +- 0.228	306.67 +- 1.77	0.0210-0.7950	225	66.5	305	0.646
	NSLS	2.9 mg/mL	0.02096	1.39-1.72	66.2 +- 0.145	586.1 +- 2.15	0.0210-0.7950	210	64.2	560	0.696
	NSLS	5.0 mg/mL	0.01300	0.850-1.50	65.4 +- 0.298	1964.9 +- 9.52	0.0130-0.8000	220	63.9	1920	0.713
ADP	NSLS	2.5 mg/mL	0.01000	0.663-1.49	66.3 +- 0.0374	1365.4 +- 0.709	0.0078-0.8050	240	67	1370	0.636
	NSLS	5.0 mg/mL	0.01051	0.704-1.47	67.0 +- 0.0384	2807.5 +- 1.40	0.0078-0.7300	245	67.9	2820	0.601
	SSRL	2.9 mg/mL	0.01499	0.985-1.52	65.7 +- 0.225	16.606 +- 0.0616	0.0140-0.4435	210	64.8	16.3	0.723
	SSRL	5.9 mg/mL	0.01499	0.994-1.53	66.3 +- 0.182	33.548 +- 0.100	0.0140-0.4435	215	64.6	32.6	0.731
	NSLS	1.5 mg/ml	0.01201	0.799-1.53	66.6 +- 0.0935	287.34 +- 0.410	0.0120-0.7950	225	66.1	284	0.649
No nucleotide	NSLS	2.5 mg/mL	0.00750	0.538-1.51	71.7 +- 0.106	490.30 +- 0.773	0.0090-0.2240	245	71.6	487	0.646
	NSLS	5.0 mg/mL	0.00899	0.616-1.49	72.5 +- 0.0647	971.03 +- 0.856	0.0090-0.1590	260	73.6	975	0.635
	SSRL	2.9 mg/mL	0.01497	1.09-1.53	72.8 +- 0.340	18.995 +- 0.105	0.0140-0.4435	255	73.3	18.9	0.746
	SSRL	5.9 mg/mL	0.01501	1.11-1.56	74.2 +- 0.334	38.935 +- 0.214	0.0140-0.4384	255	74.7	38.7	0.764
	NSLS	1.5 mg/mL	0.01400	0.990-1.49	70.7 +- 0.177	344.72 +- 0.945	0.0110-0.7950	225	70	341	0.701
	NSLS	2.9 mg/mL	0.01397	1.01-1.52	72.3 +- 0.116	688.30 +- 1.25	0.0110-0.7950	225	71.3	678	0.7

Table 1 continued. Parameters derived from SAXS/WAXS of WT and ΔN Hsp104.

Hsp104 WT		MM by Qr		GASBOR		Situs dimensions		Channel				
									Diameter			
Volume	P	Exp. MM	Theor. MM	No. included	NSD	Damaver	Damfilt	Volume	Avg.	Max.	Min.	Slices
AMP-PNP												
1727702	3.9	645000	612000	10	2.588 +- 0.495	252x224x188.090	154x126x89.095					
1706347	3.9	650000	612000	9	2.373 +- 0.549	234x234x156.270	143x169x91.924	1.71E+05	29	56	0	90
1700962	3.9	624000	612000	9	2.366 +- 0.341	228x240x127.280	156x180x84.853					
ATPγS												
1711825	3.9	609000	612000	10	2.053 +- 0.266	221x234x156.271	130x143x91.924					
1708074	3.9	620000	612000	9	2.096 +- 0.169	237.5x225x150.261	150x137.5x88.388					
1660568	3.8		612000	9	2.267 +- 0.394	238x224x158.391	140x154x89.095					
1647299	3.8		612000	9	2.173 +- 0.551	246.5x232x133.289	145x159.5x92.277					
1654519	3.9	617000	612000	9	1.912 +- 0.292	216x228x144.25	156x156x84.853					
1692549	3.9	630000	612000	9	1.641 +- 0.114	228x228x135.765	168x156x93.338	1.05E+05	28	47	18	80
ATP												
1654371	3.9	631000	612000	10	2.034 +- 0.189	216x228x135.764	132x144x93.338					
1674270	3.9	640000	612000	9	2.013 +- 0.512	225x237.5x150.260	187.5x187.5x88.388	1.82E+05	38	50	28	95
1684247	3.9		612000	9	1.801 +- 0.203	237.5x237.5x141.422	187.5x175x97.227					
1679654	3.9		612000	9	2.829 +- 0.653	234x221x165.463	143x143x101.117					
			612000									
1654772	3.8	603000	612000	10	1.706 +- 0.080	216x228x135.764	156x168x93.338					
ADP-AlFx												
1642119	3.9		612000	9	2.412 +- 0.634	225x212.5x159.099	175x150x97.227					
1641887	3.9		612000	9	2.343 +- 0.286	225x225x141.421	150x175x79.550					
1593390	3.9		612000	9	1.806 +- 0.288	228x216x135.764	180x156x84.853					
1625506	3.9		612000	10	2.108 +- 0.220	216x216x144.250	168x156x84.853					
1580239	3.8	564000	612000	8	1.904 +- 0.132	216x228x135.764	180x180x93.338	6.51E+05	26	32	25	80

Table 1 continued. Parameters derived from SAXS/WAXS of WT and ΔN Hsp104.

Hsp104 WT		MM by Qr		GASBOR		Situs dimensions		Channel				
									Diameter			
Volume	P	Exp. MM	Theor. MM	No. included	NSD	Damaver	Damfilt	Volume	Avg.	Max.	Min.	Slices
ADP												
1595855	3.8	617000	612000	9	2.004 +- 0.286	250x225x141.421	175x150x88.389	8.50E+04	27	40	15	75
1596676	3.9	622000	612000	9	2.034 +- 0.247	234x247x137.885	143x156x82.731					
1644595	3.9		612000	9	1.847 +- 0.193	207x218.5x138.24	172.5x195.5x105.712					
1629344	3.8		612000	10	2.807 +- 0.487	216x216x200.465	135x148.5x95.460					
1610198	3.9	596000	612000	10	2.034 +- 0.245	216x228x144.250	168x168x84.852					
No nucleotide												
1977362	3.8		612000	10	2.359 +- 0.158	243x243x152.736	148.5x148.5x85.914					
1979811	3.9		612000	9	2.663 +- 0.613	256.5x256.5x133.644	148.5x.148.5x95.460					
2064711	3.9		612000	9	2.692 +- 0.958	256.5x256.5x152.736	162x175.5x85.914					
2066202	3.9		612000	9	2.525 +- 0.676	243x256.5x143.190	175.5x229.5x105.006					
2069872	3.8	668000	612000	9	2.530 +- 0.527	234x234x156.27	156x195x101.116	1.86E+05	27	57	17	100
1969839	3.9		612000	9	2.714 +- 0.420	234x234x156.271	143x143x91.924					

Table 1. Parameters derived from SAXS/WAXS of WT and ΔN Hsp104. Rg values from the Guinier region of the scattering curves were determined using the program PRIMUS (Konarev 2003). Distance distribution functions P(r) were calculated by the program GNOM using an indirect Fourier transform (Svergun 1992). The maximum dimension of the particle (Dmax) was determined by examining the quality of fit to the experimental data for a Dmax range of 180 to 280 Å varied in 5-Å increments. Values for Rg were computed from the second moment of the P(r). The Porod volume and p value were calculated by the java-based program ScÅtter (www.bioisis.net/tutorial/9). The mass of the particle was calculated from Qr as described (Rambo 2013). GASBOR (Svergun 2001) was run on the raw scattering data and DAMAVER (Volkov 2003) used to avergae the envelopes and calculate normalized spatial discrepancy (NSD). Damaver and damfilt pdb files were converted using the prgram pdb2vol from the SITUS suite of programs (Wriggers 2011). Channel dimensions of the reconstructed volumes were determined using MATLAB. See also Experimental Procedures.

Hsp104 ΔN			Guinier				GNOM				
	Location	Conc.	q_{min}	qRg range	Rg	I(0)	Angle range	Dmax	Rg	I(0)	Porod total estimate
AMP-PNP	NSLS	5.0 mg/mL	0.01150	0.768-1.50	66.8 +- 0.0553	869.53 +- 0.732	0.0118-0.7490	235	67.2	864	0.654
	NSLS	1.5 mg/mL	0.01000	0.651-1.50	65.1 +- 0.0976	254.35 +- 0.394	0.0100-0.7950	235	65.8	255	0.568
	NSLS	2.0 mg/mL	0.00801	0.523-1.50	65.3 +- 0.0822	339.88 +- 0.435	0.0080-0.7950	235	66.5	342	0.571
ATPγS	NSLS	2.5 mg/mL	0.01099	0.723-1.48	65.7 +- 0.0747	434.39 +- 0.492	0.0113-0.7890	235	67.1	434	0.61
	NSLS	5.0 mg/mL	0.01100	0.733-1.50	66.6 +- 0.0610	933.47 +- 0.851	0.0113-0.7860	235	68	933	0.606
	SSRL	2.3 mg/mL	0.01398	0.996-1.50	71.2 +- 0.290	16.918 +- 0.780	0.0140-0.2414	220	69.6	8.25	0.681
	SSRL	4.6 mg/mL	0.01399	0.970-1.53	69.4 +- 0.336	8.3718 +- 0.470	0.0150-0.2515	220	69.6	16.1	0.628
	NSLS	1.5 mg/mL	0.01200	0.787-1.51	65.6 +- 0.0864	298.48 +- 0.392	0.0120-0.7950	220	66	295	0.589
	NSLS	2.0 mg/mL	0.01200	0.790-1.52	65.9 +- 0.0904	404.09 +- 0.565	0.0120-0.7950	220	66.4	400	0.616
ATP	NSLS	2.5 mg/mL	0.00650	0.712-1.49	64.8 +- 0.0769	379.69 +- 0.454	0.0068-0.7900	240	67.2	387	0.504
	NSLS	5.0 mg/mL	0.01100	0.717-1.50	65.2 +- 0.0491	862.45 +- 0.638	0.0113-0.7900	235	65.9	859	0.571
	SSRL	2.3 mg/mL	0.01499	0.957-1.54	63.8 +- 0.276	7.0681 +- 0.033	0.0140-0.2919	225	64.6	7.08	0.779
	SSRL	4.6 mg/mL	0.01499	0.972-1.50	64.8 +- 0.238	13.913 +- 0.534	0.0140-0.2919	225	65.1	13.8	0.674
	NSLS	1.5 mg/mL	0.01000	0.629-1.51	62.9 +- 0.0795	220.52 +- 0.277	0.0110-0.7950	230	63.4	221	0.488
	NSLS	2.0 mg/mL	0.01000	0.629-1.51	62.9 +- 0.0792	220.94 +- 0.276	0.0110-0.7950	240	63.8	222	0.481

Table 1 continued. Parameters derived from SAXS/WAXS of WT and ΔN Hsp104.

Hsp104 ΔN			Guinier				GNOM				
	Location	Conc.	q_{min}	qRg range	Rg	I(0)	Angle range	Dmax	Rg	I(0)	Porod total estimate
ADP-AlFx	SSRL	2.3 mg/mL	0.01399	0.852-1.53	60.9 +- 0.249	6.9066 +- 0.0289	0.0140-0.2666	205	60.9	6.9	0.689
	SSRL	4.6 mg/mL	0.01397	0.869-1.50	62.2 +- 0.194	13.553 +- 0.0428	0.0140-0.4435	215	62.7	13.6	0.683
	NSLS	1.5 mg/mL	0.01899	1.20-1.52	63.2 +- 0.271	251.55 +- 1.41	0.0190-0.7950	220	62.2	246	0.664
	NSLS	2.0 mg/mL	0.01897	1.21-1.53	63.8 +- 0.228	337.34 +- 1.60	0.0190-0.7950	220	63.7	334	0.685
	NSLS	5.0 mg/mL	0.01400	0.889-1.52	63.5 +- 0.298	1556.8 +- 7.92	0.01400-0.800	220	62.5	1530	0.84
ADP	NSLS	2.0 mg/mL	0.00749	0.465-1.52	62.0 +- 0.0933	228.15 +- 0.370	0.0078-0.7850	233	63.5	229	0.624
	NSLS	4.0 mg/mL	0.01100	0.695-1.49	63.2 +- 0.0665	498.94 +- 0.537	0.0113-0.7860	225	63.8	496	0.605
	SSRL	2.3 mg/mL	0.01499	0.921-1.54	61.4 +- 0.241	6.7263 +- 0.0282	0.0140-0.2414	220	62.6	6.77	0.66
	SSRL	4.6 mg/mL	0.01500	0.941-1.51	62.7 +- 0.209	13.284 +- 0.0456	0.0140-0.3374	230	63.9	13.4	0.789
	NSLS	1.5 mg/mL	0.01501	0.960-1.54	64.0 +- 0.121	245.70 +- 0.525	0.0150-0.7950	230	64.4	244	0.611
	NSLS	2.0 mg/mL	0.01500	0.963-1.54	64.2 +- 0.102	320.01 +- 0.575	0.0150-0.7950	225	64.5	318	0.614
No nucleotide	NSLS	2.5 mg/mL	0.00800	0.584-1.50	72.9 +- 0.154	395.38 +- 0.881	0.0083-0.7890	245	72.7	388	0.671
	NSLS	5.0 mg/mL	0.01151	0.917-1.52	79.7 +- 0.117	956.06 +- 1.56	0.0118-0.7890	240	75.5	882	0.631
	SSRL	2.3 mg/mL	0.01497	1.10-1.54	73.2 +- 0.469	8.5800 +- 0.0659	0.0140-0.2919	235	72.2	8.36	0.807
	SSRL	4.6 mg/mL	0.01497	1.16-1.55	77.5 +- 0.490	17.835 +- 0.0141	0.0140-0.4435	235	74.4	16.7	0.727
	NSLS	1.5 mg/mL	0.01399	1.00-1.50	71.5 +- 0.153	328.19 +- 0.792	0.0140-0.7950	230	70.6	321	0.688
	NSLS	2.0 mg/mL	0.01299	0.938-1.52	72.2 +- 0.123	435.05 +- 0.815	0.0130-0.7950	240	71.8	429	0.682

Table 1 continued. Parameters derived from SAXS/WAXS of WT and ΔN Hsp104.

Hsp104 ΔN		MM by Qr		GASBOR		Situs dimensions		Channel				
									Diameter			
Volume	P	Exp. MM	Theor. MM	No. included	NSD	Damaver	Damfilt	Volume	Avg.	Max.	Min.	Slices
AMP-PNP												
1521470	3.9	563000	506000	10	1.717 +- 0.069	228x240x118.794	144x156x67.882	7.80E+04	32	46	27	60
1441966	3.9	530000	506000	10	2.182 +- 0.167	237.5x237.5x123.743	175x187.5x70.711					
1455462	3.9	537000	506000	9	2.066 +- 0.182	240x240x118.794	204x204x67.883					
ATPγS												
1351120	3.9	523000	506000	9	1.661 +- 0.182	230x230x113.844	184x195.5x73.186					
1441596	3.9	538000	506000	9	1.726 +- 0.235	241.5x230x113.844	172.5x149.5x73.186					
1543621	3.9		506000									
1571916	3.9		506000									
1335332	3.9	515000	506000	9	1.338 +- 0.072	198x209x116.672	154x154x77.782	5.70E+04	22	25	16	80
1328161	3.9	520000	506000	9	1.458 +- 0.227	209x209x108.894	143x154x77.782					
ATP												
1353560	3.9	512000	506000	9	1.899 +- 0.116	230x241.5x105.713	195.5x195.5x73.185					
1436818	3.9	519000	506000	9	1.757 +- 0.176	230x207x113.844	184x149.5x65.054	1.25E+05	34	61	24	70
1382322	3.9		506000	9	1.645 +- 0.135	230x230x121.976	195.5x172.5x81.317					
1364062	3.9		506000	10	1.419 +- 0.036	230x218.5x105.712	207x207x73.186					
1348699	3.9	478000	506000									
1349023	3.9	468000	506000									
ADP-AlFx												
1237425	3.8		506000	9	1.466 +- 0.245	210x199.5x96.52	189x168x81.671					
1325795	3.9		506000	9	1.462 +- 0.074	220x209x108.894	209x187x70.004					
1416628	3.9	527000	506000	10	1.538 +- 0.074	209x209x116.673	154x154x62.225					
1408572	3.9	544000	506000	9	1.421 +- 0.056	209x209x108.895	165x165x70.003					
1309244	3.9	488000	506000	9	1.832 +- 0.259	220x220x108.895	176x176x70.004	1.51E+05	30	53	23	65

Table 1 continued. Parameters derived from SAXS/WAXS of WT and ΔN Hsp104.

Hsp104 ΔN		MM by Qr		GASBOR		Situs dimensions		Channel				
									Diameter			
Volume	P	Exp. MM	Theor. MM	No. included	NSD	Damaver	Damfilt	Volume	Avg.	Max.	Min.	Slices
ADP												
1226602	3.8	476000	506000	9	1.688 +- 0.216	209x220x108.894	165x176x70.004					
1257546	3.9	490000	506000	9	1.523 +- 0.076	231x209x108.895	187x176x70.003	9.30E+04	26	50	15	70
1239575	3.9		506000									
1261388	3.9		506000									
1364382	3.9	512000	506000									
1356323	3.9	513000	506000									
No nucleotide												
1847354	3.9	497000	506000	9	1.675 +- 0.093	230x230x113.844	161x172.5x65.054	1.28E+05	47	52	42	60
2180685	3.9	567000	506000									
1903839	3.8		506000									
1944172	3.9		506000									
1933427	3.9	529000	506000									
2251878	3.9	536000	506000									

Table 2.
Average R_g and D_{max} values from GNOM analysis of SAXS data

	WT		ΔN	
Nucleotide	R_g	D_{max}	R_g	D_{max}
AMP-PNP	68.7 ± 0.3	240 ± 8	66.5 ± 0.4	235 ± 0
ATPγS	69.7 ± 0.4	234 ± 2	67.8 ± 0.6	225 ± 3
ATP	67.3 ± 0.2	228 ± 2	65.7 ± 0.6	231 ± 4
ADP-AlF_x	64.9 ± 0.5	219 ± 2	62.2 ± 0.4	213 ± 3
ADP	66.1 ± 0.6	227 ± 7	63.8 ± 0.3	227 ± 2
No Nucleotide	72.4 ± 0.7	244 ± 6	72.9 ± 0.7	238 ± 2

Distance distribution functions P(r) were calculated by the program GNOM using an indirect Fourier transform (Svergun 1992). The maximum dimension of the particle (D_{max}) was determined by examining the quality of fit to the experimental data for a D_{max} range of 180 to 280 Å, varied in 5-Å increments. Values for Rg were computed from the second moment of the P(r). Values reported are averaged from scattering data collected at various concentrations and beamlines (See methods for beamline details). Full details of each sample are given in Table 1.

The R_g and D_{max} values indicate that in the absence of nucleotide the Hsp104 hexamer is expanded relative to the hexamer in the presence of nucleotide (Figure 4B, Tables 1 and 2). A decrease in hexamer dimensions occurs upon addition of nucleotide, the magnitude of which is reproducibly dependent on the identity of the nucleotide (Figure 4B, Tables 1 and 2). Compared to the WT Hsp104 hexamer, the magnitude of the decrease in the ΔN Hsp104 hexamer dimensions is markedly more pronounced in the transition from the no nucleotide to nucleotide bound state (Figure 4B, Table 2). This decrease indicates that in the absence of nucleotide the ΔN Hsp104 hexamer is more expanded than the full-length protein. For both proteins AMP-PNP and ATPγS, non-hydrolysable and slowly hydrolysable ATP analogs respectively, have the largest R_g values (Figure 4B, Tables 1 and 2). The ADP-AlF_x states have the smallest R_g (Figure 4B, Tables 1 and 2). These data suggest that both WT and ΔN Hsp104 hexamers contract upon nucleotide binding, reaching their smallest dimension in the presence of the transition state mimic ADP-AlF_x, and then expanding slightly in the ADP state (Figure 4B, Table 2). This finding indicates that the hexamer contracts and expands in concert with ATP hydrolysis (Figure 4B,

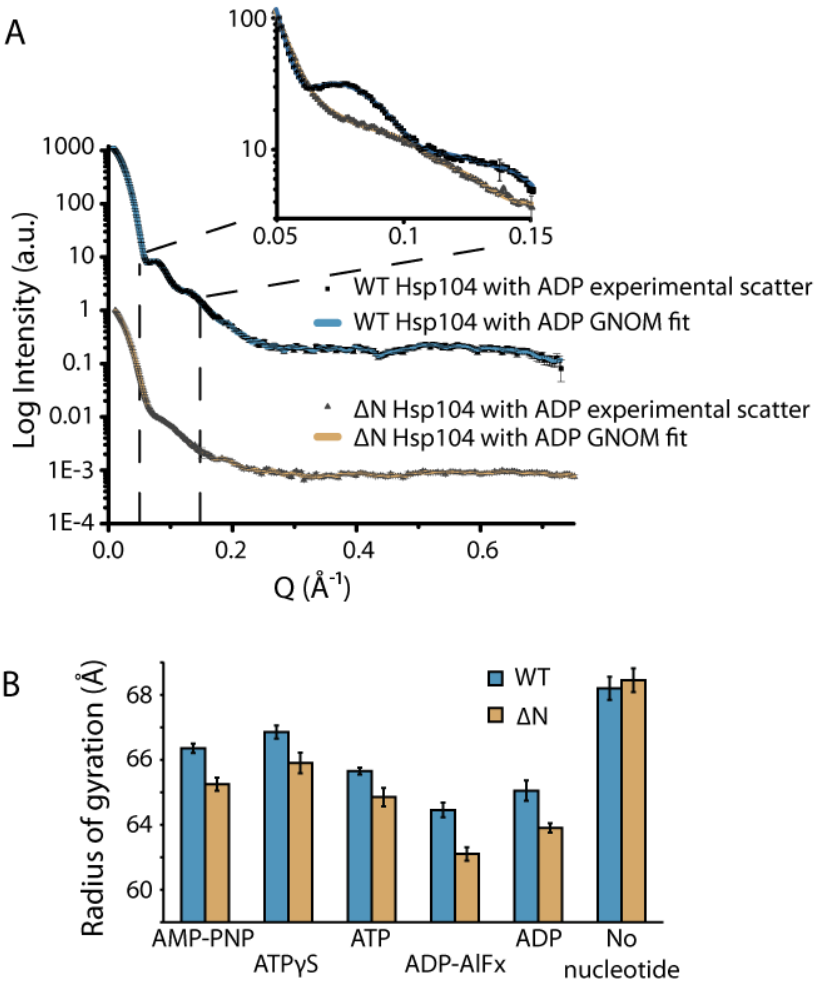

Figure 4. Representative raw scattering profiles and changes in R_g for WT and ΔN Hsp104 from Small Angle X-ray Scattering (SAXS) measurements. A) Representative scattering profiles for WT and ΔN Hsp104 (arbitrary intensity scale versus momentum transfer Q). The curves are scaled for better visualization. Inset shows enlargement of the region outlined with dashed lines. The curves are overlaid in the enlargement to reveal the regions of the scattering profiles where the WT protein consistently differs from ΔN Hsp104 in all nucleotide states (AMP-PNP, ATPγS, ATP, ADP-AlFx, ADP and no nucleotide). Overlaid onto the experimental curves is the GNOM (Svergun, 1992) fit to the data. GNOM implements an indirect Fourier transform to reveal real space information about the particle including radius of gyration (R_g) and a pairwise density distribution plot (P(r)). B) Bar graph displaying the change in radius of gyration (R_g) in the presence of different nucleotides for both WT and ΔN Hsp104 as calculated by GNOM. These values also closely match the Guinier approximations for R_g (See Table 1). Both WT and ΔN Hsp104 have the largest Rg in the absence of nucleotide. Since ΔN Hsp104 is smaller than the WT protein, the increase in R_g relative to the other nucleotide states is enhanced. The trend in R_g values for the WT and ΔN Hsp104 indicate that the hexamer contracts as it processes through the ATP hydrolysis cycle. Each bar represents 3-7 replicates +- SEM at varying concentrations and different beamlines (SSRL BL4-2 and NSLS X9).

Tables 1 and 2). The D_{max} values for the WT and ΔN Hsp104 hexamers are comparable to each other for all of the nucleotide states, suggesting that the maximum dimension maybe a longitudinal rather than a simple N- to C- terminal vector (Tables 1 and 2).

Additional information about the conformational changes of the hexamers can be garnered from the real-space pairwise density distribution function, or P(r), which is also obtained by the indirect Fourier transform of the raw scattering data by the program GNOM [200]. Representative P(r) curves for the WT (Figure 5A) and the ΔN (Figure 5B) hexamers are shown for all nucleotide states. For ease of comparison the curves have been normalized to the area under the curve and overlaid. The area surrounding the peak of the P(r) curves has been enlarged as an inlay to show the differences between nucleotide states (Figure 5). As with the R_g values there are clear changes in shape dependent upon the identity of the nucleotide. Not surprisingly, the most striking difference is seen in the ΔN Hsp104 hexamer in the absence of nucleotide, where the particle is enlarged compared to the nucleotide bound states (Figure 5B).

The P(r) curves demonstrate that the addition of nucleotide, and the identity of the nucleotide, induces specific conformational changes in both the WT and ΔN Hsp104 hexamers. However, how the Hsp104 hexamer responds to nucleotide, both in terms of the magnitude and the specific effect of a given nucleotide, differs in the absence of the NTD. To visualize these changes, and how they differ between the WT and ΔN Hsp104 hexamers we used an *ab initio* modeling program GASBOR [201] to acquire volume reconstructions of the average shape of the particles in each nucleotide state (Figures 6 and 7). For each state, GASBOR was run on the raw scattering data 10 times. The outputs of each GASBOR run were then averaged together to give a filtered and unfiltered density using the program DAMAVER [202]. An overlay of every GASBOR output for each state is shown in Figure 6. The WT shape reconstructions were oriented using the ΔN hexamers (Figure 7B) which when overlaid showed where density for the missing domain would fit. The large conformational changes are clearly visible, in particular the

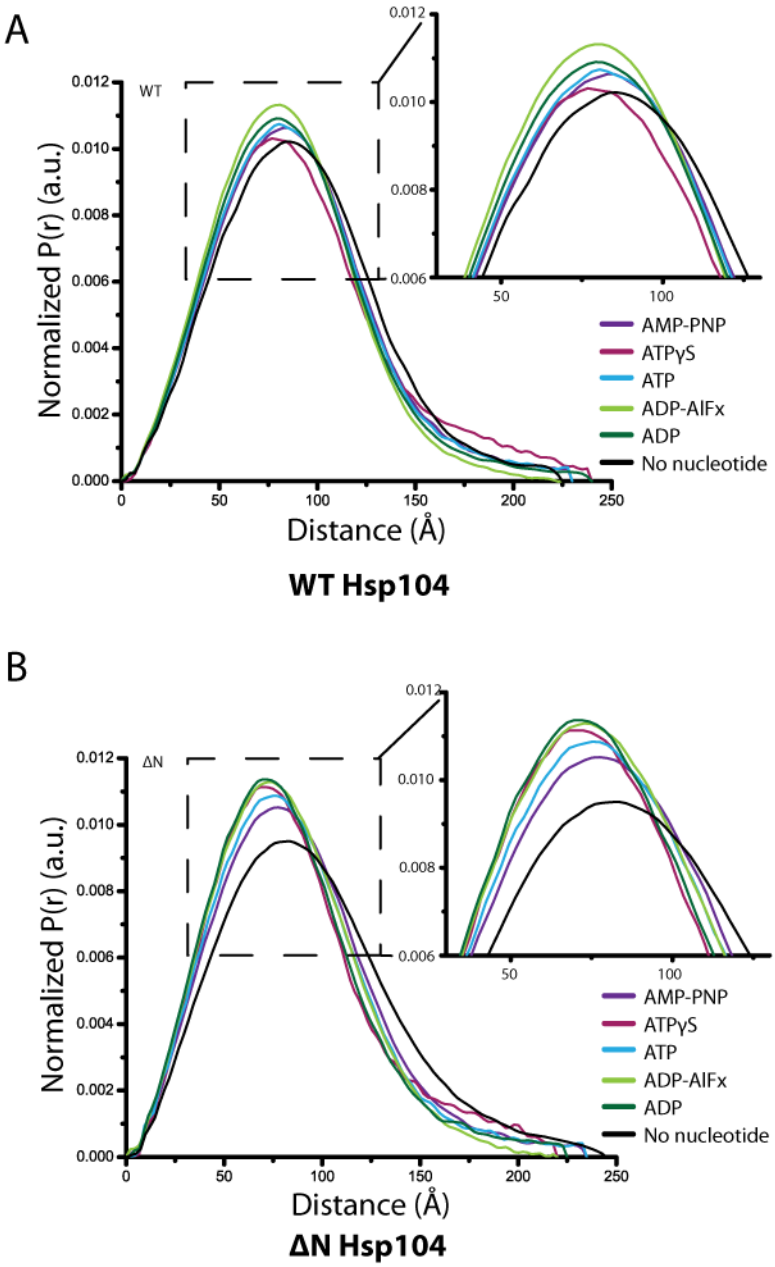

Figure 5. Real-space shape information from Small Angle X-ray Scattering (SAXS) measurements. Normalized P(r) curves (density distribution plots) generated by GNOM (Svergun 1992) for WT (A) and ΔN (B) Hsp104 in the presence of six different nucleotides: AMP-PNP, ATPγS, ATP, ADP-AlFx, ADP and no nucleotide. The P(r) plots have been normalized to the area under the curve and overlaid to show differences between the nucleotide states. The inset displays the P(r) peak, showing some of the variability between the nucleotide states. Compared to the WT protein, ΔN Hsp104 in the absence of nucleotide has an expanded center of mass relative to its nucleotide states.

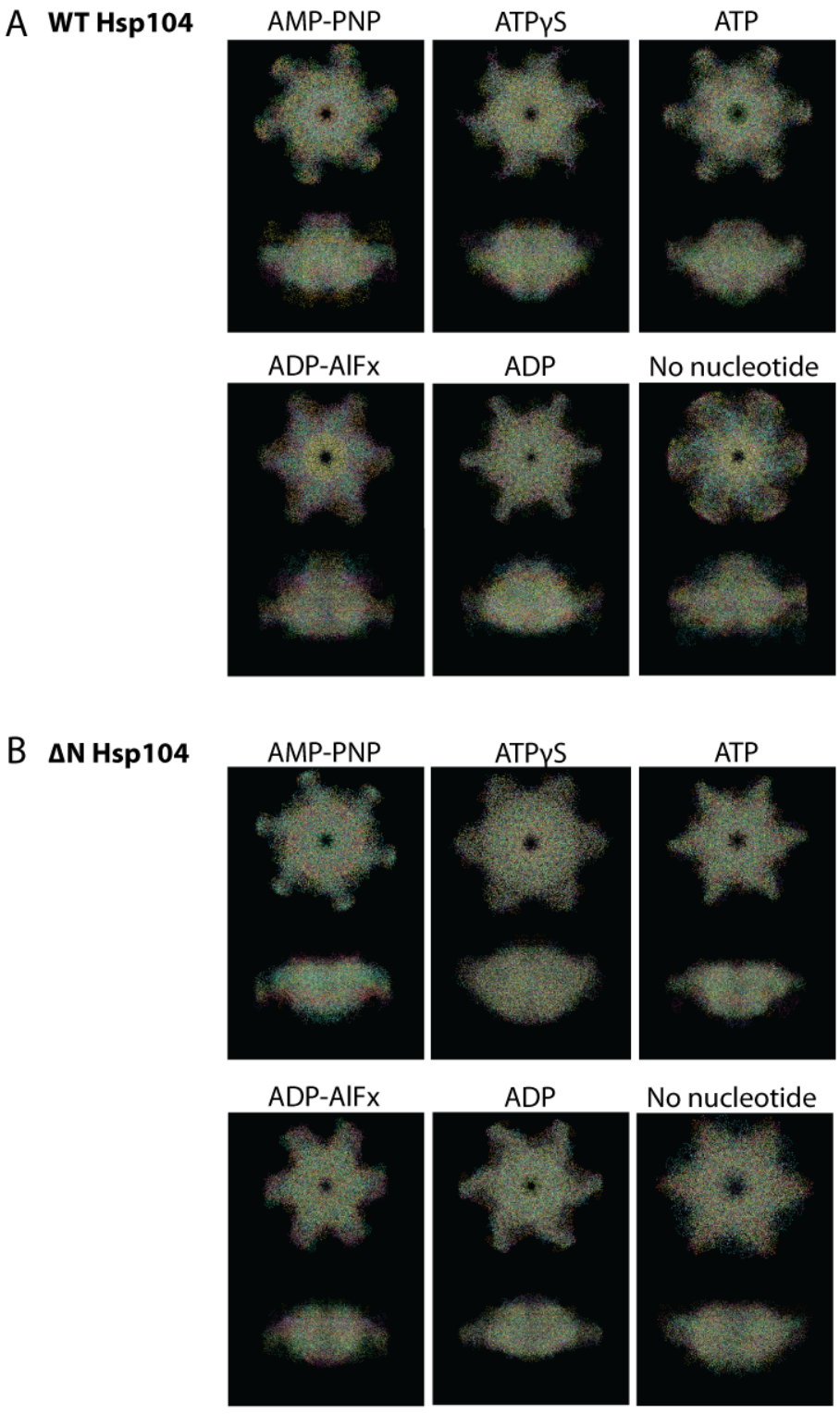

Figure 6. GASBOR replicates. Each GASBOR (Svergun 2001) model of A) WT and B) ΔN Hsp104 are overlaid to show agreement of the individual GASBOR solutions for each of the nucleotide states (AMP-PNP, ATPγS, ATP, ADP-AlF$_x$, ADP and no nucleotide).

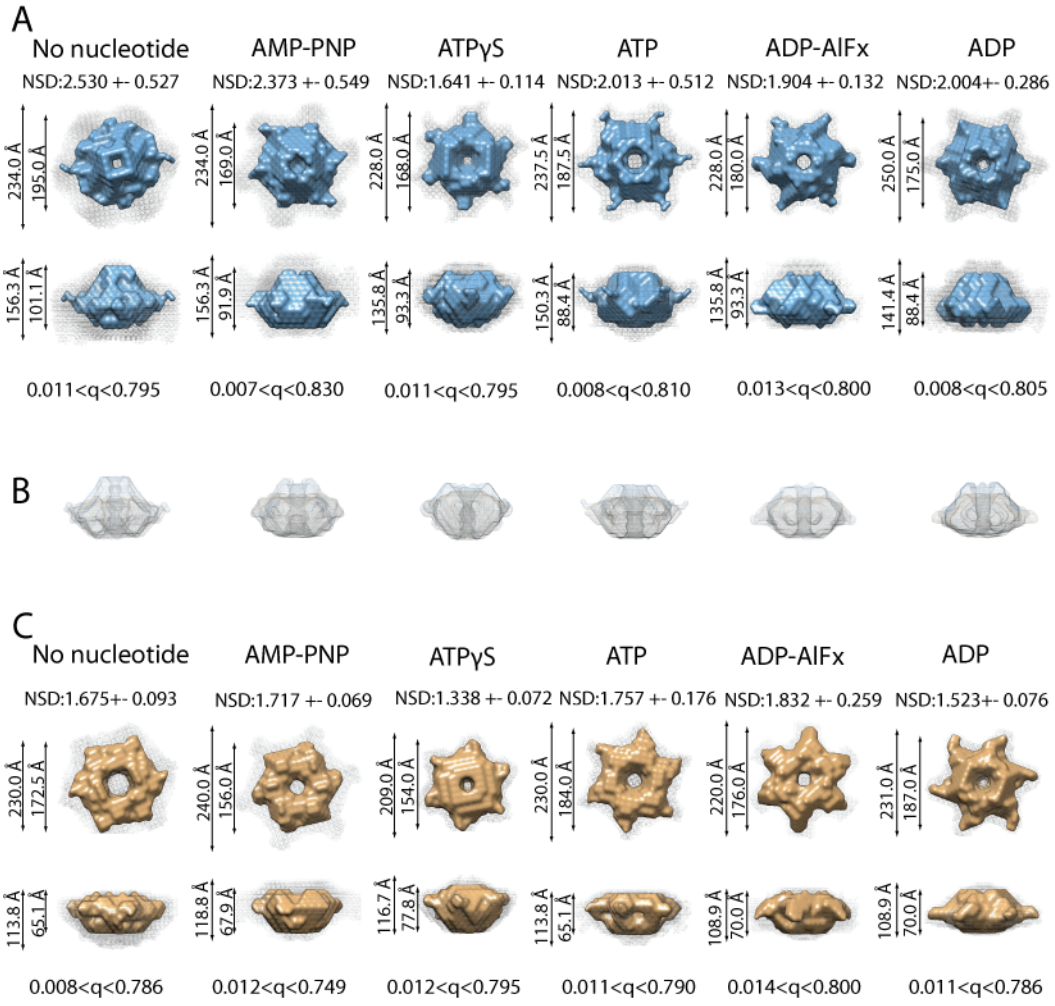

Figure 7. Volume envelope reconstructions from SAXS data. Averaged *ab initio* GASBOR (Svergun 2001) volume reconstructions of A) WT and C) ΔN Hsp104 from the SAXS data. Filtered density is solid blue (WT) or orange (ΔN) overlaid with the unfiltered average shown in gray mesh. Normalized spatial discrepancy (NSD) of the averaged models and the q range used for the reconstructions are shown along with average particle dimensions. B) Overlay of the WT and ΔN Hsp104 average reconstructions for each state, which was used to orient the particles. The Hsp104 hexamer undergoes large changes in shape dependent upon the identity of the nucleotide. Reconstructions are oriented with the N-terminus pointing toward the top of the page.

placement of a projection of external density. This projection is evident in the P(r) as well, as a population of large vectors evidenced by the P(r) tails that start around 175 Å, that represent a small amount of overall density (Figure 5). Both the WT and ΔN Hsp104 hexamers appear to have dynamic projections that travel from more N- to C- terminal positions through the simulated ATPase cycle (Figure 7A and C). The relatively large R_g and broadened P(r) curve of the ΔN Hsp104 hexamer in the absence of nucleotide is explained by the expanded cavity as seen by the view down the center of the reconstruction (Figure 7C).

Being able to visualize the average shape of the hexamers in each nucleotide state allows us to define how the particle changes through the nucleotide cycle. However, we know that the remodeling activity of Hsp104 is dependent upon translocation of substrate either fully or partially, through the central pore of the hexamer [167]. To understand how the central channel changes through the ATPase cycle we reconstructed the volume of the channel from the averaged GASBOR reconstructions (Figure 8). The average diameter of the channel reconstructions, N- C- terminally, are shown as bar graphs in Figure 8A (for WT) and Figure 8B (for ΔN). Each bar represents one angstrom, and the number of bars represents the length of the channel that is closed for 360 degrees. The motions of the WT Hsp104 channel are highly reminiscent of a peristaltic wave (Figure 8A). In a peristaltic wave there is a relaxation at the site of substrate entrance, followed by a wave of constriction that travels in the direction the substrate is being pumped . Experiments have shown that substrate enters N-terminally and can be fully translocated out the C-terminal end of the channel [111]. In the ATPγS/ATP states, when the hexamer is capable of binding substrate, the extreme N-terminal side is open (Figure 8A). After the opening there is a region of constriction, still N-terminal (Figure 8A, arrow). As we step through the simulated ATPase cycle, the channel first constricts fully, correlating with the smallest R_g, in the ADP-AlF_x transition state mimic, and then the point of constriction moves toward the C-terminus in the ADP state (Figure 8A). This peristaltic pumping motion, similar to how an esophagus moves food boluses, explains how the Hsp104 hexamer is able to transduce energy from ATP hydrolysis to conformational change and substrate remodeling using physical force.

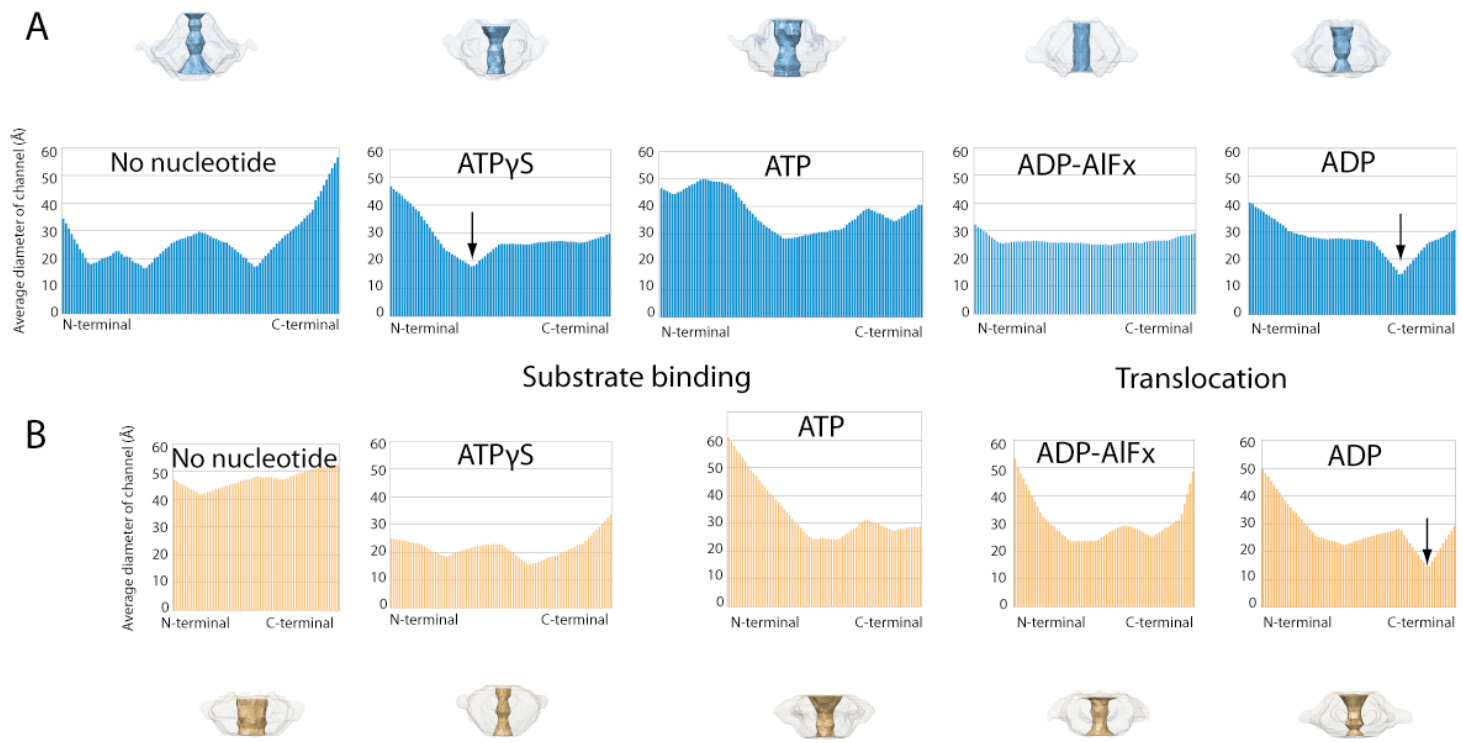

Figure 8. Channel motions of the Hsp104 hexamer. Mapping of the A) WT and B) ΔN Hsp104 hexamer channels. The volume of the channel was reconstructed in Chimera (Pettersen 2004) using the filtered average volumes for each nucleotide state. The bar graphs display the average diameter of each z slice of the channel volume starting from the N-terminus as calculated using Matlab. Substrate binds in the ATPγS/ATP states of the hexamer and translocation occurs from the N to C-termini. The WT Hsp104 channel displays a peristaltic wave motion; relaxation at the N-terminal region followed by a contraction of the entire channel and finally a shift in the location of a constriction from the N to C- terminal region. The ΔN Hsp104 hexamer channel displays defects in the peristalsis motion, especially in the N-terminal region, which appears to fail to fully contract. This defect is most notable in the transition state analog, ADP-AlFx. Arrows denote constricted regions of the hexamer channel.

The role of the NTD in facilitating the peristaltic pump motion is both simple and significant. It becomes clear looking at the channel reconstructions why, in the absence of nucleotide, the ΔN Hsp104 hexamer is expanded (Figure 8B). In the absence of nucleotide, in the WT Hsp104 channel, the N-terminal region is contracted and the entire assembly elongated and open on the C-terminal end (Figure 8A). In the absence of the NTD the channel is unable to contract, rather, the entire hexamer is smaller in the N- to C-terminal direction, and the channel appears to have a uniformly large diameter throughout (Figure 8B). As the ΔN Hsp104 channel progresses through the ATPase cycle, it is clear that the missing domain is essential for the proper movements of the channel. This defect is most obvious in the transition state mimic ADP-AlF_x, which is constricted in the center but open on both sides (Figure 8B). While there still appears to be an area of contraction that shifts N to C-terminally, it is clear that the peristaltic motion is greatly perturbed in the ΔN hexamer (Figure 8B). Specifically, it appears that substrate could more readily diffuse out of the N-terminal opening of the channel of the ΔN Hsp104 hexamer.

Our SAXS/WAXS findings indicate that deletion of the NTD results in expansion of the ends of the central cavity (similar to a cryo-EM study of the ΔN Hsp104 hexamer [136]), as well as abnormal changes of the central channel during the ATPase cycle (Figure 8). Since ΔN Hsp104 is unable to undergo nucleotide-dependent changes in the central channel similar to WT Hsp104, we hypothesized that these structural defects may result in a diminished ability to translocate substrate through the Hsp104 hexameric channel.

2.2.5 Deletion of the HAP NTD results in an increase in Km, and a decrease in Vmax for casein degradation

To determine whether ΔN Hsp104 had a translocation defect as implied by the SAXS/WAXS data we determined a Km and Vmax of casein degradation (Figure 9A) for both the full length and ΔN versions of HAP. HAP is an Hsp104 mutant (739-GSK-741 to 739-IGF-741) that is able to interact with the chambered peptidase ClpP [111]. HAP and ΔN HAP retain ATPase

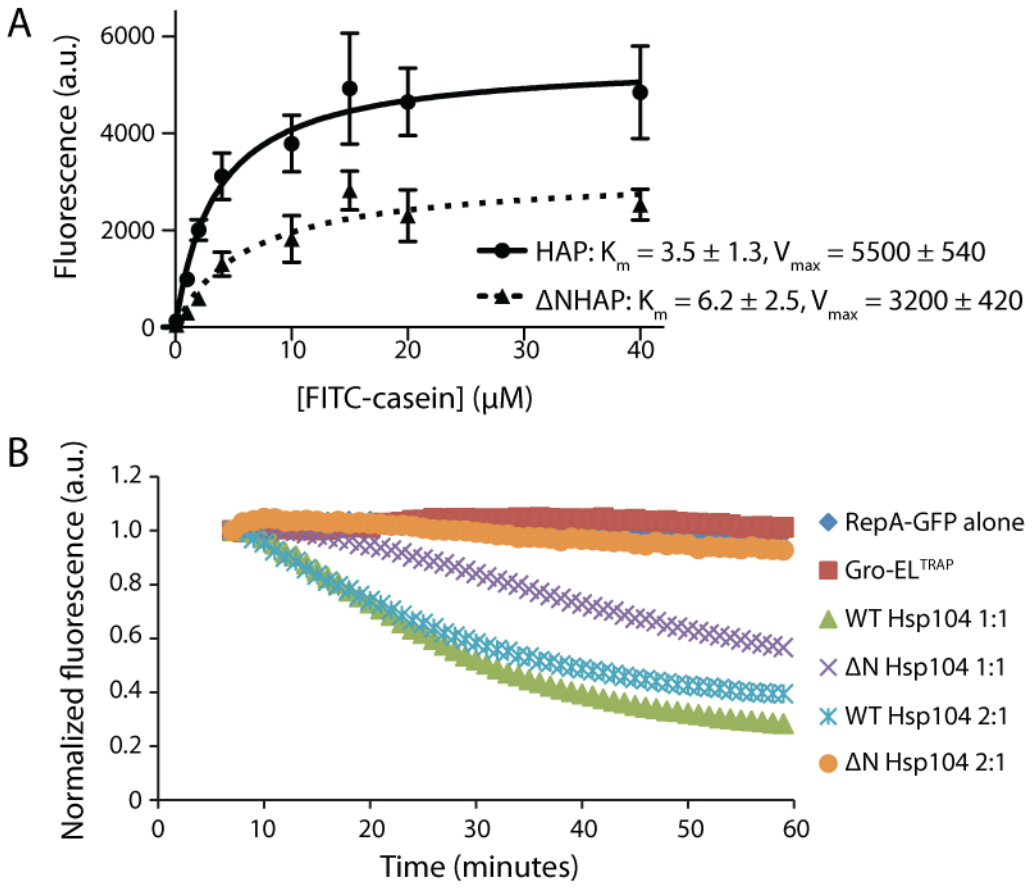

Figure 9. The N-terminal domain is necessary for robust substrate translocation and unfolding activity. A) Translocase activity was measured using FITC-casein (100 nM-40 μM) incubated for 60 minutes at 25˚C with HAP or ΔNHAP (1 μM), ClpP (21 μM monomer), 5.1 μM ATP and an ATP regenerating system. HAP or ΔNHAP translocate casein into ClpP for degradation. Degradation of FITC-casein was monitored by measuring fluorescence of free FITC. K_m and V_{max} were calculated by fitting the curves to Michaelis-Menten kinetics. Values represent mean ± S.E. (n=5). HAP and ΔNHAP values are statistically different, with $p < 0.05$ for K_m and V_{max}. Unfoldase activity was measured using a $RepA_{1-70}$-GFP assay. B) Displays a representative $RepA_{1-70}$-GFP unfolding curve. Unfolding of GFP was monitored by the decrease in fluorescence over time of $RepA_{1-70}$-GFP (0.7 μM) in the presence of Gro-EL^{TRAP} (1.5 μM), WT or ΔN Hsp104 (1 μM), either 2.6 mM ATP and 2.5 mM ATPγS (1:1) or 3.43 mM ATP and 1.67 mM ATPγS (2:1) and an ATP regenerating system.

activity that is indistinguishable from WT and ΔN Hsp104 respectively (Figure 2A). In the presence of ClpP, substrates that are translocated through the Hsp104 variant HAP are degraded rather than released [111]. Therefore, using FITC-casein as a substrate we are able to assess translocation efficiency by monitoring increases in FITC fluorescence as a proxy for casein degradation, as FITC-casein is translocated and degraded, FITC is released. The ΔN HAP variant displayed an increased Km as well as a reduced Vmax (Figure 9A), revealing that it is a less effective translocase as predicted from the SAXS/WAXS data.

2.2.6 Deletion of the NTD results in a defect in substrate unfolding

Next we wanted to ascertain whether ΔN Hsp104 also displayed a defect in substrate unfolding. To assess unfoldase activity we used a $RepA_{1-70}$-GFP unfolding assay [113], where decreases in fluorescence are used to measure GFP unfolding. To track unfolding of our $RepA_{1-70}$-GFP substrate in the absence of subsequent refolding, we added $GroEL^{TRAP}$ [203], which captures the unfolded $RepA_{1-70}$-GFP and prevents it from refolding [203]. By using permissive ratios of ATP:ATPγS we see that WT Hsp104 robustly unfolds the $RepA_{1-70}$-GFP substrate (Figure 9B and C). WT unfolding activity is strongest with a 1:1 ATP:ATPγS, but remains strong at a 2:1 ratio (Figure 9B and C). In contrast, ΔN Hsp104 has partial $RepA_{1-70}$-GFP unfoldase activity at a 1:1 ATP:ATPγS, but is unable to unfold $RepA_{1-70}$-GFP at a ratio of 2:1 ATP:ATPγS (Figure 9B and C). This result indicates 1) that ΔN Hsp104 retains some, but not WT levels of unfoldase activity, and 2) Hsp104 unfoldase activity is more sensitive to changes in ATP:ATPγS than luciferase reactivation is (Figures 2B and 9B), indicating that productive disaggregation of disordered luciferase aggregates makes different demands on the Hsp104 hexamer than full substrate unfolding.

2.2.7 The NTD of Hsp104 is essential for hexamer cooperativity

Recent work in our lab revealed that WT Hsp104 employs different degrees of intersubunit coordination to remodel disordered aggregates versus amyloid aggregates [132]. Dissolution of disordered aggregates does not require global cooperativity (i.e., all subunits binding substrate and hydrolyzing ATP in concert, or in a specific order), rather, non-cooperative probabilistic substrate binding and ATP hydrolysis are sufficient (i.e., subunits binding substrate and hydrolyzing ATP independently of each other) [132]. In contrast, dissolution of amyloid aggregates requires global cooperativity of the hexamer subunits [132], and Hsp104 hexamers that contained subunits with defects in cooperativity were unable to remodel amyloid substrates [132]. Since ΔN Hsp104 is also unable to remodel amyloid substrates (Figure 1), displays defects in ATPase regulation (Figure 2A), and is unable to undergo conformational changes reminiscent of the WT Hsp104 hexamer (Figure 8), we hypothesized that the NTD may be necessary for hexamer cooperativity.

To test this hypothesis, we used a mutant subunit doping strategy [132]. Hsp104 subunits with specific defects (such as ATP binding or hydrolysis) are mixed with WT, or in our case, ΔN subunits, to generate ensembles of heterohexamers. Incorporation of the mutant subunits to create heterohexamer ensembles occurs according to a binomial distribution dependent upon the ratio of WT:mutant [132] (Figure 10A). Since the heterohexamers assemble based on a binomial distribution, and the Hsp104 mutants retain no activity on their own, theoretical activities for each ratio of WT:mutant can be determined based on the fraction of each type of heterohexamer present at each WT:mutant ratio, and how many active subunits are required for activity [132] (Figure 10B). If cooperativity is dispensable for activity, then only one WT subunit per hexamer is required, and a linear decrease in activity would be expected [132] (Figure 10B, orange line). If global cooperativity is required, a steep decline in activity would be expected [132] (Figure 8B, blue line), and if some form of sub-global cooperativity (i.e., more than one but less than six

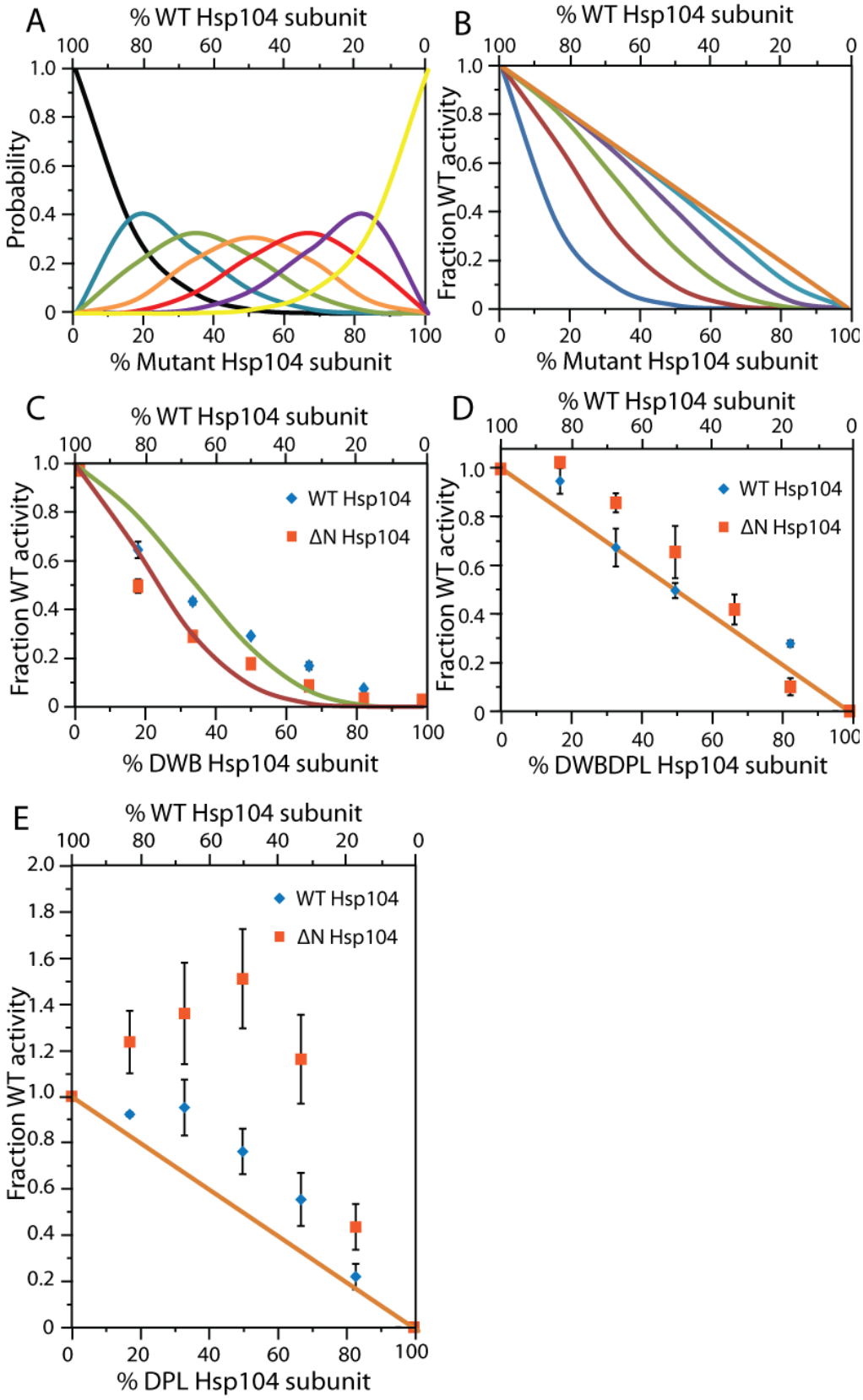
A
% WT Hsp104 subunit
100 80 60 40 20 0
Probability
1.0 0.8 0.6 0.4 0.2 0
0 20 40 60 80 100
% Mutant Hsp104 subunit
B
% WT Hsp104 subunit
100 80 60 40 20 0
Fraction WT activity
1.0 0.8 0.6 0.4 0.2 0
0 20 40 60 80 100
% Mutant Hsp104 subunit
C
% WT Hsp104 subunit
100 80 60 40 20 0
Fraction WT activity
1.0 0.8 0.6 0.4 0.2 0
WT Hsp104
ΔN Hsp104
0 20 40 60 80 100
% DWB Hsp104 subunit
D
% WT Hsp104 subunit
100 80 60 40 20 0
Fraction WT activity
1.0 0.8 0.6 0.4 0.2 0
WT Hsp104
ΔN Hsp104
0 20 40 60 80 100
% DWBDPL Hsp104 subunit
E
% WT Hsp104 subunit
100 80 60 40 20 0
Fraction WT activity
2.0 1.8 1.6 1.4 1.2 1.0 0.8 0.6 0.4 0.2 0
WT Hsp104
ΔN Hsp104
0 20 40 60 80 100
% DPL Hsp104 subunit

Figure 10. Hsp104 N-terminal domain is essential for productive hexamer cooperativity. A) Theoretical ensembles of Hsp104 hexamers containing zero (black), one (blue), two (green), three (orange), four (red), five (purple), or six mutant subunits (yellow) as a function of the percent of mutant subunit present. B) Theoretical activity curves for heterohexamer ensembles when six (blue), five (red), four (green), three (purple), two (light blue), or one WT subunits (orange) are needed for hexamer activity. C-E) Urea-denatured luciferase aggregates were incubated for 90 min at 25˚C with WT (blue) or ΔN (orange) Hsp104 (1 μM), Hsp72 (1 μM), Hdj2 (1 μM), 5.1 mM ATP, an ATP regenerating system (1 mM creatine phosphate, 0.25 μM creatine kinase) plus increasing percentages of C), DWB Hsp104 D), DWBDPL Hsp104 or E) DPL Hsp104. Luciferase reactivation was then assessed by measuring luminescence and plotted as fraction of WT Hsp104 activity. Values represent means ± SEM (n = 3–4). Theoretical disaggregase activity if one (orange line [D and E]), four (green line [C]), or five (red line [C]) WT Hsp104 subunits are needed for activity.

subunits binding substrate or hydrolyzing ATP cooperatively) were required, an intermediate curve [132] (Figure 10B) would be expected. For our doping experiments we used the full-length WT Hsp104 with mutants in the full-length background, as well as ΔN Hsp104 and mutants in the ΔN Hsp104 background. The mutants we used were double Walker B (DWB, E285Q:E287Q) which can bind, but not hydrolyze ATP, double pore loop (DPL, Y257A:Y662A) which is defective in substrate binding [204], and the combination mutant, DWBDPL (E285Q:E287Q:Y257A:Y662A) which cannot hydrolyze ATP or bind substrate. In doping experiments with DWB or DWBDPL, we saw that ΔN Hsp104 behaved similarly to WT Hsp104 (Figure 10C and D). Luciferase reactivation was very sensitive to DWB subunits, ~5-6 WT/ΔN subunits per hexamer are necessary for activity (Figure 10C). By contrast, luciferase reactivation was much less sensitive to DWBDPL subunits, and luciferase reactivation required only one functional subunit per hexamer (Figure 10D). These findings indicate that defects in ATP hydrolysis are tolerated as long as the subunits defective in hydrolysis do not bind substrate (the DWB variant has been described as a substrate 'trap' [161], since substrate binds in the ATP state, and therefore substrate would be prevented from translocating through the Hsp104 channel if some subunits were bound to ATP as well as substrate). It also tells us that even though ΔN Hsp104 displays deregulated ATPase activity, it behaves similarly to WT Hsp104 in response to the addition of ATPase-dead subunits. We

obtained very different results with the DPL subunits, which are defective in substrate binding. When we doped these subunits into the ΔN and full length WT Hsp104, we found that in the absence of the NTD results in a dramatic enhancement of activity in the presence of the DPL subunits (Figure 10E). This finding implies that in the absence of the NTD the Hsp104 subunits are behaving in a negatively cooperative manner in respect to substrate binding. This finding suggests that the NTD is essential for productive cooperativity of the Hsp104 hexamer, a finding strongly supported by the defects in the conformational changes seen in the SAXS/WAXS data (Figures 5, 7 and 8).

2.2.8 Intersubunit cooperativity mediated by the NTD is essential for potentiation of the Hsp104 hexamer

Through random mutagenesis our lab has discovered Hsp104 mutants that are potentiated and capable of remodeling diverse substrates involved in human proteinopathies that are intractable to WT Hsp104 [179]. These mutations, in motif 2 of the middle domain (MD), appear to relieve autoinhibition of the hexamer and display increased activity in a variety of *in vitro* assays as well as suppressing toxicity of human disease associated proteins in both *S. cerevisiae* and *C. elegans* [179]. We decided to test whether these potentiating mutations (A503S and A503V) could overcome the defects in cooperativity of ΔN Hsp104. We found that in the ΔN Hsp104 background the potentiating mutations were unable to suppress toxicity of TDP-43, FUS (TDP-43 and FUS are connected to amyotrophic lateral sclerosis [205]), or α-synuclein (α-synuclein is connected to Parkinson's disease [206]) (Meredith Jackrel, Figure 11A-C). Since we know that global cooperativity is required for remodeling amyloid substrates [132], and that TDP-43, FUS and α-synuclein form highly recalcitrant aggregates, this finding provides further evidence that the NTD is essential for global cooperativity of the Hsp104 hexamer. Further, it would appear that cooperativity of the hexamer trumps potentiation conveyed through these missense mutations.

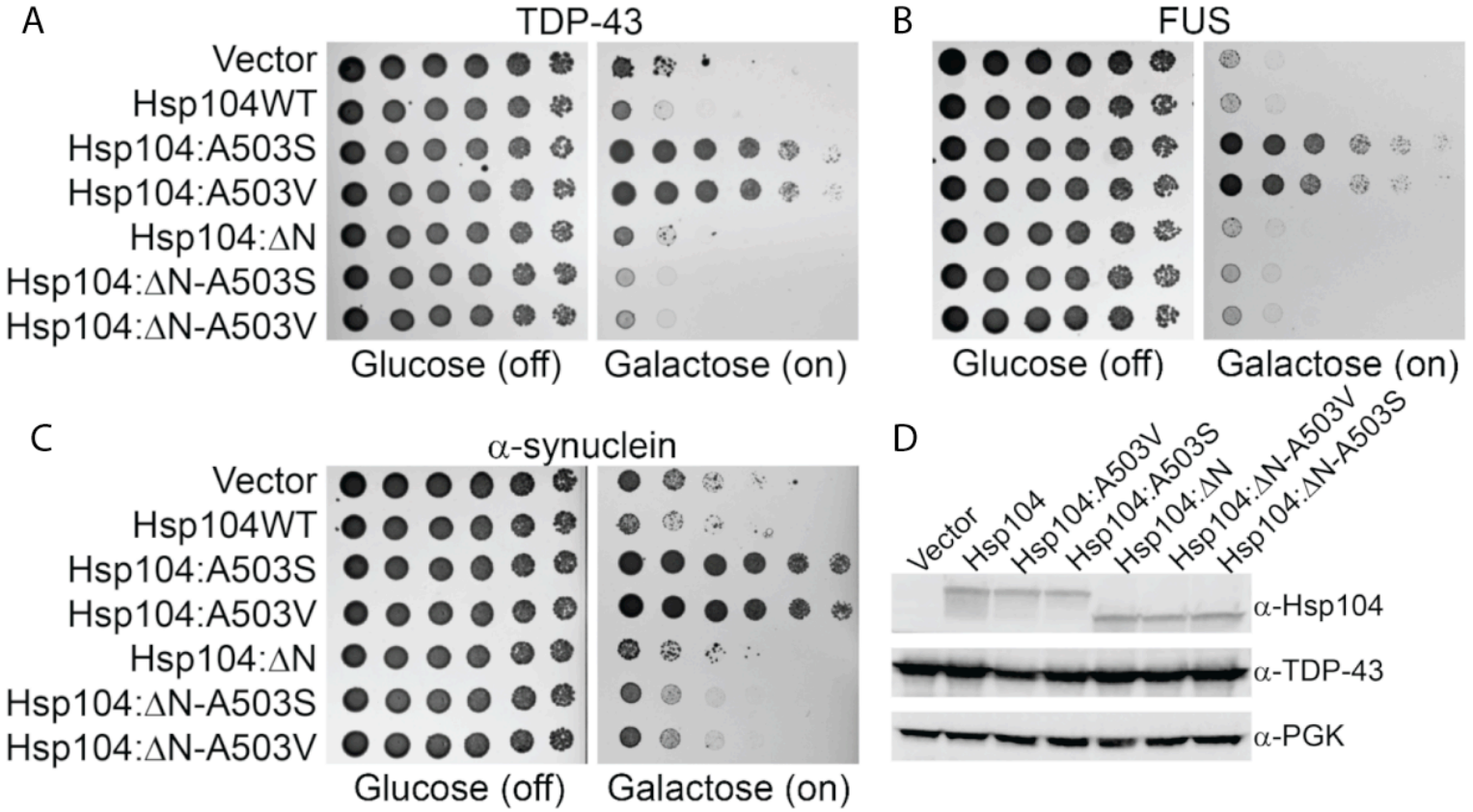

Figure 11. The N-terminal domain is required for hyperactivation of the hexamer. A-C) *Δhsp104* yeast strains integrated with galactose-inducible A) TDP-43 B), FUS, or C) α-synuclein, were transformed with the vector control or Hsp104 variant indicated. The strains were then spotted in a 5-fold dilution series on glucose (off) or galactose (on) media. D) Strains from A) were induced for 5 hr, lysed, and immunoblotted for Hsp104 and the disease protein TDP-43. 3-Phosphoglycerate kinase (PGK1) is a loading control. (Work of Dr. Meredith Jackrel, Shorter lab)

2.3 Conclusions

We have found that the Hsp104 NTD is necessary for nucleotide-dependent conformational changes that allow productive hexamer cooperativity. While cooperativity is dispensable for disordered aggregate dissolution, it is necessary for robust and adaptable hexamer function. This deficiency in hexamer cooperativity due to defects in conformational changes results in a deregulated ATPase rate, diminished unfoldase and translocase activity, and an inability to remodel exceptionally stable substrates such as amyloid, even in the presence of potentiating mutations. This role in global cooperativity is unexpected and novel for an Hsp100 NTD, and if unique to Hsp104 could explain why amyloid substrate remodeling has only been observed with Hsp104 and not its bacterial homologue ClpB.

Chapter 3: X-ray footprinting (XF) as a probe of Hsp104 solvation

3.1 XF introduction

The functional Hsp104 hexamer is large and highly dynamic with an expansive, solvent filled channel running the length of the macromolecule [136, 171]. In response to nucleotide binding and hydrolysis, the hexamer undergoes substantial changes in conformation [137, 176]. These changes in conformation are coupled to remodeling diverse substrates, from thermally-denatured aggregates [110] to amyloid conformers [20, 81, 113]. To understand the details of these conformational changes and how they may be driving substrate remodeling, a clearer picture of Hsp104 structure and dynamics is necessary. Hsp104 is too large for NMR analysis and has been refractory to crystallization attempts, therefore high-resolution structural information is lacking. The bacterial homologue tClpB has been crystallized, but as a monomer [102]. Two hexameric models have been proposed, based on rigid body fits of homology-modeled Hsp104 into cryo-EM maps [136, 171]. However, the models disagree dramatically, and dynamics of the hexamer have been poorly defined. Elucidating details about the hexameric Hsp104 and how it changes in response to nucleotide is important to understanding how these changes mediate substrate remodeling.

We aimed to use a hybrid approach to learn structural and mechanistic details of the Hsp104 hexamer. By combining homology modeling of the individual domains, volume information from small angle x-ray scattering, crosslinking and mutational analysis, secondary structure information from hydrogen-deuterium exchange and solvation information from x-ray footprinting, we aimed to develop structural and mechanistic models that can explain observations from the literature as well as allow us to predict novel mechanistic details that can be tested biochemically. Central to our approach is the information garnered from synchrotron x-ray footprinting experiments. X-ray footprinting is a technique that probes the solvent accessibility of the side-chains of a protein [207-209]. This allows for the identification of regions that are involved in conformational changes and protein-protein interactions [207-209].

Synchrotron x-ray footprinting uses millisecond bursts of high-flux x-rays to produce large amounts of hydroxyl radicals through the radiolysis of water [207, 210]. Hydroxyl radicals are ideal footprinting reagents because of their similarity to water molecules, making them excellent probes for solvation, and their high and well-characterized reactivity with 19 of the 20 of the amino acid side chains [207, 211, 212] (excluding glycine). Once hydroxyl radical-mediated footprinting has been carried out on a protein sample, the oxidized products can be detected using quantitative liquid-chromatography-coupled mass spectrometry [211, 213] (Figure 1). Identification of the reaction products can be achieved using methods based on hydrogen-deuterium (HD) exchange analyses [214, 215]. The abundance of unmodified and oxidatively modified versions of a peptide is used to calculate the fraction unmodified [207, 208, 216] (Figure 1). For any given peptide, there can be a number of different modified versions, since each residue can undergo different modifications, and different side chains on the same peptide may be modified [207, 212, 213]. All singly modified peptides are quantified and added to the sum of modified peptide [207, 208, 213]. Peptides that have more than one modification are not included in the sum, as they may represent solvation-independent oxidation which can occur after the initial, solvent-dependent modifications [211, 217]. The fraction unmodified for each identified peptide is determined for a number of millisecond time points (Figure 1). The rate of hydroxyl radical-mediated oxidative modification of each peptide is determined by fitting the dose response curve to a first order decay [208, 213, 216] (Figure 1). At the longest timepoints deviation from the curve indicates solvation-independent over-oxidation and therefore must be removed from the fit [213]. MS2 data can be used to identify specific residues that are modified. There are also a few modifications that can only occur on specific residues, although the majority of modifications, +16 and +14, can occur on 18 and 8 of the 20 amino acids respectively [212, 213]. Modification rates of peptides can be compared across samples by using a normalization factor [218, 219]. The normalization factor is determined by measuring the x-ray dose dependent oxidation and decay of a fluorescent dye, Alexa488 in each of the sample conditions [218].

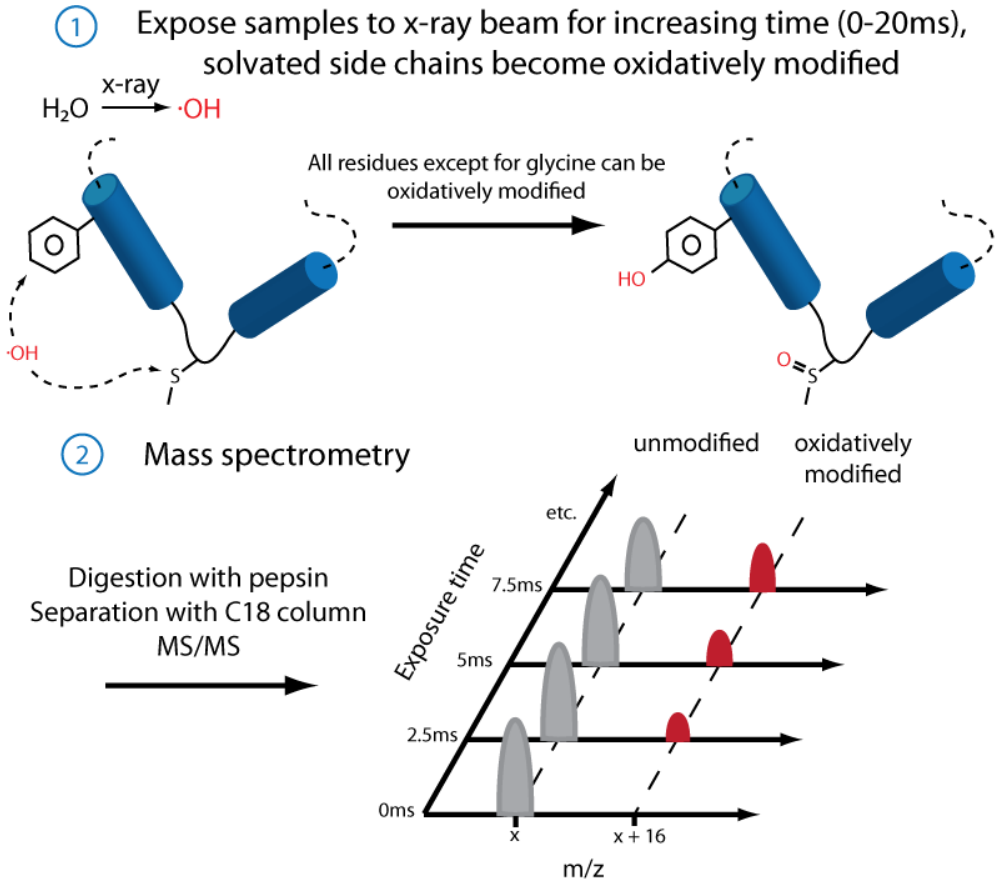

Figure 1. Schematic for synchrotron x-ray footprinting. 1) Using a stopped flow device protein sample is exposed to millisecond doses of synchrotron x-rays which react with water to form hydroxyl radicals. The hydroxyl radicals react with protein side chains. After exposure oxidation is quenched and the samples are frozen. 2) Samples are digested with pepsin, separated using a C18 column and analyzed using MS/MS. Unmodified and oxidatively modified versions of peptides are identified. 3) For each timepoint the fraction unmodified is calculated by dividing the intensity of the unmodified peptide by the sum of all the unmodified and modified versions of the peptide. The fraction unmodified over time can then be fit to a first order exponential decay to give the rate of modification.

In this study we present the hydroxyl radical footprinting of Hsp104 in three states: monomer, hexamer with ADP and hexamer with ATPγS. We used pepsin proteolysis and mass spectrometry followed by peptide analysis using a modified version of an HX processing program called ExMS-CL [220]. We used homology modeled Hsp104 domains, based off the tClpB crystal structure [102], as a foundation for our examination of the solvation state of each domain in different nucleotide bound states (see Figure 2 for rigid body fits into the SAXS/WAXS envelope). Our solvation results allowed us to explain phenomena reported in the literature, to make testable predictions about the role different regions play in Hsp104 structure and activity and to make a new mechanistic model of how conformational changes are coupled to substrate remodeling.

3.2 Results

3.2.1 Experimental logic

Samples of the Hsp104 monomer and the Hsp104 hexamer in the presence of either ADP or ATPγS were exposed to millisecond bursts of synchrotron x-rays and immediately quenched as described in the methods. On this timescale of hydroxyl radical exposure, the main reaction products are oxidative modification of the side-chains rather than backbone cleavage or crosslinking [212, 216]. Using a pepsin column, followed by separation with a C18 column, Hsp104 peptides were injected into a mass spectrometer as described in methods. Using a modified version of ExMS [220], an unmodified pool of peptides for each Hsp104 state was created from four 0 ms timepoint MS/MS runs. Using this unmodified pool, ExMS-CL was used to search for modified versions of the peptides. The possible modifications vary by amino acid but have been well characterized [207, 211, 212]. ExMS-CL uses the primary oxidation products for each amino acid published by Kaur, Kiselar and Chance [213]. Each timepoint (2.5, 5, 7.5, 10, and 20 ms) was run through MS/MS in triplicate. Using the identification of modified and unmodified peptides by ExMS-CL and their intensities, Matlab was used to determine the fraction unmodified for each of the three MS/MS runs for each of the samples timepoints. Only singly

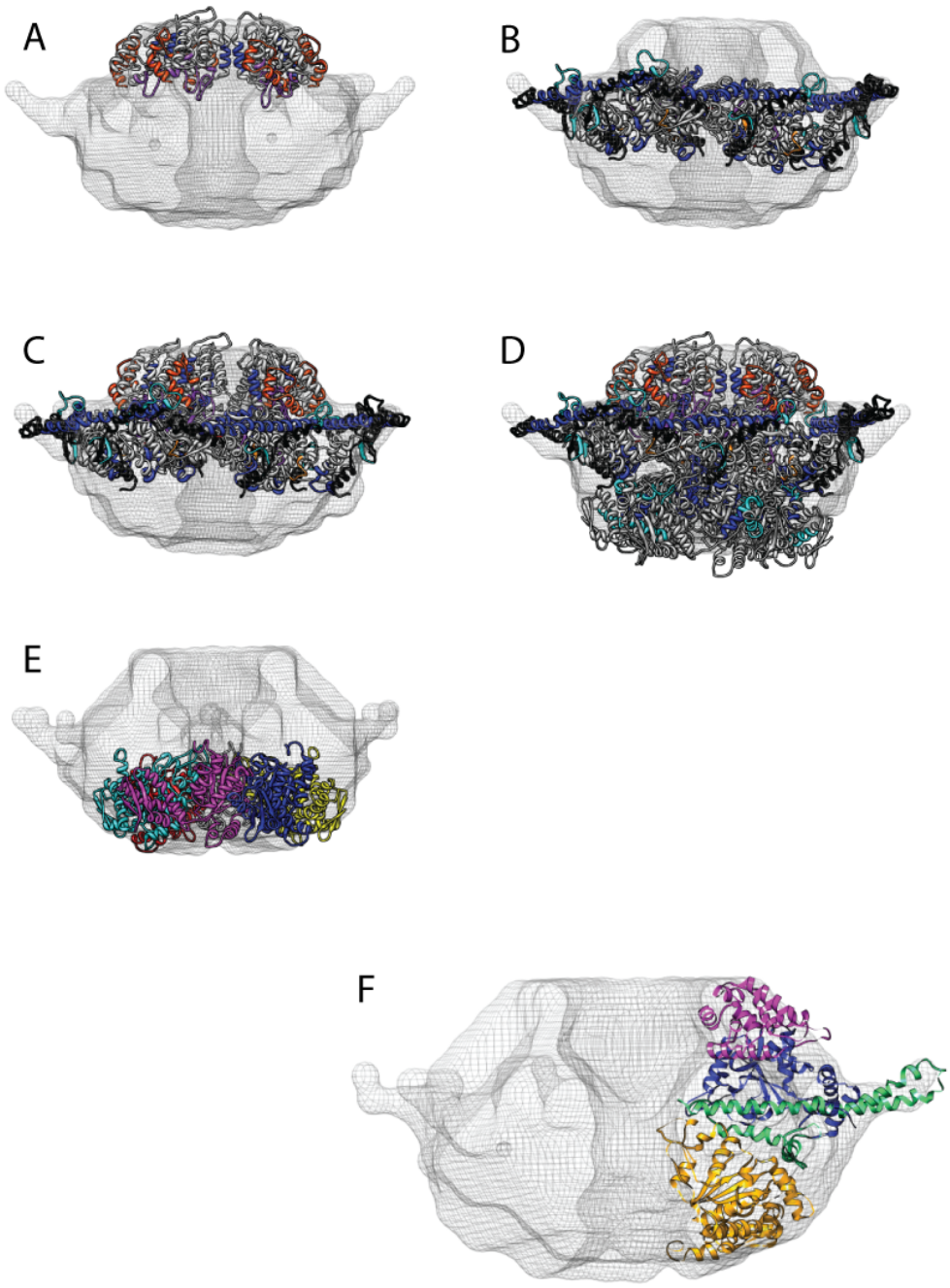

Figure 2. Rigid body fitting into a SAXS/WAXS volume reconstruction. Individual Hsp104 domains were homology modeled based on the ClpB crystal structures 1khy (N terminal domain, NTD) and 1qvr (for nucleotide binding domain 1, NBD1, the middle domain, MD, and nucleotide binding domain 2, NBD2). The domains were then rigid-body fit into the volume envelope generated from SAXS/WAXS data of the Hsp104 hexamer in the presence of ATP. A) Six NTDs, B) six NBD1s and six MDs C) six NTDs, six NBD1s and six MDs, and D) six copies of each domain are fit into the SAXS/WAXS volume envelope. E) Six NBD2 domains are fit into the SAXS/WAXS volume envelope. F) An Hsp104 monomer is shown in the SAXS/WAXS volume density.

modified versions of the peptides were used, as further modification is likely to be solvent-independent [211, 217]. Additionally, there are often more than one version of the modified peptide, due to the possibility of multiple types of modification occurring to any given residue, as well as the ability of many residues within a peptide to become modified (e.g. an entire loop may be exposed to solvent and contain several residues with approximately equal reactivities, and each of these can undergo multiple reactions resulting in products of different masses) [207, 212, 213]. Which modification takes place, and which residue it takes place upon, is to some degree determined stochastically [207, 212, 213]. To circumvent these concerns, each example of the modified peptide was summed and added to the modified pool when calculating the fraction unmodified using Matlab. For each timepoint, these values were averaged together and the standard error determined. Each peptide was binned into one of three categories by the Matlab program; no time-dependent modification, sporadic modification, and time-dependent modification. For the peptides that displayed time-dependent modification, the program used the first four timepoints (0, 2.5, 5, and 7.5 ms) to determine the rate of modification by fitting to a first order exponential decay. The earliest timepoints were used due to evidence of over-oxidation in many of the 10 and 20 ms timepoints. Each of the fits was visually checked and manually refitted using Origin 8.1 when the Matlab program failed to converge onto a visually accurate fit to the data. If manual re-fitting of the curve was impossible, often due to low signal-to-noise, the peptide was discarded. There was background modification of many of the peptides, and most of the sporadically modified peptides when examined manually, did not appear to display any time-dependent modification. For those peptides that did display time-dependent modification but were classified as sporadically modified by the Matlab program, Origin 8.1 was used to manually fit the curve. In a few cases, there does appear to be time-dependent modification, however, a good fit to the data was impossible. In those cases the rate of modification is listed as not determined (ND).

To complement the solvation data from XF, we have also included HD exchange data generated by Alec Ricciuti in the Englander lab, biochemical data using a variety of techniques,

and an investigation of the mechanistic basis of mutation based on phenotypes found in the literature. Finally, we have used the data generated from our hybrid approach to understand local and global changes of the Hsp104 hexamer during the ATPase cycle and to build a model of how large conformational changes of the hexamer function to remodel substrate in an ATP-dependent manner.

3.2.2 Peptide overview

The monomer, hexamer with ADP, and hexamer with ATPγS have 339, 359 and 342 peptides found in all three replicates of all six timepoints, respectively (Table 1). 122 (monomer) 135 (ADP) and 78 (ATPγS) of those peptides showed time-dependent modification, although several had to be discarded because of irregularities, mostly due to the presence of methionine residues within the peptide, or poor signal to noise. After discarding suspect peptides we were left with 81 (monomer), 117 (ADP), and 54 (ATPγS) peptides that showed time-dependent modification that could be fit to a first order decay curve to yield rate information (Table 1). Tables 2, 3 and 4 list all of the filtered modified and unmodified peptides for the monomer, hexamer with ADP and hexamer with ATPγS, respectively. In instances where the modified peptide was selected for fragmentation and MS2 analysis, the identity of the specific site of modification was determined. The majority of identified peptides are unmodified. For an overall assessment of the general solvation state, the peptide with the highest rate of modification is used to describe the rate of modification for all amino acids contained on that peptide. This method of displaying the data will result in an overestimation of modification rate (and therefore solvation) but this overestimation will be consistent through and between the three states. This display method allows us to uncover large changes in solvation between the samples for a given region. For example, when peptides in one sample show no or very low modification - such as < 1 per second – while similar peptides in another state show very high rates of modification – such as > 50 per second. For a direct comparison of rates, we need to look at the rate information for the

Table 1: X-ray footprinting peptide summary. Peptides reported were identified using ExMS-CL, and found in all three replicates for each timepoint. Filtered peptides represent the peptides remaining after those that displayed irregularities were removed.

Sample	Peptides	Modified	Filtered modified	Final peptide count	Percent coverage
Monomer	339	122	81	259	90%
Hexamer with ADP	359	135	117	310	89%
Hexamer with ATPγS	342	78	54	269	88%

Table 2: Hsp104 peptides found in the monomer state. Peptides reported were identified using ExMS-CL, and found in all three replicates for each timepoint. Modification rates calculated using Matlab, and specific sites of modification are also listed.

Start	End	Modified residues (ID'd by MS2)	Modification rate (s^{-1})	Error
8	38		0.028	0.03700
8	39		0	
12	36		0	
12	38		0	
12	39		0	
14	38		0	
14	39		0	
16	36		0	
16	37		0	
16	38		0	
16	39		0	
17	36		28.1910	14.7120
17	38		0	
17	39		0	
18	36		5.13290	0.49692
18	38		0	
18	39		0	
22	38		0	
39	54		1.55530	0.16430
40	54		0.09956	0.03047
54	64		0	
55	64		0	
65	73		1.41090	0.12515
65	85	81	0.34331	0.00742
65	90		0	
65	98		0.75152	0.06122
73	85		0	
73	90		nd	
74	85	74,76,77	0.35975	0.04651
74	90		1.39000	0.43000
74	110		0.71446	0.45186
86	98	97	3.28770	0.27465
86	99		0	
86	110	87,88,90,91,95,96,100,101,104,108	0.80289	0.35492
91	98		0	
91	110		0	
92	110		0	
94	110		0.45903	0.12619
99	110		1.04650	0.54010
119	128	121	9.82930	0.69402
119	130		0	
119	132		0	
119	134		0	

Table 2: Hsp104 peptides found in the monomer state. Peptides reported were identified using ExMS-CL, and found in all three replicates for each timepoint. Modification rates calculated using Matlab, and specific sites of modification are also listed.

Start	End	Modified residues (ID'd by MS2)	Modification rate (s^{-1})	Error
119	135		0	
119	136		0	
119	138		0	
119	139		0	
120	130		0	
121	132		54.3580	23.8680
121	134		0	
121	135	134	2.45180	1.88490
121	136		0	
121	138		0	
121	139		0	
122	130		0	
122	138		0	
122	139		0	
129	136	131,132,135	58.2380	31.1270
129	139		0	
146	166		0	
148	166		0.21532	0.01415
166	173		0	
167	173		9.22380	0.44315
167	174		0	
175	190		0	
175	192		0.33606	0.03790
175	200		0	
192	200		0	
211	221	219	1.27000	0.67000
211	223		0	
211	224		0	
211	226		0	
211	227		0	
211	231		0	
211	238		0	
211	243		0	
225	243		15.90000	11.23000
227	243		0	
228	243		0	
244	261		0	
244	271		31.29100	6.06930
248	261		0	
249	261		0	
249	262		0	
249	263		0	
249	269	252	1.07270	0.12336

Table 2: Hsp104 peptides found in the monomer state. Peptides reported were identified using ExMS-CL, and found in all three replicates for each timepoint. Modification rates calculated using Matlab, and specific sites of modification are also listed.

Start	End	Modified residues (ID'd by MS2)	Modification rate (s^{-1})	Error
249	277		0	
249	278		2.44960	0.36993
249	281		0	
251	261		0	
262	269		0	
262	277		0	
262	278		2.70020	0.01221
270	277		0	
282	295		0	
300	310		0	
300	320		nd	
300	331		0	
306	320		0	
311	320		nd	
311	321		0	
321	330		0	
321	331	321	0.66927	0.20251
331	350		0	
331	352		0	
332	349		2.36770	0.29395
332	350		0	
332	352	333,334	nd	
343	352		0	
351	372		0	
353	368		18.24000	9.56000
353	369		11.24100	0.57337
353	371		0	
353	372		0	
360	372	362,365,369	46.79800	0.60671
379	393		2.24130	0.16359
398	414		2.36260	0.47969
401	414		0.24421	0.09590
401	423		10.04000	2.68910
401	425		4.56000	2.51000
403	414		0.40740	0.31957
403	423		0	
405	423		0	
415	425		0	
424	447		0.22000	0.19000
424	455		0	
426	455		0	
427	447		0	
428	447		0	

Table 2: Hsp104 peptides found in the monomer state. Peptides reported were identified using ExMS-CL, and found in all three replicates for each timepoint. Modification rates calculated using Matlab, and specific sites of modification are also listed.

Start	End	Modified residues (ID'd by MS2)	Modification rate (s^{-1})	Error
431	445		0	
431	447	441,447	1.80690	0.57006
431	455		0.22000	0.09500
438	455		0	
456	466		0	
467	486		0.88988	0.17631
467	493		0	
476	493		0	
477	493		0	
479	493		95.16700	13.15200
480	493		0	
493	504		0	
505	520	508,510,512,513,514,515	76.24600	5.12860
505	522	518	6.30890	4.94880
506	520	507,512	18.13300	3.48700
506	522		6.20000	4.30000
506	525		0	
506	527		0	
508	518		0	
508	520	508	nd	
508	522	516,518	0.63125	0.04214
508	523		0	
508	525		2.41350	0.37531
508	526	516,519	0	
508	527		0.01900	0.00820
508	535		0	
535	553		0	
537	545		0.99278	0.11777
537	550		5.89000	3.43000
537	569		0	
546	569		2.33900	0.59246
549	569		0	
550	569		0	
551	565		0	
551	566		0	
551	569		0	
551	584		0	
554	565		0	
554	569		0.01700	0.00730
585	592	587	20.98200	9.17530
585	593		0	
585	610		0	
593	610		0	

Table 2: Hsp104 peptides found in the monomer state. Peptides reported were identified using ExMS-CL, and found in all three replicates for each timepoint. Modification rates calculated using Matlab, and specific sites of modification are also listed.

Start	End	Modified residues (ID'd by MS2)	Modification rate (s^{-1})	Error
597	610		0	
597	611		1.26000	0.45000
611	623		0	
611	630		0	
611	631	613,615,626	2.30000	0.76000
612	623		0.01900	0.00670
612	631	616,621	0.98921	0.07043
613	623		0	
613	631		0	
614	631		0	
616	631		0	
624	631		0	
638	645		0	
639	645	645	36.57600	0.73520
646	655	646,649	2.00940	0.65427
646	661		0	
646	662		0	
646	670		0	
647	655		0	
647	670		0	
656	670		nd	
656	675		0	
662	670		0	
662	674		0	
662	675		0	
663	670		0	
663	674		1.37000	0.33000
671	683		0	
675	684		0	
676	683	680	0.26000	0.14000
684	696		0	
684	697		20.20200	1.33330
685	696	685,690	0.54260	0.00268
685	697		0	
700	720		0	
703	717		0	
703	720		0	
703	721		0	
704	721		0	
706	720		0	
706	721		0	
707	721		0	
733	744		1.60200	0.07239

Table 2: Hsp104 peptides found in the monomer state. Peptides reported were identified using ExMS-CL, and found in all three replicates for each timepoint. Modification rates calculated using Matlab, and specific sites of modification are also listed.

Start	End	Modified residues (ID'd by MS2)	Modification rate (s^{-1})	Error
733	748		0	
733	751		0	
734	748		0	
734	751		0	
734	753		2.10810	1.33330
752	763		0	
753	763		0	
769	785	773,774,776,778,779,780,781,782,784	1.14590	0.09697
769	788		0.38000	0.16000
769	793		0	
773	785		0	
773	788		1.18410	0.20305
786	806		0	
786	809		0	
789	809		2.67000	1.00000
791	806		0.33906	0.02153
791	812		0	
794	806		0	
794	809		4.24350	2.84430
794	812		0	
794	814		3.60000	1.50000
810	831		0	
813	820		0	
813	822		0	
813	823		0	
843	856		0	
843	857		0	
857	872		0	
857	873		0.27548	0.03262
857	874	863	1.10000	0.43000
857	875		0	
857	876		10.74700	3.24910
857	877		10.38200	6.56650
860	873		0	
860	875		0	
877	898	886	0.10817	0.08657
877	900		0.43000	0.10000
878	889		0	
878	898		0	
878	900		0	
878	901		0	
885	898		0	
889	898		0	
890	898		0	

Table 3: Hsp104 peptides found in the hexamer with ADP state. Peptides reported were identified using ExMS-CL, and found in all three replicates for each timepoint. Modification rates calculated using Matlab, and specific sites of modification are also listed.

Start	End	Modified residues (ID'd by MS2)	Modification rate (s^{-1})	Error
8	38		0	
8	39		0	
12	38		0	
12	39		0	
14	38		0	
16	36		0	
16	37		31.0999	2.14952
16	38		0	
16	39		0	
17	38		0	
17	39		0	
18	36		0	
18	38		0.37424	0.00259
18	39		0	
22	36		0	
22	39		0	
39	53		25.0228	0.00544
40	54		0.16685	0.12455
54	64		0.17165	0.01086
55	64		3.60161	0.00893
65	73		0	
65	85		0.00376	0.00132
65	90		0	
65	91		0	
65	93		0	
65	98		6.06206	0.04369
73	85		0.20849	0.00297
73	90		43.5549	3.995
73	110		0	
74	85		0	
74	90		10.3165	2.4205
74	91		0	
74	110		5.48396	0.15566
86	98	95	4.49673	0.14847
86	99		0	
86	110	90,94,96,102,107	0.58534	0.01194
88	110		0	
91	98	92,95	6.6975	2.491
91	110		0.36439	0.02859
92	110		0	
94	110		0.31502	0.01409
99	110		1.92733	0.03709
100	110		0	

Table 3: Hsp104 peptides found in the hexamer with ADP state. Peptides reported were identified using ExMS-CL, and found in all three replicates for each timepoint. Modification rates calculated using Matlab, and specific sites of modification are also listed.

Start	End	Modified residues (ID'd by MS2)	Modification rate (s^{-1})	Error
119	130		0	
119	132		0	
119	135		0	
119	136		0	
119	138		0	
119	139		0	
120	130		0	
121	134		6.48200	0.29459
121	136		0	
121	138		0	
121	139		0	
122	138		0	
122	139		0	
129	136		0	
129	139		19.0491	0.39959
145	166		0	
146	166		0	
148	166		0.10132	0.00229
152	165		0	
166	173		0.28385	0.00123
174	190		0	
174	192		0	
175	190		0	
175	192		1.164801	0.016751
211	221		0	
211	223		32.61095	1.892455
211	224		5.621905	0.096486
211	226		0	
211	227		0	
211	231		0	
211	232		0	
211	238		0	
211	243		0	
225	243		0	
228	243		0	
248	261		0	
249	261		0	
249	263		0	
249	269		nd	
249	271		1.15408	0.08080
249	277		0	
249	278		0.51465	0.1222
249	281		0	

Table 3: Hsp104 peptides found in the hexamer with ADP state. Peptides reported were identified using ExMS-CL, and found in all three replicates for each timepoint. Modification rates calculated using Matlab, and specific sites of modification are also listed.

Start	End	Modified residues (ID'd by MS2)	Modification rate (s^{-1})	Error
251	261		0	
252	261		0	
262	277		0	
262	278		0.442011	0.034674
270	277		17.57964	0.321433
282	295		0	
282	298		0	
282	299	285,286,288,289,290,292,294,298,299	74.97205	0.587241
282	310		0	
282	320		48.23845	0.188209
283	298		nd	
283	299		28.0731	0.421472
283	310		0	
286	310		26.9075	0.331420
299	310		3.1725	1.4805
300	310		0	
300	320		145.5754	3.382825
300	331		0	
306	320		0	
311	320	311	2.284317	0.030648
321	330		17.72534	1.027138
321	331		0	
322	331		0	
331	350		133.53875	3.370135
332	345		4.584615	0.139773
332	349	333	3.774805	0.257325
332	350		0	
332	352		0.298027	0.012935
343	352		0	
351	368		0	
351	369		nd	
351	372		0.108586	0.006867
353	371		0	
353	372	356,357,358,367,370	66.62485	1.590856
360	372		0	
379	393		0.92355	0.21855
379	395		0	
396	414		0	
398	414		9.353	3.9715
398	423		0	
401	414		0	
401	423		0	
403	414		0	

Table 3: Hsp104 peptides found in the hexamer with ADP state. Peptides reported were identified using ExMS-CL, and found in all three replicates for each timepoint. Modification rates calculated using Matlab, and specific sites of modification are also listed.

Start	End	Modified residues (ID'd by MS2)	Modification rate (s^{-1})	Error
403	423		0	
405	414		21.5074	0.39282
405	423		0.77315	0.5828
415	423	415,416,417,418,421,423	35.5085	0.79437
415	425		0.99407	0.07798
424	437		0	
424	447		0	
424	455	454	0.05358	0.01261
426	455		0	
427	447		0	
428	447		38.2016	4.10075
428	455		0	
431	445		0	
431	447		0	
431	455		0.56522	0.00851
438	447		0	
438	455		0	
456	466	457,460	1.8142	0.50525
467	486		0	
467	493		0	
475	493		3.29	1.175
476	493		0	
477	493		0	
480	493		0	
505	525		0	
505	526		349.139	0.94651
506	520		0	
506	522		20.1390	1.22559
506	525		0	
506	527		0	
508	518		0	
508	520	517	0.25922	0.01159
508	522		1.45824	0.05233
508	523		0	
508	525		0	
508	526		0	
508	527		0	
508	535		0	
508	536	511,517,523	88.80885	3.409615
511	520		0	
511	522		0	
511	525		0	
528	536		0	

Table 3: Hsp104 peptides found in the hexamer with ADP state. Peptides reported were identified using ExMS-CL, and found in all three replicates for each timepoint. Modification rates calculated using Matlab, and specific sites of modification are also listed.

Start	End	Modified residues (ID'd by MS2)	Modification rate (s^{-1})	Error
535	545	536	129.076	8.43415
536	550	546,547	24.2355	0.03798
536	569		0	
537	545		5.29079	0.07757
537	548		29.2269	0.50562
537	569		0	
537	572		21.3194	0.05508
546	569		6.3685	4.982
546	572		0	
549	569		8.3425	2.9845
549	572		0	
550	569		0	
550	572		0	
551	563		0	
551	565		0	
551	566	552	4.60694	0.02460
551	569		0	
551	572		0	
551	578		0	
551	584		0	
552	569		0	
554	565		35.9315	12.737
554	566		0	
554	569		nd	
554	579		6.45122	0.08124
573	584	573,574,575,579	69.8044	6.16898
585	592	587,590	20.68	8.46
585	593		8.601	5.7575
585	610		0	
594	610		0.57593	0.03974
597	611		6.14595	0.09690
611	623		0	
611	630		0	
611	631		4.935	2.2325
611	632		0	
612	623		0.04056	0.00477
612	631		0	
613	623		0	
613	631		0	
614	631		0	
624	631		0	
638	645		1.32286	0.03287
638	646		nd	

Table 3: Hsp104 peptides found in the hexamer with ADP state. Peptides reported were identified using ExMS-CL, and found in all three replicates for each timepoint. Modification rates calculated using Matlab, and specific sites of modification are also listed.

Start	End	Modified residues (ID'd by MS2)	Modification rate (s^{-1})	Error
646	655		0	
646	661		0	
646	662		0	
646	670		0	
647	655		0	
647	670		0	
656	670		0	
656	675		0	
662	670		0	
663	670		0	
671	683	677	5.71778	0.07360
675	683		0	
675	684		0	
676	683		0	
684	696		0	
684	697	684,687	49.1197	1.27066
685	696		0.28999	0.00070
690	696		0	
700	717		0	
700	718		6.439	2.303
700	720		0	
700	721		1.11625	0.6345
701	720		0	
703	717	715	4.38016	0.03760
703	720		0	
703	721		0	
704	721		17.8200	0.69656
706	720		0	
706	721		0	
707	717		0	
733	744		1.82383	0.01648
733	748		103.056	2.96852
733	751		0	
733	752		0	
733	762		4.03236	0.31946
734	748		0	
734	752	734,738,743,744	211.166	0.01532
734	763		0	
745	763	759	36.3357	0.00716
749	762	754,756	4.52751	0.19481
749	763		0	
752	762		0	
752	763		0	

Table 3: Hsp104 peptides found in the hexamer with ADP state. Peptides reported were identified using ExMS-CL, and found in all three replicates for each timepoint. Modification rates calculated using Matlab, and specific sites of modification are also listed.

Start	End	Modified residues (ID'd by MS2)	Modification rate (s^{-1})	Error
753	763		0	
769	785	772,774,781,782,783,784	0.63596	0.00262
769	788		0	
769	790		0	
769	793		0	
770	785		0	
771	785		0	
773	785		0	
786	806		17.5545	6.345
786	809		0	
786	812		0	
789	795	792,793	21.1774	0.73183
789	806		22.3123	0.30601
789	809		20.0842	0.15006
789	812			
789	814		0	
791	806		0	
791	809		47.4418	0.91495
791	812		0	
794	806		0	
794	809	796,800,809	18.6279	1.10099
794	812		0	
794	814		16.0497	0.14408
807	831		0	
810	831		0	
813	819		0	
813	822		3.055	0.564
813	823		4.982	1.786
813	831	819,821,822,823	41.8911	0.18060
814	831		40.9816	0.70774
815	831		26.4398	0.51674
823	831	823,825,829,830	26.649	0.16948
838	856		0	
843	856	854	0.03631	0.00229
843	857	843,850,853,855	3.77245	0.13598
857	872	864	102.894	4.06926
857	873		2.44987	0.00543
857	874	871	1.60502	0.17772
857	875		0.2209	0.07755
857	876		0	
857	877		15.2216	1.79112
860	872		0	
860	873		0.72988	0.03264

Table 3: Hsp104 peptides found in the hexamer with ADP state. Peptides reported were identified using ExMS-CL, and found in all three replicates for each timepoint. Modification rates calculated using Matlab, and specific sites of modification are also listed.

Start	End	Modified residues (ID'd by MS2)	Modification rate (s^{-1})	Error
877	889		49.82	0.39828
877	898	877,886,897	nd	
877	900		0	
877	901		0	
878	889		0	
878	898	886	0.59650	0.00157
878	900		7.31437	0.73120
885	898		0	
890	898		0	

Table 4: Hsp104 peptides found in the hexamer with ATPγS state. Peptides reported were identified using ExMS-CL, and found in all three replicates for each timepoint. Modification rates calculated using Matlab, and specific sites of modification are also listed.

Start	End	Modified residues (ID'd by MS2)	Modification rate (s^{-1})	Error
8	38		1.85083	0.32579
8	39		0	
12	36		0	
12	38		0	
12	39		0	
14	38		0	
14	39		0	
16	36		15.07458	0.63493
16	37		0	
16	38		0	
16	39		0	
17	36		0	
17	38		0	
17	39		0	
18	36		0	
18	37		42.0546	8.81484
18	38		0	
18	39		0.61159	0.31614
22	36		0	
22	39		0	
39	53		4.28094	1.49826
40	54		0	
54	64		0	
55	64		0.85554	0.17676
65	73	65	0.4794	0.23256
65	85		0	
65	90		0.05479	0.03465
65	91		0	
65	93		0	
65	98		9.30484	1.02673
73	85		0	
73	110		0	
74	85		0	
74	90		0	
74	110		0	
86	98		2.7336	0.4488
86	99		0	
86	110	87,90,91,94,96,103,109	5.35051	0.35412
91	98		0	
91	110		0	
92	110		0	
94	110		0	

Table 4: Hsp104 peptides found in the hexamer with ATPγS state. Peptides reported were identified using ExMS-CL, and found in all three replicates for each timepoint. Modification rates calculated using Matlab, and specific sites of modification are also listed.

Start	End	Modified residues (ID'd by MS2)	Modification rate (s^{-1})	Error
99	110		0	
111	118		0	
119	130		0	
119	132		0	
119	135		0	
119	136		0	
119	138		0	
119	139		0	
120	130		0	
121	130	124,125	0.11559	0.03178
121	132		0	
121	134		1.14648	0.408
121	135	134	76.3021	46.6996
121	136		0	
121	138		0	
121	139		0	
122	139		0	
129	136		0	
129	139		0	
147	167		0	
148	166		0	
152	165		0	
152	167		0	
166	173		0.3468	0.1224
167	173		0	
174	190		0	
175	190		0.10812	0.02856
175	192		0	
177	192		0	
211	221		0	
211	223		0	
211	226		0	
211	227		0	
211	231		0	
211	232		0	
211	238		0	
211	243		0	
222	238		0	
225	243		0	
227	243		0	
228	243		0	
244	261		0	

Table 4: Hsp104 peptides found in the hexamer with ATPγS state. Peptides reported were identified using ExMS-CL, and found in all three replicates for each timepoint. Modification rates calculated using Matlab, and specific sites of modification are also listed.

Start	End	Modified residues (ID'd by MS2)	Modification rate (s^{-1})	Error
248	261		18.2002	0.37167
249	261		0	
249	263		0	
249	269		0	
249	271		0	
249	277		10.608	5.304
249	278		0	
251	261		0	
252	261		0	
262	269		0	
262	277		0	
262	278		3.5196	0.63456
270	277		0	
282	298		0	
283	299		0	
286	310		0	
299	310		0	
300	310		0	
300	320		0	
306	320		0	
311	319		0	
311	320	311	0.37187	0.07452
311	321		0	
321	330		0	
321	331		0	
322	331		0	
331	345		0	
331	350		0	
331	352		0	
332	345		0	
332	347		0	
332	349		0	
332	350		0	
332	352		0	
340	352		0	
351	368		0	
351	369		57.7789	3.5230
351	371		5.04247	1.5985
351	372		0	
352	372		16.4350	10.394
353	368		0	
353	371		0	

Table 4: Hsp104 peptides found in the hexamer with ATPγS state. Peptides reported were identified using ExMS-CL, and found in all three replicates for each timepoint. Modification rates calculated using Matlab, and specific sites of modification are also listed.

Start	End	Modified residues (ID'd by MS2)	Modification rate (s^{-1})	Error
353	372		0	
360	372		0	
379	393		0.04692	0.02448
396	414		0	
398	414		0.714	0.612
401	414		0	
401	423		0	
403	414		1.65319	0.12001
403	423		0	
403	425		0	
405	414		52.8094	9.52108
405	423		0	
415	423		0	
415	425		0	
424	437		0	
424	447		0	
424	455		0.28604	0.02770
426	455		0	
427	447		0	
431	437		0	
431	445		0	
431	447		0	
431	455		0.07998	0.05058
432	447		0	
438	447		0	
438	455		0	
456	476		0	
467	493		0.83926	0.11563
469	493		0	
476	493		0	
477	493		0	
494	502		0	
505	522		0	
505	526		0	
506	520	506	5.98311	0.25342
506	522		1.50949	1.04292
506	525		0	
506	526		0	
506	527		0	
508	518		0	
508	520		0	
508	522		0	

Table 4: Hsp104 peptides found in the hexamer with ATPγS state. Peptides reported were identified using ExMS-CL, and found in all three replicates for each timepoint. Modification rates calculated using Matlab, and specific sites of modification are also listed.

Start	End	Modified residues (ID'd by MS2)	Modification rate (s^{-1})	Error
508	523		0	
508	525		0.41261	0.23440
508	526		0	
508	527		0	
508	535		0	
537	545		0	
537	548		0	
537	550		0	
537	569		0	
546	569		12.0262	1.16073
549	569		9.12308	0.63721
550	569		0	
551	565		0	
551	566		0	
551	569		0	
552	569		0	
554	565		0	
554	569		0	
585	592		0	
585	593		0	
594	610		0	
597	610		0.45043	0.16747
597	611		0	
611	623		0	
611	630		0	
611	631		0	
611	632		0	
612	623		0	
612	631		0	
613	623	616,618	9.53618	0.28223
624	631		0	
646	655		0	
646	661		0	
646	662		0	
647	655		4.182	1.3872
647	670		0	
656	670		0	
656	675		0	
662	674		0	
662	675		0	
666	683	672	29.7248	1.64740
671	683		0	

Table 4: Hsp104 peptides found in the hexamer with ATPγS state. Peptides reported were identified using ExMS-CL, and found in all three replicates for each timepoint. Modification rates calculated using Matlab, and specific sites of modification are also listed.

Start	End	Modified residues (ID'd by MS2)	Modification rate (s^{-1})	Error
675	683		0	
676	683		0	
684	696		0	
684	697		0	
685	696		0	
685	697		0	
686	696		0	
688	696	694	57.171	9.3903
700	720		0	
703	717		0	
733	744		0	
733	748		0	
734	748		0	
752	762		0	
752	763		0	
753	763		0	
769	785	772,774,776,777,780,782	0.14076	0.02448
769	788		0	
769	790		0	
769	793		0	
770	785		0	
773	785		0	
773	788		15.5419	6.63
786	806		0	
789	806		0	
789	809		0	
789	812		0	
791	806		0	
791	809		0	
794	806	801	0.52210	0.07790
794	809		2.51715	0.16020
794	812		0.9792	0.408
794	813		0	
794	814		nd	
810	831		0	
813	820		16.6608	0.14824
813	822		0	
813	823		0	
813	831		0	
813	837		0	
838	856		0.12265	0.00860
841	856		0	

Table 4: Hsp104 peptides found in the hexamer with ATPγS state. Peptides reported were identified using ExMS-CL, and found in all three replicates for each timepoint. Modification rates calculated using Matlab, and specific sites of modification are also listed.

Start	End	Modified residues (ID'd by MS2)	Modification rate (s^{-1})	Error
843	856		0	
843	857	843,845,846,848,849,850,852,857	6.12	4.488
857	872		120.36	75.888
857	873		nd	
857	874		0	
857	875		1.2076	0.204
860	872		0	
860	873		0	
860	875		0	
877	889	884	27.132	13.872
877	898		0	
877	900		0	
878	889		0	
878	890		0	
878	892		21.42	7.038
878	898		0	
878	900		0	
885	898		0	
890	898		0	

Table 5: Selected peptide list. Peptides that are found in two or more states, which cover important regions of Hsp104. Modification rates and modified residues are listed side by side for ease of comparison.

		Monomer		Hexamer with ADP		Hexamer with ATPγS	
Start	End	Modified residues (ID'd by MS2)	Modification rate (s^{-1})	Modified residues (ID'd by MS2)	Modification rate (s^{-1})	Modified residues (ID'd by MS2)	Modification rate (s^{-1})
8	38		0.03 ± 0.04		0		1.85 ± 0.33
39	53		pnf		25.02 ± 0.01		4.28 ± 1.50
55	64		0		3.60 ± 0.01		0.86 ± 0.18
86	110	87,88,90,91,95,96,100, 101,104,108	0.80 ± 0.35	90,94,96,102,107	0.59 ± 0.01	87,90,91,94,96,103, 109	5.35 ± 0.35
121	134		0		6.48 ± 0.29		1.15 ± 0.41
148	166		0.22 ± 0.01		0.10 ± 0.002		0
211	223		0		32.61 ± 1.89		0
225	243		15.90 ± 11.23		0		0
282	299		nd	285,286,288,289,290, 292,294,298,299	74.97 ± 0.59		nd
283	299		nd		28.07 ± 0.42		0
286	310		nd		26.91 ± 0.33		0
300	320		nd		145.58 ± 3.38	311	0
311	320		nd	311	2.28 ± 0.03		0.37 ± 0.07
331	350		0		133.54 ± 3.37		0
332	349		2.37 ± 0.29	333	3.77 ± 0.26		0
405	414		pnf		21.51 ± 0.39		52.81 ± 9.52
415	423		pnf	415,416,417,418,421, 423	35.51 ± 0.79		0
431	455		0.22 ± 0.10		0.57 ± 0.01		0.08 ± 0.05
467	493		0		0		0.84 ± 0.12
505	526		pnf		349.14 ± 0.95		0
506	522		6.20 ± 4.30		20.14 ± 1.23		1.51 ± 1.04

Table 5: Selected peptide list. Peptides that are found in two or more states, which cover important regions of Hsp104. Modification rates and modified residues are listed side by side for ease of comparison.

		Monomer		Hexamer with ADP		Hexamer with ATPγS	
Start	End	Modified residues (ID'd by MS2)	Modification rate (s^{-1})	Modified residues (ID'd by MS2)	Modification rate (s^{-1})	Modified residues (ID'd by MS2)	Modification rate (s^{-1})
508	536		nd	511,517,523	88.81 ± 3.41		nd
611	631	613,615,626	2.30 ± 0.76		4.94 ± 2.23	616,618	0
613	623		0		0		9.54 ± 0.28
684	697		20.20 ± 1.33	684,687	49.12 ± 1.27		0
733	744		1.60 ± 0.07		1.82 ± 0.02		0
733	748		0		103.06 ± 2.97		0
769	785	773,774,776,778,779, 780,781,782,784	1.15 ± 0.10	772,774,781,782,783, 784	0.64 ± 0.00	772,774,776,777,780, 782	0.14 ± 0.02
786	806		0		17.55 ± 6.35		0
789	806		pnf		22.31 ± 0.31		0
789	809		2.67 ± 1.00		20.08 ± 0.15		0
813	831		pnf	819,821,822,823	41.89 ± 0.18		0
843	857		0	843,850,853,855	3.77 ± 0.14	843,845,846,848,849, 850,852,857	6.12 ± 4.49

same peptide for all the states. Table 5 lists identical peptides found in two or three of the states, which cover some of the regions of interest. The presence of nucleotide in our buffer affects the effective hydroxyl radical population (i.e. nucleotide quenches the oxidation of the sample). Therefore, all of the rates have been normalized to the monomer sample based on the Alexa488 decay data [218, 219], with normalization factors of 2.35 and 2.04 for the hexamers with ADP and ATPγS, respectively.

To begin my analysis of the XF solvation data of the Hsp104 hexamer, and to tease out relevant mechanistic implications I started by looking at each individual domain. I examined 1) regions of known functional importance, 2) regions that are heavily modified, and therefore solvated, and 3) regions that undergo large changes in solvation between states. I then used the XF data to make mechanistic and structural predictions about regions in each domain. After investigating each domain separately, I combined the findings to present an overall picture of changes in solvation in the Hsp104 hexamer and what they mean for its activity and regulation.

3.2.3 The N-terminal domain (NTD)

3.2.3.1 NTD overview

As we learned from Chapter 2, the NTD of Hsp104 is crucial for hexamer cooperativity. However, details of how it functions remained unclear. The crystal structures of the N-terminal domains of various Hsp100 proteins, including the Hsp104 bacterial homologues ClpA [141], ClpB [142], and ClpC [143] have been solved. The NTDs are highly structurally conserved despite low sequence identity (e.g. 28% sequence identity between the ClpA and ClpB NTDs). They are very stable globular domains [141] made up of two imperfect repeats of four helical bundles [141] and are connected to the D1 domain by a highly mobile linker [141]. The repeated subdomains, R1 and R2, each contain four helices, H1-H4 and H1'-H4' (Figure 3A). Hsp100 proteins such as ClpA [141] and ClpX [221] contain a zinc binding site in their NTDs. Hsp104 retains the histidine residues involved in zinc [141] binding but not the essential glutamic acid, while ClpB is missing both the acidic residue as well as one of the histidine residues. A loop

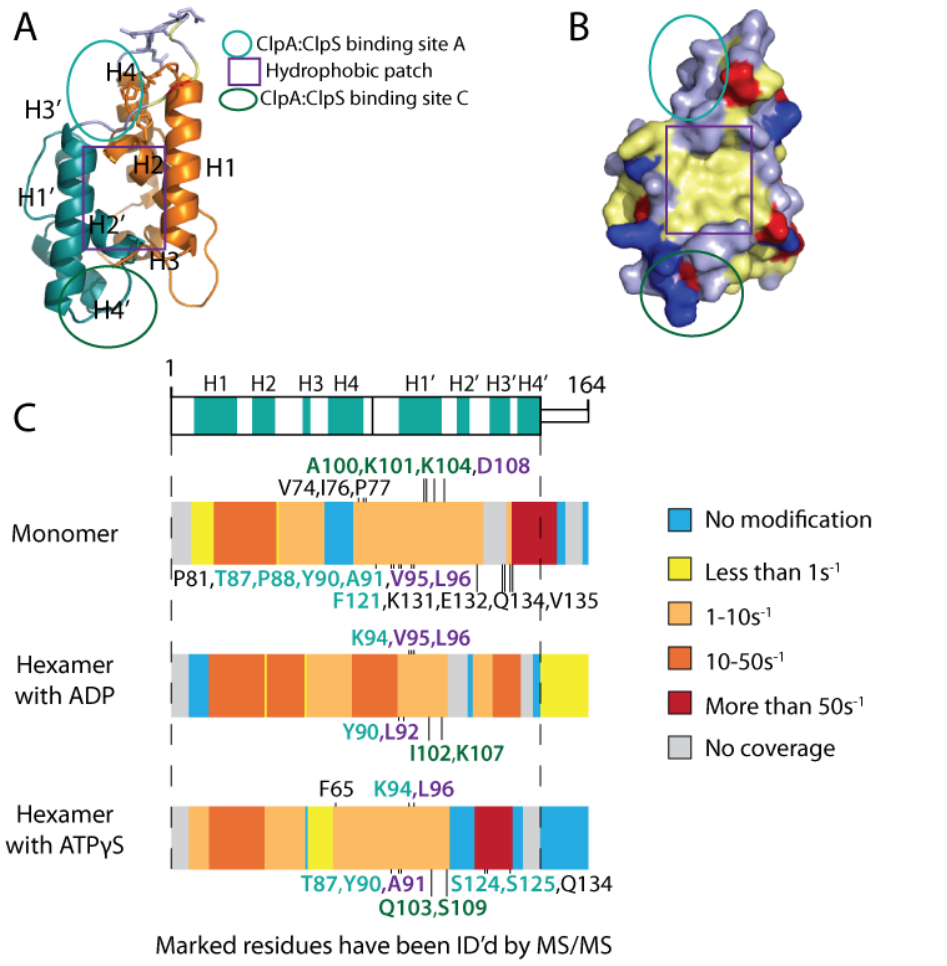
A
ClpA:ClpS binding site A
Hydrophobic patch
ClpA:ClpS binding site C
H4
H3′
H2
H1
H1′
H2′
H3
H4′
B
C
1
H1 H2 H3 H4 H1′ H2′ H3′H4′ 164
A100,K101,K104,D108
V74,I76,P77
Monomer
P81,T87,P88,Y90,A91,V95,L96
F121,K131,E132,Q134,V135
K94,V95,L96
Hexamer with ADP
Y90,L92
I102,K107
F65 K94,L96
Hexamer with ATPγS
T87,Y90,A91
S124,S125,Q134
Q103,S109
No modification
Less than 1s-1
1-10s-1
10-50s-1
More than 50s-1
No coverage
Marked residues have been ID'd by MS/MS
D
Y90
K94
L92
L96
I102
K107
Hexamer with ADP
E
Y90
T87
K94
L96
Q103
S109
Hexamer with ATPγS

Figure 3. Hsp104 N-terminal domain (NTD) organization and x-ray footprinting (XF) solvation information. A) Hsp104 NTD homology modeled off the crystal structure of the *E. coli* ClpB NTD (pdb: 1khy) with helices 1-4 for each repeat labeled. Residues shown as sticks are residual zinc binding histidines as well as unique polar residues in what is usually an acidic loop. Circled regions are important in the structurally conserved ClpA (pdb: 1r6c) NTD for ClpS binding, site A in green, site C in teal, and the hydrophobic patch for substrate binding in purple. B) Surface rendering of Hsp104 NTD showing the conservation of the surface hydrophobic patch. Acidic residues shown in red, basic residues shown in blue, and hydrophobic resides in yellow. C) Bar graph showing XF modification rates of peptides covering the Hsp104 NTD. Peptides with the highest rate for a given region are on the top layer. Blue is unmodified, yellow less than 1 s^{-1}, light orange 1-10 s^{-1}, dark orange 10-50 s^{-1}, red more than 50 s^{-1}, and gray is no coverage. Marked residues have been identified as modified by MS2 and are colored by proximity to the ClpA:ClpS binding sites, site A in green, site C in teal, and the hydrophobic patch in purple. D) and E) the Hsp104 homology modeled NTD colored based on the XF modification rates for the hexamer with D) ADP and E) ATPγS. Residues identified by MS2 as modified are shown as spheres and labeled when visible. Blue is unmodified, yellow less than 1 s^{-1}, gold 1-10 s^{-1}, orange 10-50 s^{-1} red more than 50 s^{-1}, and gray is no coverage. The NTD-NBD1 linker is drawn in as a dashed line and colored as described.

connecting the two repeats, which in ClpA is highly acidic [141], is instead enriched in glutamines and prolines in Hsp104. The three glutamines in a row, 78-QQQ-80 are an interesting divergence from bacterial homologues considering that many yeast prions are asparagine and glutamine rich [90]. I have homology modeled the Hsp104 NTD based on the NTD of the *E. coli* ClpB [142] (Figure 3A, B, D, and E). Support for the accuracy of the Hsp104 NTD homology model, despite the low sequence identity, is the solvation state of helix H2' (Figure 3A), residues 113-117. This helix, based on the homology model, is shielded from solvent, and indeed, a peptide 111-118 that covers the H2' helix, while found only in the ATPγS hexamer, is unmodified (Table 4, Figure 3E).

3.2.3.2 The N-terminal domain is involved in substrate binding

When the Hsp104 NTD, homology modeled off the NTD of *E. coli* ClpB, is compared to the well-characterized NTD of ClpA [141], there is strong structural homology despite the low sequence identity (there is 25% and 30% sequence identity between the NTD of Hsp104 and ClpA or ClpB respectively, similar to the identity between the two bacterial homologues). A

conserved feature of the Hsp100 NTDs is a hydrophobic patch between H1 and H1' [141]. We see that in the homology model of the Hsp104 NTD this hydrophobic patch appears to be conserved (Figure 3B). Interestingly, the hydrophobic patch region appears to be solvated in all three states (peptide 86-110, Table 5) and in fact, 4 hydrophobic residues in that region were identified by MS2 analysis as being specific sites of hydroxyl radical modification (residues A91, L92, V95, and L96, Table 5, Figure 3C-E). This indicates that this conserved region may have the capacity to interact with substrate in both the ADP and ATPγS states. Two acidic residues, D108 and D114, which have been implicated in large-aggregate substrate binding in ClpB [150], are also near the hydrophobic patch. However, in a surface rendering of the domain it appears they may have only minimal surface exposure, and modification of D108 was only seen in the monomeric Hsp104 sample (modification of D114 was not seen in any state and the peptide that covers the area was unmodified in the hexamer with ATPγ).

To test whether the NTD of Hsp104 is involved in substrate binding, we measured the affinity for a fluorescent substrate, FITC-casein, using a fluorescence polarization assay. We used the purified wild-type protein (WT) and a truncation mutant (ΔN) missing the NTD as well as the NTD-NBD1 linker. In the presence of ATPγS WT Hsp104 binds FITC-casein robustly with a K_d of 55 +- 7 nM (Figure 4A). In the same conditions ΔN Hsp104 binds FITC-casein with a K_d of 194 +- 60 nM, showing a 3 - 4 fold decrease in affinity (Figure 4A). This result supports a role for the Hsp104 NTD in substrate binding. Mutagenesis studies would allow us to pinpoint specific residues involved in the substrate interaction. The hydrophobic residues identified through MS2 as being oxidatively modified would be a good starting point. Since the binding surface may consist of a large, non-specific hydrophobic patch it may be necessary to substitute a number of residues (there are approximately 10 residues involved in the hydrophobic patch) or replace the hydrophobic residues with charged residues.

3.2.3.3 The N-terminal domain is involved in productive interaction with Hsp70

Additional residues that were identified as oxidatively modified by MS2 analysis fall into two clusters, either A, in the beginning of the H1' helix and in the H2'-H3' loop, (residues T87, Y90, K94, S124, and S125) or C, at the end of H1' and in the H1'-H2' loop (residues I102, Q103, K107 and S109) (Table 1, 3 and 4, Figure 3). These two clusters of residues are in the same regions that were identified in ClpA to be involved in interactions with an adapter protein ClpS [141], which protects ClpA from autodegradation and targets ClpA to aggregated substrates [191]. This was surprising, since the middle domain (MD) of Hsp104 and its bacterial homologue ClpB have previously been identified as the site of interaction with Hsp70 proteins (the Hsp70 chaperones are essential for *in vivo* Hsp104 activity) [172-175]. However, in the Hsp100 protein ClpC, which has a truncated version of the middle domain (motif 1 only) the crystal structure of the hexamer revealed that the adapter protein MecA made extensive contacts with both the MD as well as the NTD [143]. This could well be the case for Hsp104 as well, considering that the region of the MD found to interact with Hsp70, namely residues within motif 2 near the C-terminal end of helix 2 [178], are adjacent to the NTD in every hexameric model of Hsp104 [171, 222]. The second cluster of modified residues (C), at the end of H1', is covered by peptides 99-110 and 100-110 which display a 10-fold protection from HD exchange upon formation of an apo hexamer (Table 6). An increase in secondary structure upon hexamerization further suggests that the region may be available for protein-protein interactions, especially since the XF data indicates that it remains solvated and is therefore unlikely to be involved in a hexamer interface. Additionally, the residues 100-102 (which contains the oxidatively modified I102, Figure 3C, D) were identified as a potential Hsp70:Hsp104 binding site using peptide array technology [178], although the authors did not investigate the region beyond an initial identification. Their dismissal of the importance of this interaction may have been premature; NTD:Hsp70 interactions, especially so close to the substrate-binding hydrophobic patch may facilitate substrate release from Hsp70 for hand-off to Hsp104.

Table 6: Hydrogen-deuterium exchange protection factors between Hsp104 oligomeric states. Data from Alec Ricciuti, Englander lab.

		Fold-protection					Fold-protection		
Start	End	Mon: Apo	Mon: ADP	Mon: ATPγS	Start	End	Mon: Apo	Mon: ADP	Mon: ATPγS
16	36	1	1	1	378	393	1	20	100
17	36	1	1	1	379	393	1	20	100
18	36	1	1	1	379	395	1	20	100
18	38	1	1	1	396	400	n/a	n/a	n/a
39	53	1	1	1	401	414	1	10	100
55	64	1	2	10	401	423	1	5	100
65	72	1	1	2	403	423	1	2	50
73	90	1	1	1	405	423	1	2	50
74	85	1	1	1	424	430	1	10	100
74	90	1	1	1	431	447	1	1	1
74	98	n/a	1	1	431	455	1	1	5
74	110	2	2	2	448	455	1	10	50
86	110	n/a	2	5	456	476	1	1	n/a
91	110	5	5	5	467	493	2	10	50
99	110	10	10	10	494	502	2	10	50
100	110	10	10	10	494	504	2	10	50
111	118	1	1	1	508	520	2	10	20
119	130	1	1	1	508	522	2	10	20
139	147	5	5	5	508	526	2	10	20
140	146	10	10	10	511	520	2	20	n/a
140	147	10	10	10	511	522	2	20	n/a
146	165	1	1	n/a	526	536	1	1	1
174	192	1	10	100	528	536	n/a	1	1
175	192	n/a	10	100	536	545	n/a	1	5
177	190	n/a	10	100	546	550	5	10	20
177	192	1	10	100	551	569	1	2	10
200	210	1	10	100	554	569	1	2	n/a
201	210	1	10	200	573	579	1	10	20
211	223	1	100	1000	585	592	10	20	50
211	226	1	200	5000	585	593	10	20	50
224	238	1	1	2	587	593	5	20	50
249	278	1	1	n/a	594	610	1	1	5
252	261	1	1	2	597	610	1	2	10
262	269	2	2	10	611	623	1	50	500
262	271	2	2	10	613	623	1	100	200
283	310	1	2	n/a	613	631	1	200	200
299	310	1	2	10	616	631	2	100	100
300	305	1	5	50	624	631	5	100	100
300	310	1	2	10	646	655	1	2	5
300	320	1	2	10	656	670	1	1	n/a
321	331	1	1	n/a	662	670	1	1	1
351	368	1	10	20	684	696	1	1	2
351	372	1	5	20	688	696	1	1	10
378	393	1	20	100	703	721	1	1	10

Table 6: Hydrogen-deuterium exchange protection factors between Hsp104 oligomeric states. Data from Alec Ricciuti, Englander lab.

		Fold-protection		
Start	End	Mon: Apo	Mon: ADP	Mon: ATPγS
733	748	1	5	5
734	744	1	5	5
734	748	1	5	5
752	762	-2	1	5
763	768	-2	2	20
769	785	1	20	20
773	785	1	50	50
776	785	1	20	20
794	806	1	2	n/a
813	822	1	20	50
813	831	1	50	100
838	856	10	10	20
843	856	10	10	20
857	875	1	1	1
878	900	1	1	1

To test the role of the Hsp104 NTD in productive Hsp70 interaction we used a luciferase reactivation assay to assess the remodeling activity of WT Hsp104 and ΔN Hsp104 in a variety of conditions. First, we verified that the ΔN Hsp104 construct was capable of Hsp70-independent luciferase remodeling. *In vitro*, in the presence of ATP, Hsp104 is inactive in the absence of Hsp70/Hsp40 [113]. However, for reasons that are poorly understood, Hsp104 is active in the absence of Hsp70/Hsp40 by the addition of permissive ratios of ATP:ATPγS [113]. WT Hsp104 has a maximal activity at a 1:1 ratio of ATP:ATPγS (Chapter 2), and at this ratio ΔN Hsp104 displays statistically insignificant differences in luciferase reactivation (Figure 4B). This finding allowed us to assess defects in productive interactions with Hsp70 proteins, since the inherent ability of ΔN Hsp104 to remodel aggregated luciferase appeared intact. Keeping the identity of the Hsp40 protein constant, we used two different Hsp70 proteins, Hsc70, which is constitutively expressed [223, 224], and Hsp72, which is expressed during heat shock [224]. In the presence of Hsc70, ΔN Hsp104 retained only 40% WT Hsp104 activity, while in the presence of Hsp72, 86% (Figure 4B). Reductions in ΔN Hsp104 activity with both Hsc70 and Hsp72 were statistically significant, with p values of $p < 0.02$ and $p < 0.05$ respectively. The difference in activity between ΔN Hsp104 in the presence of Hsc70 versus Hsp72 indicates that the Hsp104 hexamer may interact differently (or more or less robustly) with different Hsp70 proteins. Since Hsp104 is over-expressed in response to stress, it may not be surprising that there could be differences in the productivity of interactions with Hsp70 proteins whose roles vary *in vivo* (e.g. those whose main role is in helping nascent polypeptides fold versus those involved in survival during and after various stresses). Once again, mutagenic analysis would allow us to pinpoint residues directly involved in these interactions. A promising target is T87, which was identified as oxidatively modified in the hexamer with ATPγS (Figure 3C, E). This residue is just N-terminal to helix H1' (Figure 3C, E). In ClpA an equivalent residue, T81, resides within the main ClpS binding site (site A) [141] and in ClpC the residue T31 has been shown to be essential for ClpC activity by mediating the interaction with MecA [143]. An alternative possibility would be that the NTD is

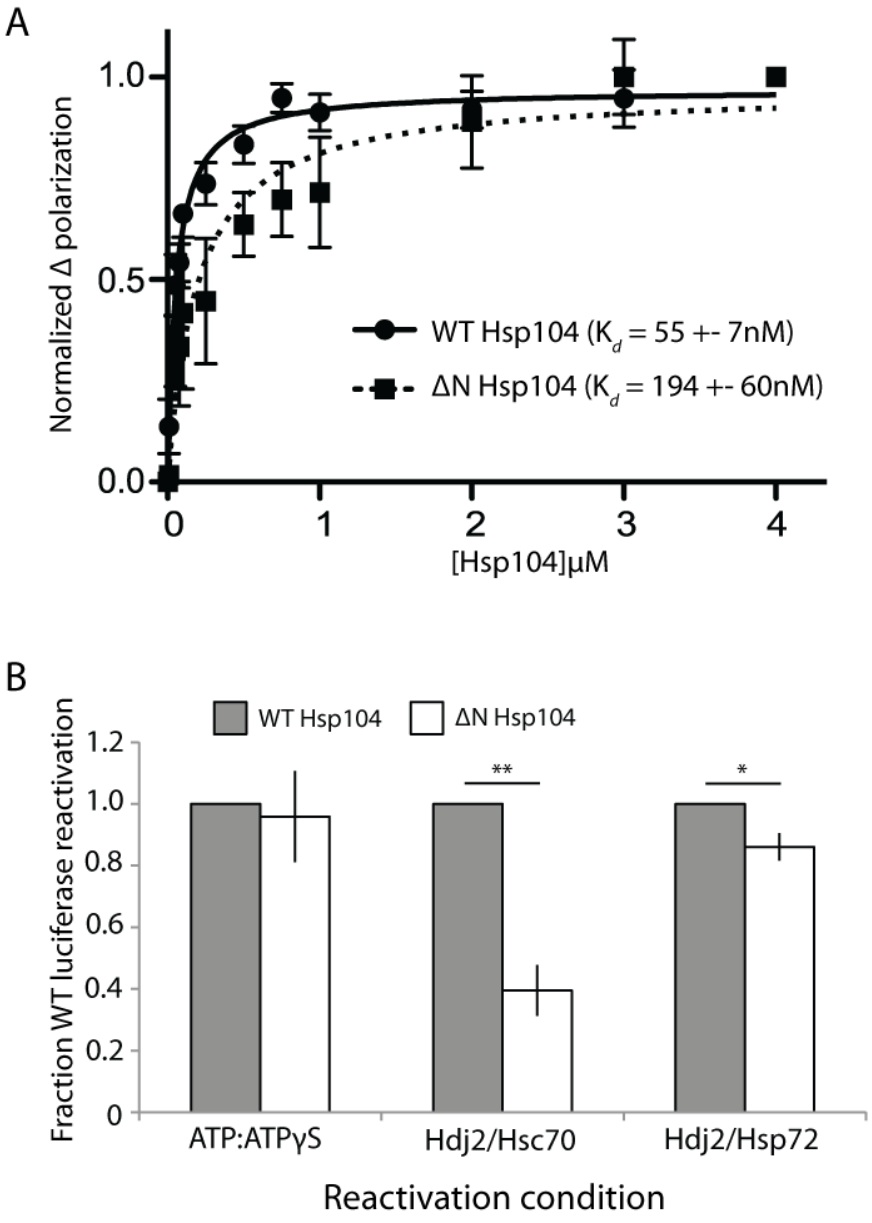

Figure 4. Substrate binding and reactivation. A) FITC-casein, 2mM ATPγS and either WT or an NTD deletion (ΔN) Hsp104 were incubated for 20 min at 25˚C. Fluorescence polarization was measured at increasing concentrations of Hsp104 and a single site Kd was calculated using a least squares fit to the data. Each data point represents mean ± S.E. (n=4-5). B) Urea-denatured firefly luciferase was incubated with either WT or ΔN Hsp104 for 90 min at 25˚C in the presence of either ATP:ATPγS; 2.6 mM ATP and 2.5mM ATPγS, or Hdj2/Hsc70; 5.1 mM ATP, 1 μM Hdj2 and 1 μM Hsc70, or Hdj2/Hsp72; 5.1 mM ATP, 1 μM Hdj2 and 1 μM Hsp72. Reactivation of luciferase was then determined by measuring luminescence and converted to fraction WT disassembly activity for each condition. Values represent mean ± S.E. (n=3-7). Two-tailed t-tests were performed with * denoting $p < 0.05$ and ** $p < 0.02$.

making contacts with the MD, stabilizing the interaction between the MD and Hsp70. Whether direct, or indirect, it is clear that the NTD plays a role in Hsp70 interaction.

3.2.3.4 The N-terminal domain controls Hsp104 cooperativity through a network of NTD:NBD1:MD interactions that include the NTD-NBD1 linker

To understand how the NTD may be communicating with neighboring domain(s) and how these interactions may change depending on the identity of nucleotide, we can first look for regions that undergo changes in solvation between different states. These regions include the beginning of helix 1 (residues 8-15), the loop between helix 2 and 3, the loop between helix 3 and 4, and the linker between the NTD and NBD1 (Figure 3C-E). A peptide that covers the beginning of H1 starting at residue 8, appears to be unmodified in the hexamer with ADP, but has a rate of 1.85 +- 0.33 s^{-1} in the hexamer with ATPγS (Table 5). The loop between H2 and H3, residues 41-51, is covered by the peptide 39-53, which has rates for the ADP and ATPγS hexamers of 25 +- 0.005 and 4.3 +- 1.5 s^{-1}, respectively (Table 5). The loop between H3 and H4, residues 58-61, is covered by the peptide 55-64. This peptide is unmodified in the monomer, and has rates for the ADP and ATPγS hexamers of 3.6 +- 0.009 s^{-1} and 0.85 +- 0.18 s^{-1}, respectively (Table 5). Additionally, this peptide displayed a 2-fold protection from hydrogen-deuterium exchange in the hexamer with ADP, and a 10-fold protection in the hexamer with ATPγS (Table 6). The linker between the NTD and NBD1 is covered by the peptide 148-166 in all three states (Figure 3C-E). It is unmodified in the hexamer with ATPγS, has a rate of 0.101 +- 0.002 s^{-1} in the hexamer with ADP, and 0.215+- 0.014 s^{-1} in the monomer (Table 5).

Then we can compare these regions from XF to the three tClpB monomer models. In the crystal structure of tClpB, each monomer of the spiral trimer (designated models A, B and C in the pdb) has a different orientation of the NTD [102]. By examining the different orientations of the NTD we discovered regions of the NTD, NBD1, and MD that appeared to be capable of

interacting in one or all of the three models. The homologous Hsp104 NTD residues include 8-20 found in models A and B, NBD1 residues 264-274 found in models A and C, MD residues 496-498 found in models A and C, and NTD residues 39-52, NTD/NBD1 residues 155-169, and NBD1 residues 230-240 found in all three of the models. Many of these regions display changes in solvation, as mentioned above. These include the beginning of helix 1, residues 8-15 in particular (Figure 5 in yellow), which are protected from solvation in the hexamer with ADP, the loop between H2 and H3, residues 39-53 (Figure 5, in orange), which shows a decrease of solvation in the hexamer with ATPγS, and the NTD-NBD1 linker region, 148-166 which shows a protection from solvation in the hexamer with ATPγS. If we briefly investigate the regions in NBD1 and the MD we find that residues 230-240 (Figure 5, in blue) are covered by a number of peptides, which are always unmodified in both hexameric states (Tables 3 and 4). In fact, the peptide 225-243 is unmodified in the hexamers while the monomer has a modification rate of 15.9 +- 11.2 s^{-1} (Table 5). Residues 262-274 display no clear trend in modification rate (Tables 2, 3 and 4), and residues 496-498 (Figure 5, in green), covered by the peptide 494-504 are found unmodified in the monomer and the hexamer with ATPγS, but the peptide was not found in the hexamer with ADP. These findings indicate that the NTD, specifically the beginning of helix 1 in the hexamer with ADP, and the H2-H3 loop and NTD-NBD1 linker in the hexamer with ATPγS may be making a stable interaction with NBD1, specifically residues 230-240, and potentially the MD, in the loop between MD helices 2 and 3 in motif 2 (Figure 5). Since we know from Chapter 2 that the NTD is involved in regulating the ATPase rate and is essential for global cooperativity of the hexamer, we suggest that these interactions may mediate signals from substrate and/or Hsp70 interactions in the NTD to the rest of the hexamer. Further support of this model is the fact that an NTD mutant, T160M, which resides in a region proposed to interact with NBD1 and/or the MD was found to mimic the NTD deletion phenotype *in vivo* [154]. Additionally, other regions identified by peptide array as potential Hsp70 binding sites include residues 34-39 [178], just N-terminal of the H2-H3 loop, and 241-249 [178], just C-terminal of the unmodified 230-240 NBD1 region, indicating that there may be a complex network of NTD-NBD1-MD:Hsp70 interactions, which the XF solvation

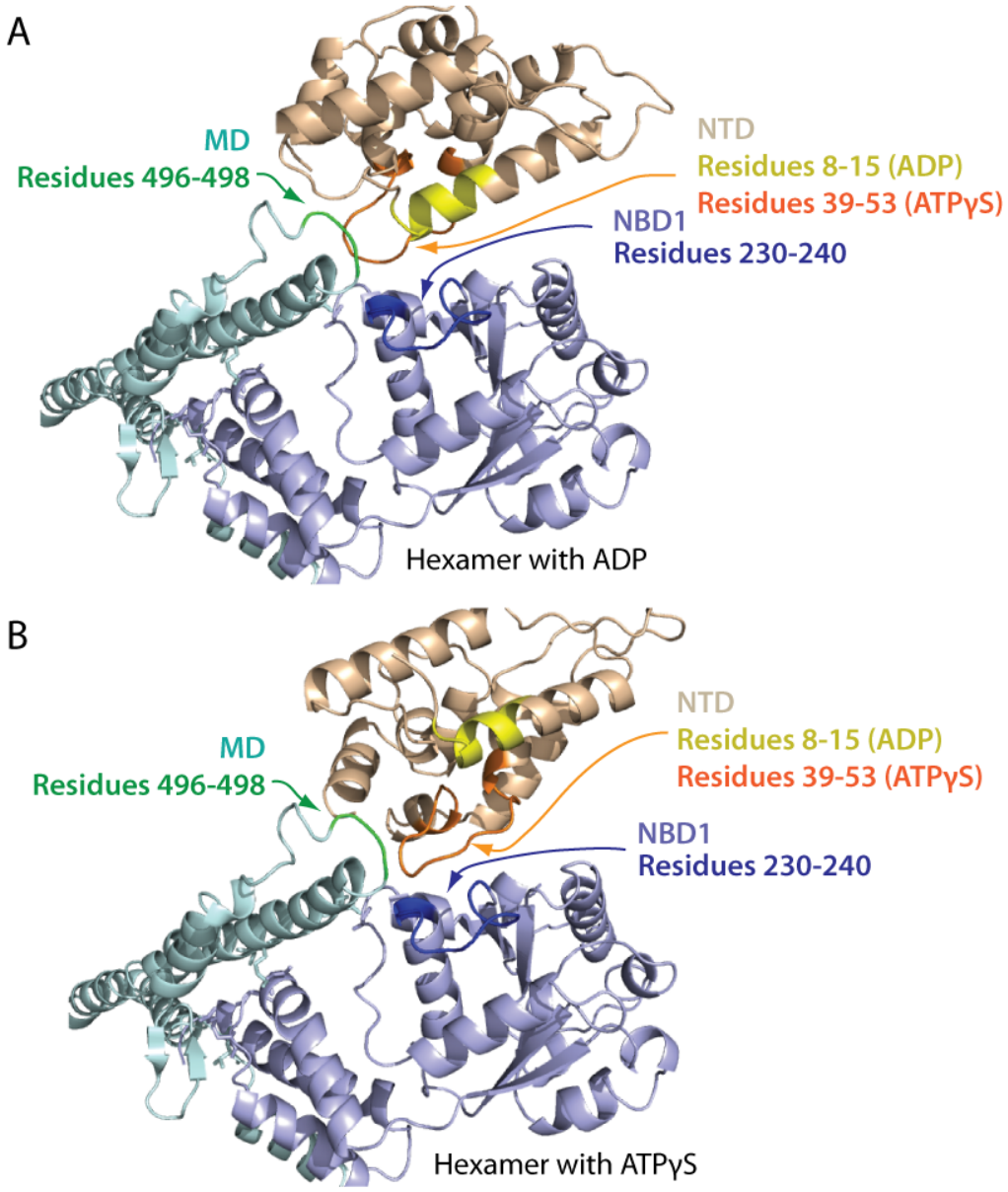

Figure 5. Potential NTD-NBD1-MD interface. Based on the solvation data from x-ray footprinting (XF) there may be regions of the Hsp104 NTD, NBD1 and MD which make contacts that are nucleotide dependent. In the NTD these regions are the beginning of helix 1 in the hexamer with ADP (residues 8-15 in yellow), and the H2-H3 loop (residues 39-53 in orange) and NTD-NBD1 linker (not pictured) in the hexamer with ATPγS. Based on the XF data as well as the three monomeric tClpB crystal structures (pdb: 1qvr), these may be making a stable interaction with NBD1 (specifically residues 230-240 in blue), and in the hexamer with ATPγS the MD in the loop between MD helices 2 and 3 in motif 2 (residues 496-498 in green). Shifts in these contacts in response to stimuli such as Hsp70 binding, substrate binding, or ATP hydrolysis could transmit signals through the hexamer and facilitate cooperativity.

data has allowed us to map (Figure 5). Mutations in this region, specifically D498V [179], T499D and I230N (Amber Tariq, Shorter lab unpublished data) lead to potentiated Hsp104 variants, and deletion of the NTD precludes this potentiation. These findings suggest that this interface is, in fact, important for hexamer regulation and activity.

3.2.4 Nucleotide-binding domain 1

3.2.4.1 AAA+ motifs

We know from the literature that NBD1 is a high affinity, high turnover site for ATP binding and hydrolysis [140]. NBD1 is the main site of ATP hydrolysis for the Hsp104 hexamer [140], but does not drive hexamerization [140]. Since we know that ATP binding and hydrolysis is required for Hsp104 activity, we wanted to examine changes in solvation of the conserved AAA+ motifs between the hexamer with ADP and hexamer with ATPγS. Overall, the domain is more modified in the hexamer with ADP than the hexamer with ATPγS (Figure 6A-C), particularly in the regions involved in the conserved ATP binding pocket. The Walker A motif, residues 212-220, the Walker B motif, residues 280-285, the sensor-1 residue, T317 and the arginine finger, R334 are covered by peptides which suggest that in the hexamer with ATPγS the ATP binding pocket is protected from solvation (Figure 6A). The peptide 211-223 shows no modification in the ATPγS hexamer, but a rate of 32.6 +- 1.9 s^{-1} in the hexamer with ADP (Table 5). The peptides 282-299, 283-299 and 286-310 also show no modification in the hexamer with ATPγS but rates of 75 +- 0.58 s^{-1}, 28 +- 0.42 s^{-1}, and 27 +- 0.3 s^{-1} respectively in the hexamer with ADP (Table 5). The peptides 300-320 and 311-320, which cover the sensor-1 residue T317, show that the hexamer with ADP is much more solvated than the hexamer with ATPγS, with rates of 145.6 +- 3.4 s^{-1} and 2.8 +- 0.03 s^{-1} for ADP and 0 and 0.37 +- 0.07 s^{-1} for ATPγS respectively (Table 5). Finally, the peptides 331-350 and 332-349 that cover the arginine finger R334 are unmodified in the hexamer

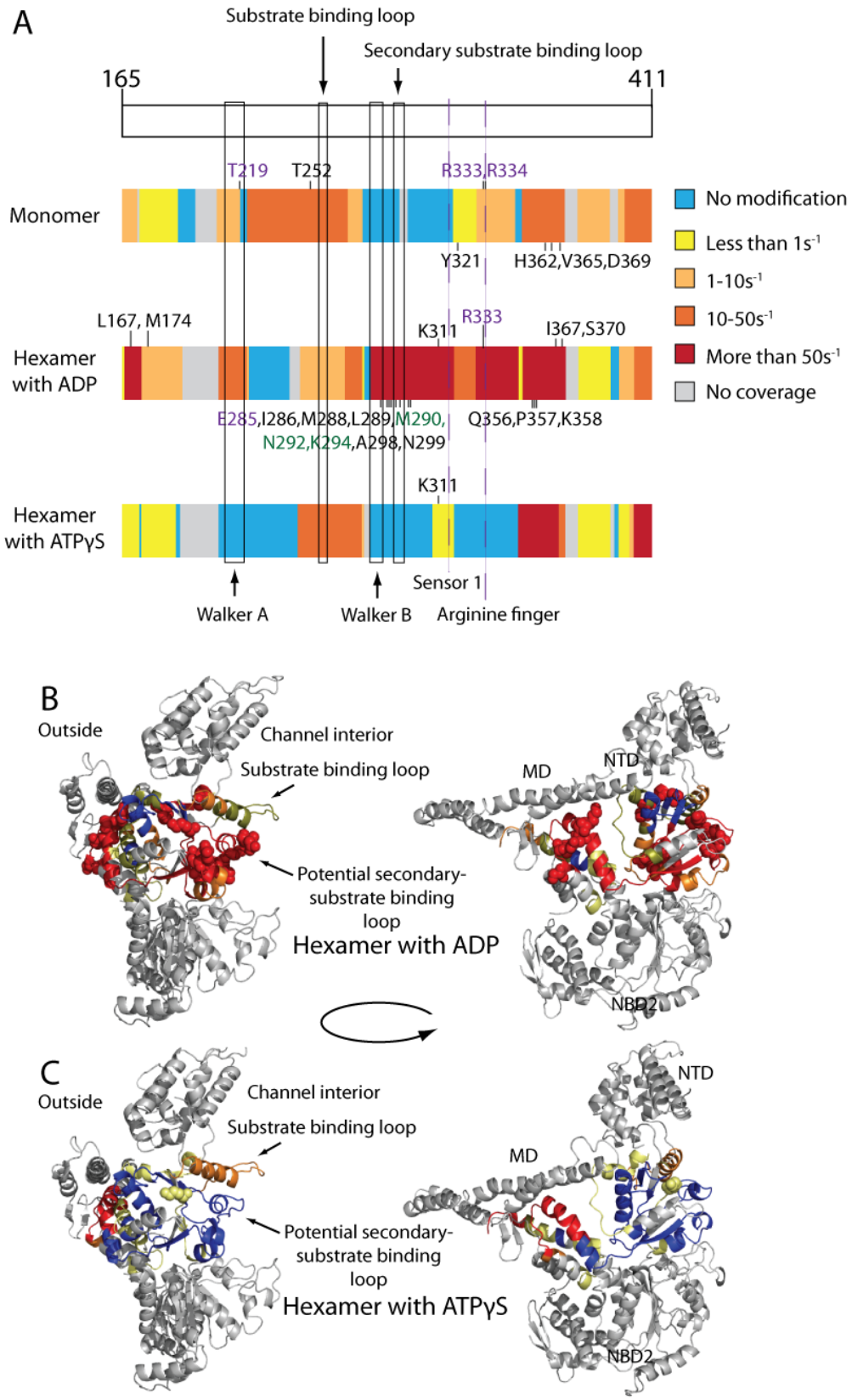
A
Substrate binding loop
Secondary substrate binding loop
165
411
T219
T252
R333,R334
Monomer
Y321
H362,V365,D369
L167, M174
R333
K311
I367,S370
Hexamer with ADP
E285,I286,M288,L289,M290,
N292,K294,A298,N299
Q356,P357,K358
K311
Hexamer with ATPγS
Sensor 1
Walker A
Walker B
Arginine finger
No modification
Less than 1s-1
1-10s-1
10-50s-1
More than 50s-1
No coverage
B
Outside
Channel interior
Substrate binding loop
MD
NTD
Potential secondary-substrate binding loop
Hexamer with ADP
NBD2
C
Outside
Channel interior
Substrate binding loop
NTD
MD
Potential secondary-substrate binding loop
Hexamer with ATPγS
NBD2

Figure 6. Hsp104 nucleotide binding domain 1 (NBD1) organization and x-ray footprinting solvation information. A) Bar graph showing XF modification rates of peptides covering the Hsp104 NBD1. Peptides with the highest rate for a given region are on the on the top layer. Blue is unmodified, yellow less than 1 s^{-1}, light orange 1-10 s^{-1}, dark orange 10-50 s^{-1}, red more than 50 s^{-1}, and gray is no coverage. Marked residues have been identified as modified by MS2 and are colored for their involvement in nucleotide binding, in purple, or the proposed secondary substrate binding loop, in green. NBD1 homology modeled off the tClpB crystal structure (pdb: 1qvr) shown in context of a rigid body fit Hsp104 monomer (fit into the SAXS volume envelope from the Hsp104 hexamer with ATP). Blue is unmodified, yellow less than 1 s^{-1}, gold 1-10 s^{-1}, orange 10-50 s^{-1} red more than 50 s^{-1}, and gray is no coverage, colored based on the XF modification rates for the hexamer with B) ADP and C) ATPγS. Residues identified by MS2 as modified are shown as spheres and colored based on rate.

with ATPγS, and have rates of 133.5 +- 3.4 s^{-1} and 3.8 +- 0.3 s^{-1} in the hexamer with ADP respectively (Table 5). Additionally, residues in these regions were identified as modified by MS2 in the hexamer with ADP including the essential Walker B glutamate, residue E285, as well as R333, the residue directly preceding the arginine finger R334 (Table 5, Figure 6A). A recent paper from the Tsai lab found that mutation of either R333 or R334 results in a loss of ATPase activity [225], indicating that both may be involved in the role of arginine finger. These differences in solvation (Figure 6A) indicate that the six conserved ATP binding pockets of NBD1 in the hexamer with ATPγS are either all occupied, or all either occupied or closed (i.e. unoccupied, but shielded from solvent). This observation would fit with hexameric structures of AAA+ proteins seen to have some sites occupied by nucleotide, and the consequent asymmetric conformational changes forcing other sites closed [226]. This steric hindrance of all sites binding ATP simultaneously has been postulated to contribute to substrate handling mechanisms [101, 137, 226]. Regardless of whether the NBD1 nucleotide-binding sites are all bound to ATPγS or some bound and the rest closed, this situation is clearly not the case for the hexamer with ADP. In the presence of ADP, there is a large degree of solvation in the nucleotide-binding, which indicates that either the ADP is either not large enough, or not rigidly bound enough to fully protect the

participating residues, or that some sites are bound to ADP while others are open and unbound to nucleotide.

3.2.4.2 Nucleotide-binding domain 1 contains a conserved loop with a potential role in substrate interaction

Though two substrate-binding loops have been identified in Hsp104 [167], the incomplete defect in thermotolerance when the NBD1 loop is mutated [167] indicates that there may be additional regions of NBD1 involved in substrate binding. The canonical substrate binding loop, 256-KYKG-259 [167], is oxidatively modified in both hexameric states, indicating that the loop is solvated and capable of substrate interaction (Figure 6A-C, Tables 3 and 4). Though rate information for identical peptides is unavailable for both states, peptides that cover the loop are have much higher rates of modification in the hexamer with ATPγS than for the hexamer with ADP (compare 10.6 +-5.3 s^{-1} and 18.2 +- 0.37 s^{-1} for peptides from the hexamer with ATPγS to 0.51 +-0.12 s^{-1} and 1.15 +- 0.08 s^{-1} for peptides from the hexamer with ADP - Tables 3 and 4). As the Hsp104 hexamer primarily binds substrate in the ATP state [204, 227], it is unsurprising that the loop would be more exposed in the hexamer with ATPγS than in the hexamer with ADP. While Y257 has been identified as one of two substrate binding residues in Hsp104, thermotolerance assays show that mutation of the tyrosine to alanine results in only minor defects in Hsp104 mediated survival [167]. This is in contrast to mutation of the NBD2 tyrosine, Y662 to alanine, which results in large defects in survival after heat shock [167]. This finding led us to hypothesize that regions of the NTD as well as other sites within NBD1 may also contribute to substrate binding. As discussed in the preceding section, the NTD is indeed involved in substrate binding (Figure 4A). This finding is further supported by thermotolerance data showing that while either deletion of the NTD or mutation of Y257 display only mild defects in thermotolerance, the combined truncation and mutation variant, ΔN:Y257A Hsp104 is severely compromised in its ability to mediate survival after heat shock (Figure 7A). To determine if there are other substrate

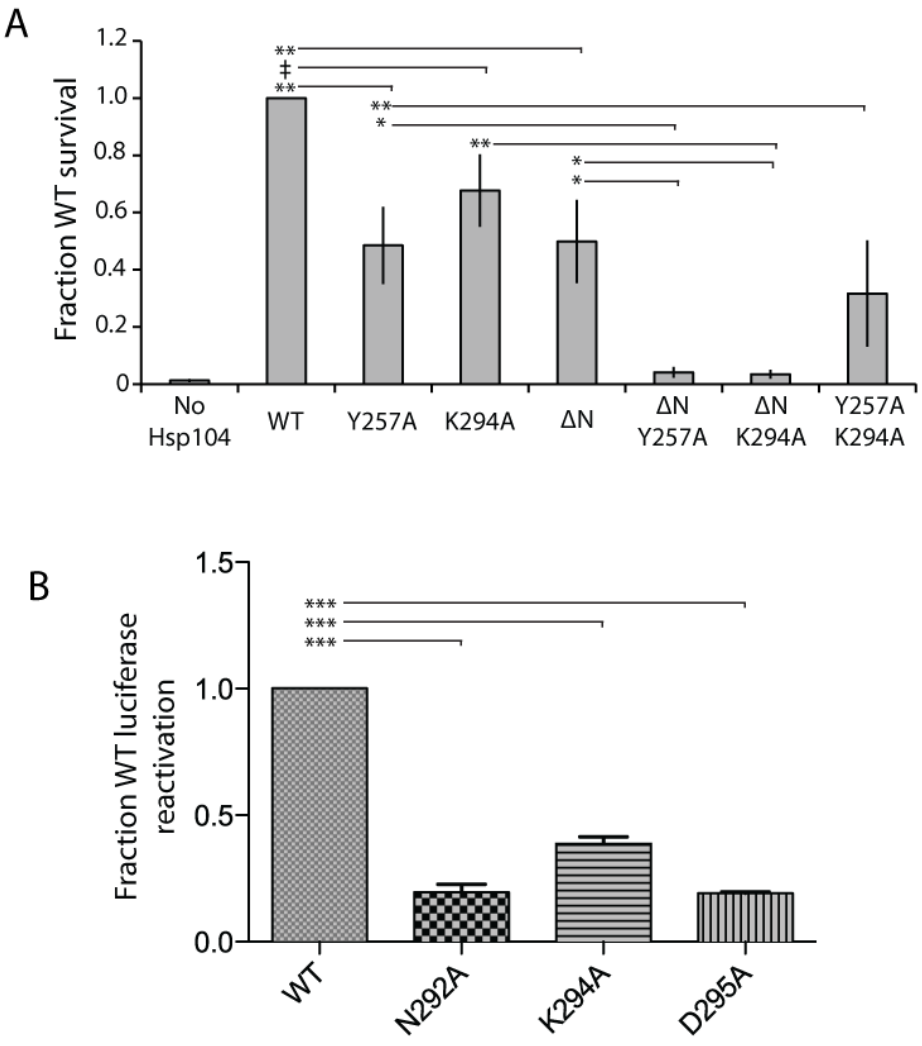

Figure 7. Thermotolerance and luciferase reactivation of NBD1 mutants. A) After incubation at 37°C for 30 min to induce Hsp104 expression, cells were heat shocked for 20 min at 50°C, immediately transferred to ice for 2 min, plated on SD-ura plates, and after a 2-day incubation at 30°C colonies were counted using an acolyte automated colony counter. Values represent mean ± S.E. (n=3-14). Equal expression levels were confirmed by immunoblot (Work of Michelle Go, Shorter lab). Comparisons between WT Hsp104 and single variants were assessed using a two-tailed t-test with ‡ denoting $p = 0.05$, * $p < 0.05$ and ** $p < 0.02$. To determine whether the defects were additive, double mutants were assessed using a single-tailed t-test with * denoting $p < 0.05$ and ** $p < 0.02$. B) Urea-denatured firefly luciferase was incubated with either WT or an Hsp104 substrate binding loop 2 variant (291-GNGKD-295), for 90 min at 25˚C in the presence of 2.6 mM ATP, 2.5mM ATPγS and an ATP regenerating system (1 mM creatine phosphate, 0.25 µM creatine kinase). Reactivation of luciferase was then determined by measuring luminescence and converted to fraction WT disassembly activity for each condition. Values represent mean ± S.E. (n=3). Two-tailed t-tests were performed with *** denoting $p < 0.0002$.

binding regions of NBD1 we looked for regions that change in solvation in the different hexamers. A striking example stood out immediately. In the homology model of the Hsp104 NBD1 there are two loops that point into what would be the interior of the hexameric Hsp104 channel (Figure 6A-C). One is the canonical 256-KYKG-259 loop and the second is the 291-GNGKD-295 loop. Peptides covering the 291-GNGKD-295 loop are unmodified in the hexamer with ATPγS, but highly modified in the hexamer with ADP (the peptides that cover the Walker B site also cover this loop) (Figure 6A-C, Table 5). In addition to the peptides (282-299, 283-299 and 286-310, Table 5) displaying high rates of modification in the hexamer with ADP (75 +- 0.58 s^{-1}, 28 +- 0.42 s^{-1}, and 27 +- 0.3 s^{-1}, respectively, Table 5) three residues within and near the 291-GNGKD-295 loop were identified as modified by MS2, including N292, and K294 (Figure 6A). This loop is homologous to the ClpC 286-GAGGA-290 [143] loop, as well as the ClpA 292-GAGAA-296 [168] loop, which are secondary substrate binding loops. Mutation or deletion of this loop results in severe defects in ClpC [143] and ClpA [168] activity.

We decided to test our hypothesis that this loop is involved in substrate processing in Hsp104. To assess whether this loop is actually necessary for Hsp104 activity, we carried out *in vivo* thermotolerance and *in vitro* luciferase reactivation assays, as well as fluorescence polarization assays to test for differences in K_ds. Fluorescence polarization experiments revealed that mutations in the loop, N292A, K294A and D295A, had no statistically significant effect on FITC-casein binding in the presence of ATPγS (Table 7). This result was to be expected since the loop appears to be protected from solvent in the hexamer with ATPγS, and is therefore unlikely to interact with substrate in this state. Since initial and robust substrate binding appears to occur in the Hsp104 hexamer with ATP, one possibility is that this second loop transiently engages the substrate during or after ATP hydrolysis to ADP. This interaction could prevent substrate diffusion as the subunits in the hexamer rebind ATP and subsequently reengage the polypeptide at a new site, thereby driving directional translocation of the substrate. We decided to test whether there were differences in FITC-casein binding in the presence of ADP. WT Hsp104 binds FITC-casein

Table 7. K_d values for mutations in the potential secondary substrate binding loop of NBD1. Changes in the fluorescent polarization of FITC-casein were measured in the presence of increasing concentrations of Hsp104 variants. Data were fit using a single-site specific binding curve. Values represent mean ± SE (n = 3) and do not display statistically significant differences.

Hsp104 variant:	K_d for FITC-casein (6 nM) with ATPγS	K_d for FITC-casein (100 nM) with ADP
WT	69 ± 9 nM	6.1 ± 1.1 μM
N292A	93 ± 31 nM	6.0 ± 1.4 μM
K294A	114 ± 21 nM	6.6 ± 0.7 μM
D295A	96 ± 13 nM	4.2 ± 0.5 μM

in the presence of ADP with a K_d of 5.9 +- 0.7 μM, 2 orders of magnitude weaker than in the presence of ATPγS. When we tested our loop mutants, we found that once again there were no statistically significant changes in affinity (Table 7). And this may not be surprising. If our model is correct, substrate would first need to engage the Hsp104 hexamer in the presence of ATPγS, and then be handed off to the second loop. In our experimental set-up the Hsp104 hexamer is incubated with ADP and then FITC-casein is added. In these conditions we may not expect substrate to bind in a manner indicative of how the Hsp104 hexamer normally processes substrate.

In vivo thermotolerance assays revealed that the K294A Hsp104 variant displayed a slight, but statistically significant (p=0.05), defect in mediating survival after heat shock compared to WT Hsp104 (Figure 7A, work of Michelle Go, Shorter lab). When the K294A mutation was combined with the NTD truncation, survival after heat shock was similar to the ΔN:Y257A variant (Figure 7A, work of Michelle Go, Shorter lab). The double mutant Y257A:K294A variant was less active than the single mutants, but more active than the single mutants combined with the NTD truncation (Figure 7A, work of Michelle Go, Shorter lab). This *in vivo* data supports a role for the loop in substrate processing. We then wanted to test the mutants in an *in vitro* assay with minimal components so that we could remove the confounding and potentially mitigating effects of the

presence of various Hsp70 and other chaperone proteins. To test the activity of the loop mutants in a minimal component situation, we carried out luciferase reactivation assays in the presence of a 1:1 ratio of ATP:ATPγS. What we found was that the loop mutants N292A, K294A and D295A were defective in luciferase reactivation, retaining only 20%, 39% and 19% of WT Hsp104 respectively (Figure 7B). This finding confirmed the importance of this loop for productive substrate remodeling, and indicates that defects caused by mutations in the loop can, in fact, be partially mitigated by the *in vivo* environment. Ideally we would be able to test whether our proposed mechanism for the loop, preventing substrate diffusion as subunits rebind ATP, is correct. An assay designed to measure release of substrate due to ATP hydrolysis after initial binding events would be able to confirm whether mutations in the loop result in more, or faster release of substrate. An alternative would be to measure processivity of the WT and mutant Hsp104 variants.

3.2.5 Solvation of the middle domain changes dramatically in the presence of different nucleotides, which supports a role in Hsp104 regulation

We aimed to use information from the literature as well as our solvation data from the XF experiments to get a holistic understanding of how local and global dynamics of the MD determine its role in regulating the hexamer. The homology model of Hsp104's anti-parallel coiled-coil middle domain (MD), based off of the tClpB structure, retains the leucine zipper-like interactions between the helices 1-4 (Figure 8B and C). The arrangement of large hydrophobic residues such as leucine and isoleucines at the helical interfaces, with polar and charged residues exposed on the other side of the helices, is an indication that the model is sound. Additionally, hydrogen-deuterium exchange experiments confirm the loop-secondary structure boundaries (data not shown, Alec Ricciuti and Walter Englander manuscript in preparation). The MD has been implicated in regulating the ATPase rate and activity of the hexamer [136, 145, 172, 173, 175-177, 228-230], transmitting signals between NBD1 and NBD2 [181, 228, 229], and

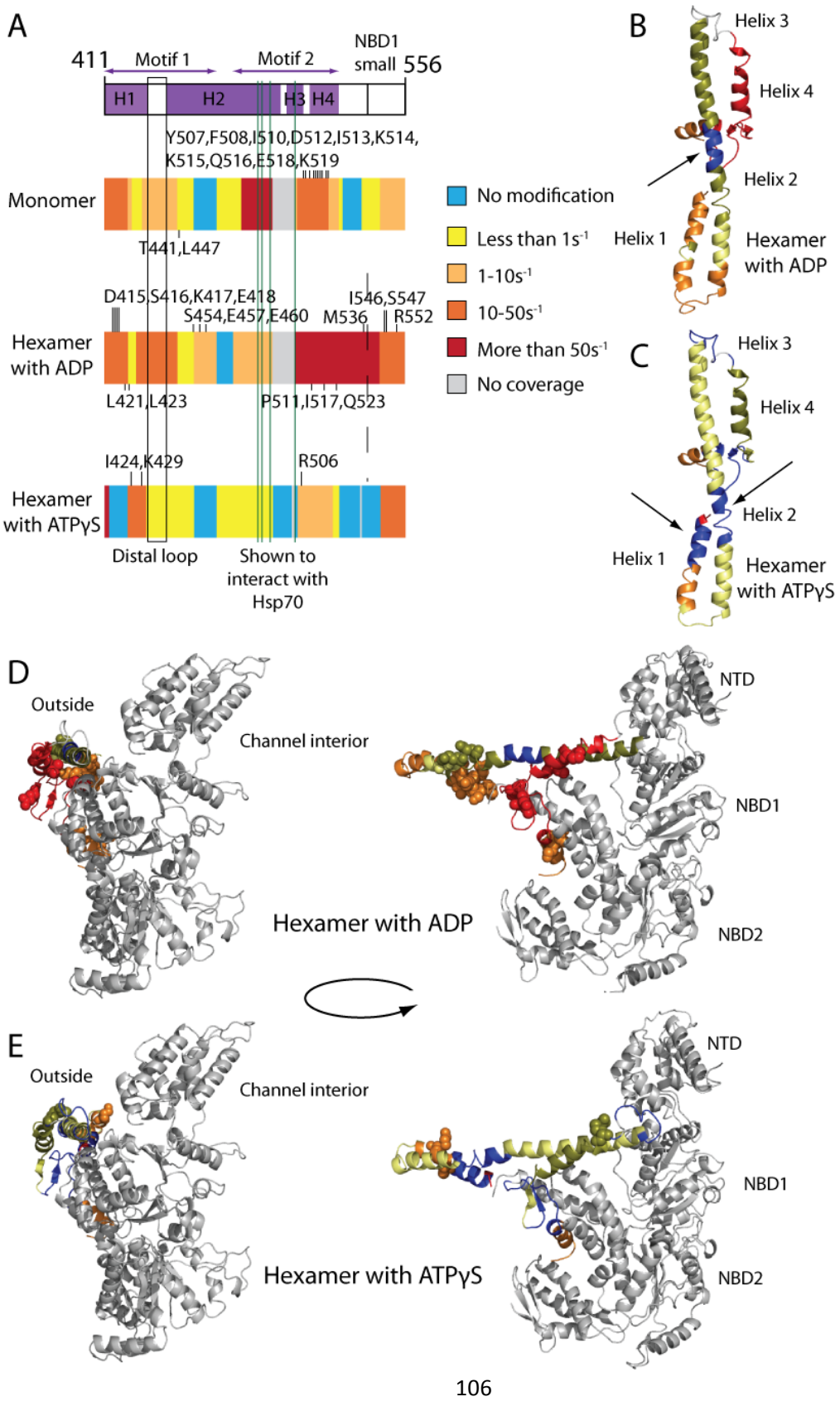
A
411
Motif 1
Motif 2
NBD1
small
556
H1
H2
H3
H4
Y507,F508,I510,D512,I513,K514,
K515,Q516,E518,K519
Monomer
T441,L447
D415,S416,K417,E418
S454,E457,E460
M536
I546,S547
R552
Hexamer
with ADP
L421,L423
P511,I517,Q523
I424,K429
R506
Hexamer
with ATPγS
Distal loop
Shown to
interact with
Hsp70
No modification
Less than 1s-1
1-10s-1
10-50s-1
More than 50s-1
No coverage
B
Helix 3
Helix 4
Helix 2
Helix 1
Hexamer
with ADP
C
Helix 3
Helix 4
Helix 2
Helix 1
Hexamer
with ATPγS
D
Outside
Channel interior
NTD
NBD1
NBD2
Hexamer with ADP
E
Outside
Channel interior
NTD
NBD1
NBD2
Hexamer with ATPγS

Figure 8. Hsp104 middle domain (MD) organization and x-ray footprinting (XF) solvation data. A) Bar graph showing XF modification rates of peptides covering the Hsp104 MD. Peptides with the highest rate for a given region are on the on the top layer. Blue is unmodified, yellow less than 1 s^{-1}, light orange 1-10 s^{-1}, dark orange 10-50 s^{-1}, red more than 50 s^{-1}, and gray is no coverage. Marked residues have been identified as modified by MS2. Green lines are sites of Hsp70 interaction. The isolated MD modeled off the tClpB crystal structure (pdb: 1qvr) and colored, blue unmodified, yellow less than 1 s^{-1}, gold 1-10 s^{-1}, orange 10-50 s^{-1} red more than 50 s^{-1}, and gray no coverage, based on the XF modification rates for the hexamer with B) ADP and C) ATPγS. Arrows highlight the regions that undergo large changes in solvation and secondary structure between the two nucletide bound states and may be responsible for transmitting signals between NBD1 and NBD2. The MD shown in context of a rigid body fit Hsp104 monomer (fit into the SAXS volume envelope from the Hsp104 hexamer with ATP but not necessarily representative of its placement or dynamics, as explained further in the text), colored as in B) and C) based on the XF modification rates for the hexamer with D) ADP and E) ATPγS. Residues identified by MS2 as modified are shown as spheres.

mediating the interaction with Hsp70 [172-175, 178]. Interactions with Hsp70 proteins have shown to take place in motif 2, specifically residues 480-KKK-482 and residue R496 [178]. We have already discussed in the preceding sections how these regions are poised to interact with the NTD as well as NBD1 (Figure 5). In ClpB a number of interactions between motif 2 of the MD and NBD1 have been identified [102, 172, 176, 231] and it has been shown that stabilization of these interactions leads to repression of the disaggregase [102, 172, 176], while destabilization leads to potentiation [102, 176, 179, 231]. While the models in Figure 8 show the MD partially projecting into solution, it is simply representative of one possible orientation. XF data as well as published crosslinking [176, 222] and structural data [176] support a model in which the domain is highly mobile, undergoing interactions with both NBD1 [102, 172, 176, 231] and NBD2 [222]. Additionally, it is likely that MDs within a given Hsp104 hexamer occupy a variety of positions [176]. The orientation shown in Figure 8 is fit into a symmetrically averaged volume envelope, and future work would include modeling the domain asymmetrically into the hexamer in a variety of positions based on a compilation of the published data and XF information

XF data of the MD shows large changes in solvation between the hexamer bound to ADP and the hexamer bound to ATPγS (Figure 8A-E). This finding is to be expected since the domain is highly dynamic, and restricting its movement through disulfide crosslinking greatly impairs Hsp104 activity [102, 172, 222]. In general, the hexamer with ADP displays greater solvation than the hexamer with ATPγS (Figure 8A-E, Tables 3-5). The only part of the MD where this is not true is the first three residues of the MD, 412-414, found on the peptide 405-414, which mainly covers the NBD1 domain (Table 5). This peptide is solvated in both hexameric states, but more so in the presence of ATPγS (compare 21.5 +- 0.4 s^{-1} to 52.8 +- 9.5 s^{-1}, Table 5). Modification rates change at the adjacent peptide. The peptide 415-423 shows that the hexamer with ATPγS is unmodified while the hexamer with ADP has a modification rate of 35.5 +- 0.8 s^{-1} and contains several residues identified as modified by MS2: D415, S416, K417, E418, L421 and L423 (Table 5, Figure 8A).

This peptide covers the first half of helix 1, and is adjacent to a region of helix 2, residues 456-466, which is also unmodified in the hexamer with ATPγS (Figure 8C, see arrows). This peptide, 456-466, has a modification rate of 1.8 +- 0.5 s^{-1} in the hexamer with ADP and contains residues identified as modified by MS2, E457 and E460 (Table 5, Figure 8A). A region more C-terminal in helix 2, residues 467-474, is unmodified in the hexamer with ADP, but is modified in the hexamer with ATPγS. A peptide that covers this region, 467-493, is unmodified in the hexamer with ADP, and has a modification rate of 0.84 +- 0.1 s^{-1} in the hexamer with ATPγS (Table 5). Interestingly, the same peptide shows large changes in protection from deuterium exchange. From monomer to apo hexamer to hexamer with ADP to hexamer with ATPγS the peptide undergoes increases in protection from 2- to 10- to 50-fold respectively (Table 6, Alec Ricciuti). The changes in solvation and secondary structure indicate that transitions in this region of helix 2 may play a role in transmission of conformational changes from motif 1 to motif 2 in response to stimuli (e.g., interaction with Hsp70, binding of substrate in the NTD and NBD1, and ATP hydrolysis at NBD1 or NBD2). It's been shown that the MD is crucial for communication

between NBD1 and NBD2 [181, 228, 229], for example, in ClpB ATP binding in NBD1 leads to large movements of the MD and subsequently promotes hydrolysis in NBD2 [229] (this communication route may be reversed in Hsp104 since the role of the two nucleotide binding domains is transposed between ClpB and Hsp104 [135], or could be bi-directional). Additionally, a mutation in this region, L462R, was discovered to disrupt intersubunit cooperativity [132], suggesting that this region is critical for communication within the Hsp104 hexamer.

Several crosslinks between motif 2 of the MD and NBD1 have been found, in ClpB: G175C:S499C [172], D178C:S499C [172], G167C:R475C[102], V350C:Q467C[102], G353C:R464C[102], R355C:E520C[102], K476C:E358C[176] and in Hsp104 there may be a salt bridge D484:D184:K358 [231]. Models proposing that this motif 2-NBD1 interaction is dynamic are supported by the solvation data which shows large increases in solvation in the hexamer with ADP compared to the hexamer with ATPγS (Figure 8A-E). These increases in solvation include the C-terminal end of helix 2 (Tables 3 and 4) as well as the end of helix 3 through the end of the MD (peptides 505-526, 506-522, and 508-536 with rates for the hexamer with ADP of 350 +- 0.9 s^{-1}, 20 +-1.2 s^{-1}, and 89 +- 3.4 s^{-1} respectively versus 0 s^{-1}, 1.5 +- 1 s^{-1}, and undetermined for the hexamer with ATPγS) (Table 5). Residues 494-504 are not found in the hexamer with ADP but are unmodified in the hexamer with ATPγS. This finding indicates that helices three and four of motif 2 are partially shielded from solvent in hexamer bound to ATPγS. If this protection from solvent is representative of the repressive motif 2-NBD1 contacts it would support a model where the repressed state of the hexamer is predominantly found in the hexamer with ATPγS. This would make sense since ATP hydrolysis is necessary for substrate remodeling. Additionally, several potentiating mutations are found in helices 3 and 4 [102, 176, 179, 231] (Dr. Meredith Jackrel, unpublished work), indicating that large changes in solvation between nucleotide bound states may indicate mechanistically important regions of the Hsp104 hexamer.

More recent work in our lab uncovered robust crosslinks between motif 1 of the MD and NBD2, A430C:F630C, and K451C:E790C [222] and mutations in the distal loop (R433-R441)

revealed that the region is crucial for transmission of Hsp70-mediated relief of the MD autoinhibition [222]. These crosslinks were predicted by a hexameric Hsp104 model in which the MD is intercalated between the NBDs [136, 137]. Confirmation of these crosslinks means that the MD cannot invariably project into solution as proposed in a second hexameric model of Hsp104 [171]. The XF data shows that the distal loop is more solvated in the hexamer with ADP than the hexamer with ATPγS (peptide 431-455 with rates of 0.57 +- 0.009 s^{-1} and 0.08 +- 0.05 s^{-1} respectively, Table 5) and that the region around residue 630 is also more solvated in the hexamer with ADP than the hexamer with ATPγS (peptide 611-631 with rates of 4.9 +- 2.2 s^{-1} and 0 s^{-1} respectively, Table 5). Peptides covering the NBD2 residue involved in the second crosslink are similar, with rates for the hexamer with ADP much higher than for the hexamer with ATPγS (peptides 789-806 and 789-809 which are unmodified in the hexamer with ATPγS but have rates of 22.3 +- 0.3 s^{-1} and 20 +- 0.2 s^{-1} respectively for the hexamer with ADP, Table 5). All of these XF modification rates match the crosslinking data well, since the crosslink was most robust with AMP-PNP, less so with ATP, and even less with ADP [222]. Therefore, data from multiple techniques confirms that the interactions of the MD and NBD2 are stabilized in the hexamer with ATPγS compared to the hexamer with ADP. These motif 1 MD-NBD2 crosslinks reveal a missing piece to the NBD1-MD-NBD2 communication network, and the changes in solvation and secondary structure at the juncture of motif 1 and motif 2 found by XF and hydrogen deuterium exchange explains how signals may be transmitted through the coiled-coil between the two nucleotide binding domains in response to ATP hydrolysis and Hsp70 binding.

3.2.6 Nucleotide-binding domain 2

3.2.6.1 AAA+ motifs

First, we will examine modification of the conserved NBD2 ATP binding motifs as well as the region that contains the nuclear localization signal (NLS) [157]. There is no coverage of either the arginine finger or the sensor 1 residue. Similarly to our findings in NBD1, a peptide 684-697

that covers the Walker B motif is unmodified in the hexamer with ATPγS but has a rate of 49 +- 1.3 s^{-1} and two residues identified by MS2 as being modified, L684, and the conserved glutamate, E687 in the hexamer with ADP (Table 5). Additionally, the peptide 813-831 that covers the sensor 2 residue (R826), is unmodified in the hexamer with ATPγS and has a rate of 42 +- 0.2 s^{-1} in the hexamer with ADP (Table 5). However, just C-terminal of the Walker B motif is a peptide 688-696, which in the hexamer with ATPγS has a modification rate of 57 +- 9.4 s^{-1}, and a peptide 613-623 which covers the Walker A motif has a rate of 9.5 +- 0.3 s^{-1} in the hexamer with ATPγS with residues 616 and 618 have been identified by MS2 as modified (Tables 4 and 5). These data indicate that in contrast to NBD1, ATPγS binding in NBD2 does not fully shield the nucleotide-binding pocket from solvent. This may be due to the presence of empty, incompletely closed sites, and/or less stable ATPγS binding, which would result in partial solvation of some of the sites with the Hsp104 hexamer population. Differences between NBD1 and NBD2 are not surprising, as they belong to different AAA+ clades [155] and are responsible for divergent functions within the Hsp104 hexamer [140].

3.2.6.2 Nucleotide-binding domain 2 nuclear localization signal (NLS)

The NLS in Hsp104, residues 773-789 [157], appears to be solvated in the monomer as well as both of the hexameric states, with the hexamer with ATPγS the least modified (Table 5, Figure 9). The NLS also includes the NBD2 hinge 773-NKLS-776, which connects the large and small subdomains of NBD2. Peptides that cover this regions include 769-785 and 786-806 with rates for the monomer, the hexamer with ADP and the hexamer with ATPγS of 1.15 +- 0.1 s^{-1}, 0.64 +- 0.003 s^{-1}, and 0.14 +- 0.02 s^{-1} respectively for 769-785 and 0 s^{-1}, 17.6 +- 6.3 s^{-1}, and 0 s^{-1} respectively for 786-806 (Table 5). There are many MS2 identified modified residues in this region, including lysines (in bold) which, when all mutated to alanine result in a loss of nuclear accumulation [157], as well as residues (in italics) that are in the NBD2 hinge. K774 may or may not be necessary for nuclear localization; since it is in the NBD2 hinge mutating it to alanine

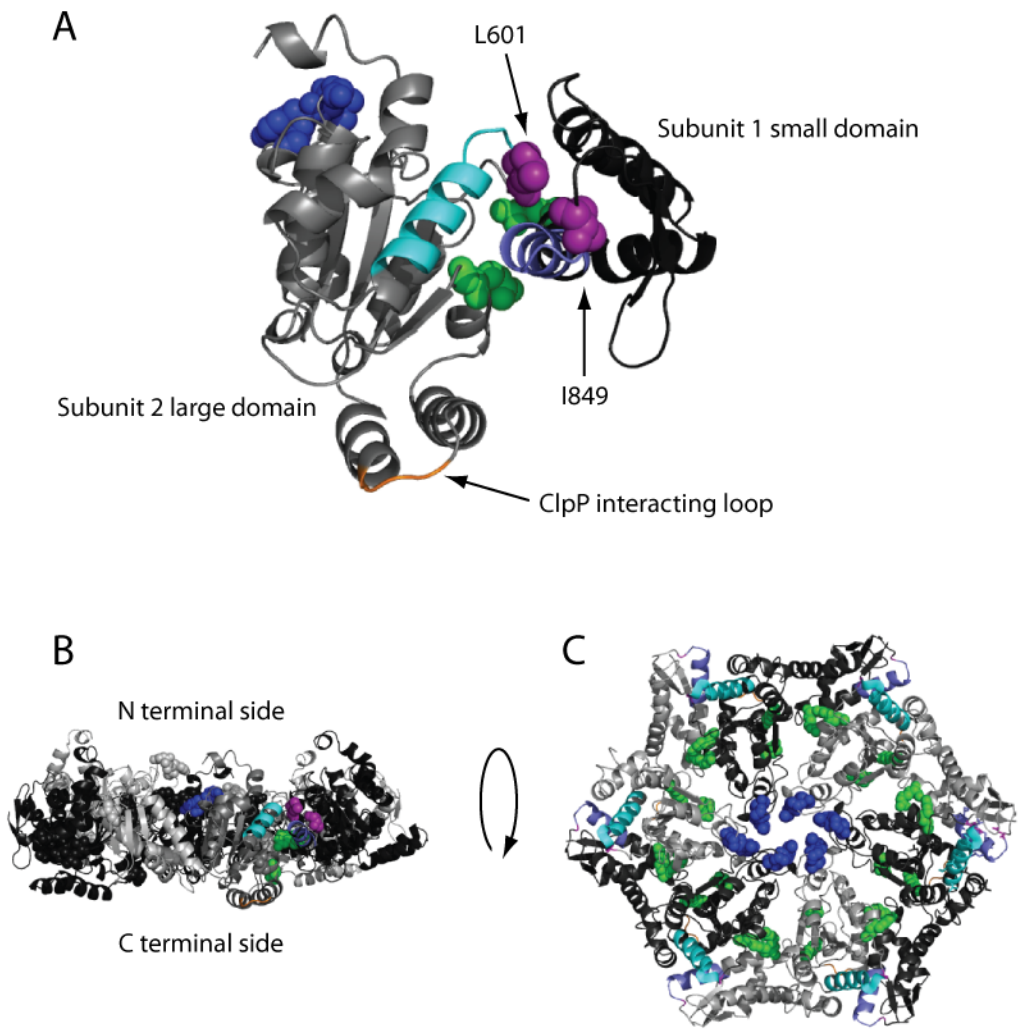

Figure 9. Proposed hexamer interface. A) Close-up of the interface between the residues 586-AIKAVSNAVRLSRSGL-601 of the large subdomain of subunit 1 in teal, and the residues 836-ILNKLALRILKNEI-849 of the small domain of subunit 2 in lavender. Conserved residues L601 (large domain) and I849 (small domain), which are in the loops immediately following the helices involved in the proposed hexamer interface, are shown as magenta spheres. The loop that can interact with ClpP when mutated (739-GSK-741, to 739-IGF-741) is shown in orange. The substrate binding loop is shown as blue spheres and AAA+ conserved residues R765 (arginine finger) and R826 (sensor 2) are shown green spheres. The entire NBD2 hexameric model is shown from the side B), or from the N-terminal side, looking down, in C). The models in B) and C) are colored as in A).

disrupts the protein's stability. The MS2 identified residues include (all found on the peptide 769-785): *N773, K774, S776*, **K778**, A779, I780, H781, **K782**, and V784 in the monomer, F772 (just before NLS), *K774*, H781, **K782,** I783, V784 found in the hexamer with ADP, and F772, *K774, S776*, R777, I780, **K782** found in the hexamer with ATPγS (Table 5, Figure 9). It would appear that K782 is always exposed to solvent, and in the monomeric state the hinge is highly exposed (3 of 4 NBD2 hinge residues were identified as modified, compared to the hexamer with ATPγS (2 of 4) and the hexamer with ADP (1 of 4)). The third essential lysine, K789 [157] is not on the peptide 769-785 and therefore we have not confirmed its solvation state.

3.2.6.3 A hexameric model of nucleotide-binding domain 2 which is consistent with the XF solvation data

The second nucleotide-binding domain (NBD2) is necessary and sufficient for Hsp104 hexamerization [160], however, a hexameric interface has yet to be described. We have used the monomeric NBD2 modeled off of the tClpB structure to create a hexameric NBD2 model (Figure 9B and C). This model uses the equivalent subunit:subunit interfaces seen in the hexameric ClpC [143] and ClpX [226] structures, and fits previously published crosslinking [225] and mutational data [182]. This interface includes helix 3 and part of its C-terminal loop in the large NBD2 subdomain (residues 586-**AI**K**AV**SN**AV**RLSRS**GL**-601, with conserved hydrophobic residues in bold), and the last helix and part of its C-terminal loop in the neighboring NBD2 small subdomain (residues 836-**I**LNK**LA**LR**IL**KNE**I**-849, with conserved hydrophobic residues in bold) (Figure 9).

There are a large number of conserved, hydrophobic residues in these regions indicating that they may be mediating the subunit:subunit interaction. If the subunit:subunit interaction was driven by hydrophobic interactions, it would explain a number of previously published phenomena. We know that the protomer interface undergoes large changes in conformation during the functional cycle of the hexamer; crosslinking the small and large subdomains results in stable hexamers with diminished function [225]. If the interface was a rigid salt bridge, it may

hinder rapid and smooth movements of the domains. If instead the region were a network of hydrophobic residues then the interface could easy change register upon conformational changes of nearby regions. The proposed interface is ideally suited to respond to changes in nucleotide – while the C-terminal end of the small NBD2 helix contains a number of conserved hydrophobic residues that we propose to be involved in the hexamer interface, the N-terminal end contains a region called the sensor and substrate discrimination (SSD) motif, which contains a sensor 2 arginine (R826) [102] (Figure 9). Additionally, the helix and loop in the NBD2 large domain that we propose to be involved in the interface is just N-terminal to a short, highly conserved β-sheet that immediately precedes the conserved Walker A motif [102].

A hydrophobic interface would also explain why the Hsp104 hexamer is sensitive to salt [140]. As salt concentrations increase, the Hsp104 hexamer becomes destabilized [140]. Upon cursory inspection, this finding would make it seem unlikely that the interface were mediated by hydrophobic interactions, however, Hsp104 undergoes continual and rapid monomer exchange [132]. Upon mixing Hsp104 hexamers with different (measurable) properties, monomer exchange occurs on a timescale of just a few minutes to yield an ensemble of hexamers containing subunits of different Hsp104 variants explained by the binomial distribution [132]. This phenomena of monomer exchange explains why high salt conditions would disrupt hexamer integrity, as a monomer is released from the hexamer into high salt conditions, there will be a propensity to make intramolecular contacts in order to bury the newly exposed hydrophobic hexamer interface. We find support for this hypothesis by examining the solvation information from the XF modification data. In the monomeric sample, which was created by adding 500 mM NaCl to the buffer, there are two regions, one N-terminal to helix 3 of the large NBD2 domain (residues 569-583), and one C-terminal of the small NBD2 domain helix (residues 843-857), which become shielded from solvent (Figure 10A, Table 2). Though there is no coverage of 569-583 in the hexamer with ATPγS, it is highly modified in the hexamer with ADP (Tables 3 and 4). The peptide 843-857 is unmodified in the monomer and modified in both of the hexamers, with a number of

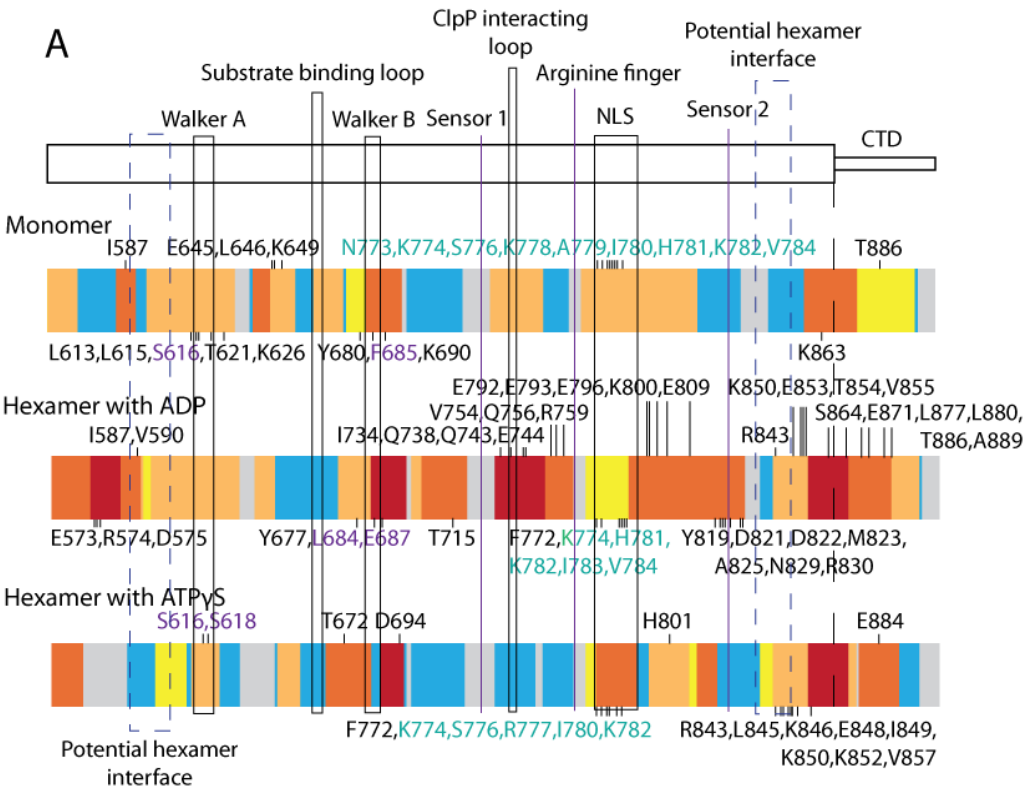
A
ClpP interacting loop
Potential hexamer interface
Substrate binding loop
Arginine finger
Walker A
Walker B
Sensor 1
NLS
Sensor 2
CTD
Monomer
I587
E645,L646,K649
N773,K774,S776,K778,A779,I780,H781,K782,V784
T886
L613,L615,S616,T621,K626
Y680,F685,K690
K863
Hexamer with ADP
I587,V590
E792,E793,E796,K800,E809
V754,Q756,R759
I734,Q738,Q743,E744
K850,E853,T854,V855
S864,E871,L877,L880,
T886,A889
R843
E573,R574,D575
Y677,L684,E687
T715
F772,K774,H781,
K782,I783,V784
Y819,D821,D822,M823,
A825,N829,R830
Hexamer with ATPγS
S616,S618
T672
D694
H801
E884
F772,K774,S776,R777,I780,K782
R843,L845,K846,E848,I849,
K850,K852,V857
Potential hexamer interface

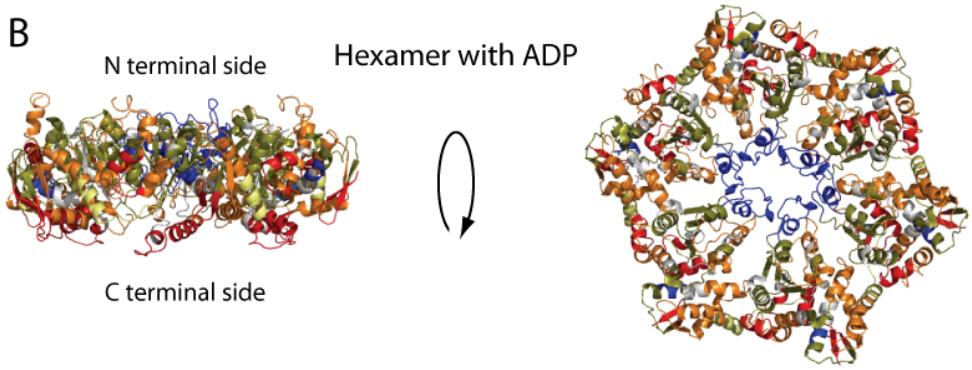
B
N terminal side
Hexamer with ADP
C terminal side

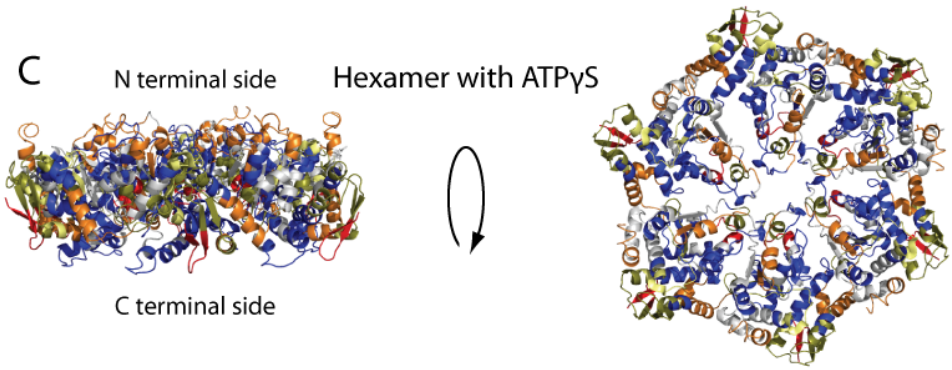
C
N terminal side
Hexamer with ATPγS
C terminal side

Figure 10. Hsp104 nucleotide binding domain 2 (NBD2) hexameric model and x-ray footprinting (XF) solvation data. A) Bar graph showing XF modification rates of peptides covering the Hsp104 NBD2. Peptides with the highest rate for a given region are on the on the top layer. Blue is unmodified, yellow less than 1 s^{-1}, light orange 1-10 s^{-1}, dark orange 10-50 s^{-1}, red more than 50 s^{-1}, and gray no coverage. Marked residues have been identified as modified by MS2 and are colored for their involvement in nucleotide binding, in purple, or the nuclear localization signal (NLS), in teal. Conserved AAA+ motifs, and the ClpP interacting loop are boxed, sensor-1, sensor-2 and arginine finger residues are marked with lines, and the potential hexamer interface regions are shown in dashed boxes. NBD2 homology modeled off the tClpB crystal structure (pdb: 1qvr) colored based on the XF modification rates with blue unmodified, yellow less than 1 s^{-1}, gold 1-10 s^{-1}, orange 10-50 s^{-1}, red more than 50 s^{-1}, and gray no coverage for the hexamer with B) ADP and C) ATPγS, and rigid body fit into a hexamer (fit into the SAXS volume envelope from the Hsp104 hexamer with ATP) that obeys published crosslinking data and Hsp100 hexameric crystal structure contacts.

residues identified as modified by MS2 (3.8 +- 0.14 s^{-1} with residues R843, K850, E853, and V855 for the hexamer with ADP and 6.1 +- 4.5 s^{-1} with residues R843, L845, K846, E848, I849, K850, K852, and V857 for the hexamer with ATPγS, Table 5). Both of these regions also contain highly conserved hydrophobic residues [102], supporting the possibility that they may be involved in intramolecular interactions that block hexamerization in high salt.

We decided to test whether we could disrupt the hexameric interactions by mutating a conserved hydrophobic residue in the proposed protomer interface to a charged residue. We chose L601 because it is in a loop region, so it was unlikely to grossly perturb secondary structure, and it is conserved in Hsp100 proteins from plants to bacteria to yeast [102]. Using a glutaraldehyde crosslinking assay [160] we assessed the ability of low concentrations of WT Hsp104, the double Walker A mutant (DWA - a variant known to severely disrupt hexamerization [160]) and a L601K variant to form hexamers under two conditions, adding either EDTA or ATP. Addition of EDTA chelates the magnesium essential for ATP binding and therefore disrupts the ability of Hsp104 to form hexamers, while addition of ATP promotes the formation of hexamers [139]. We visualized the gels using silver stain and found that WT Hsp104 exists as a mixture of monomer, dimer, trimer and hexamer in the presence of EDTA, and upon addition of ATP shifts entirely to the hexamer (Figure 11). DWA Hsp104, our negative control, shows very little hexamer

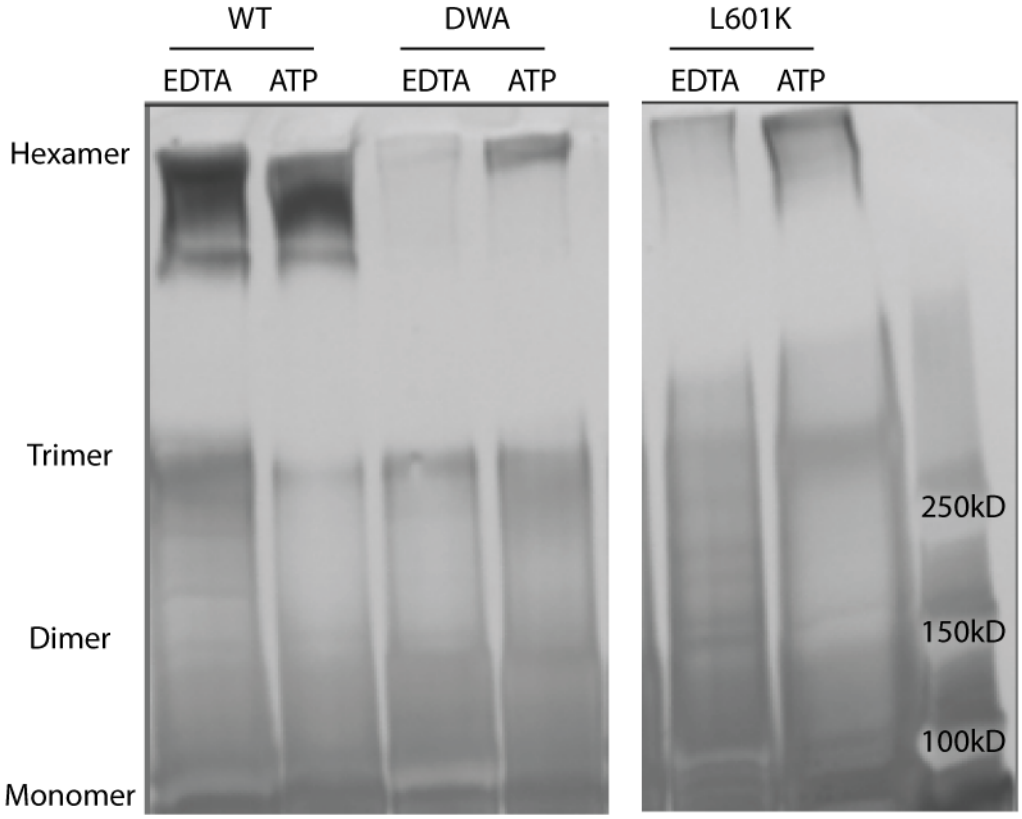

Figure 11. Glutaraldehyde crosslinking showing the effects of mutations on the oligomeric state of Hsp104. WT Hsp104 shows a robust ability to form hexamers even in the presence of EDTA and absence of ATP. The double Walker A (DWA) mutant displays defects in hexamerization even in the presence of ATP. The mutant L601K, which resides in the proposed hexamer interface but outside of any secondary structure, also displays defects in the ability to form hexamers.

in the presence of EDTA, and upon addition of ATP remains a mixture of monomer, dimer and trimer (Figure 11). The L601K Hsp104 mutant appears to strongly resemble the DWA Hsp104 variant; even upon addition of ATP there is very little hexamer but instead mostly smaller oligomers and monomer (Figure 11). This data supports the potential placement of the residue near a hydrophobic hexamer interface. Future experiments include repairing the interface with a compensatory, oppositely charged residue in the small NBD2 domain, as well as disulfide crosslinking.

Once I had a proposed interface and hexameric model, I used the XF modification rate information to assess its validity. I have colored the NBD2 hexameric model based on the XF modification rates for the hexamer with ADP as well as the hexamer with ATPγS (Figure 10B and C). Despite large differences in solvation, both of the states agree well overall with the model (Figure 10B and C). The hexamer with ADP shows a high degree of modification, with only two regions that appear to be shielded from solvation. These regions include residues 646-670 which contain the canonical substrate binding motif 661-GYVG-664, as well as residues 838-NKLAL-842, which reside within the region of the NBD2 small domain we propose to be involved in the hexamer interface (Table 3, Figure 10A). The fact that the rest of the domain appears to be solvated fits with the overall trend we have seen in both the XF solvation data and the HD exchange data, namely that the hexamer with ADP has less structure and more regions accessible to solvent. This suggests a model in which the energy of ATP binding induces the formation of stable secondary structure as well as minimizing large dynamic movements which would, due to the ensemble nature of XF experiments, result in increased regions of solvent accessibility. The implications for this finding will be explored further in a subsequent section. The hexamer with ATPγS has a number of regions that appear to have decreased modification rates and therefore solvation when compared to the hexamer with ADP (Figure 10A-C). When the modification rates are mapped onto our hexameric model we see a striking agreement (Figure 10B and C). Regions that display no oxidative modification include the core of the globular NBD2 domains, which in contrast to the hexamer with ADP, indicates that in the presence of ATPγS the domain is rigid, thereby protecting the interior of the domain from solvent. The substrate binding region is also unmodified in the hexamer with ATPγS, indicating that hydrolysis in NBD1 may be necessary to prime the GYVG loop for substrate engagement (Table 4). There is also substantial protection of the regions we believe to be involved in the hexamer interface. Though there is no coverage of the N-terminal part of the NBD2 large subdomain helix, residues in the middle show no modification, while residues on the helix near the surface of the hexamer show a low rate of modification (peptide 597-610 with a rate of 0.45 +- 0.17 s^{-1}, Table 4). Similarly, the NBD2 small

subdomain helix is unmodified in the N-terminal end, which is the interior of the hexamer, while modifications increase C-terminally. The region of the helix positioned near the outside of the hexamer becomes increasingly modified (peptides 838-856 and 843-857 with rates of 0.12 +- 0.009 s^{-1} and 6.12 +- 4.5 s^{-1} respectively, Tables 4 and 5).

3.2.7 C-terminal domain

Hsp104 has a unique C-terminal extension (CTD). The role of the CTD is poorly understood, though it is required for hexamerization [180, 182]. The XF data revealed a surprisingly unmodified stretch of acidic residues in the C-terminal extension (CTD), residues 893-GDDDNEDS-900 (Table 4, Figure 10A). The protection of this acidic patch, predicted to be unstructured, may be an important clue to its role, however, since the region is unique and therefore cannot be modeled based off homology it is hard to predict where it might be interacting with the rest of the hexamer. One possibility is a region of low homology in the NBD2 large domain helices 10 and 11 [102], which is protected in the hexamer with ATPγS (peptides 733-744 and 733-748 are unmodified in the hexamer with ATPγS and have rates of 1.8 +-0.02 s^{-1} and 103 +- 3 s^{-1} respectively in the hexamer with ADP). In Hsp104 this region has a large number of polar residues as well as two lysine residues. Whether the two regions interact could be tested using disulfide crosslinking.

3.2.8 Overall changes in solvation and hydrogen-deuterium exchange supports a new model for substrate remodeling by Hsp104

Overall, the hexamer with ADP shows more modification in our XF experiments as well as more HD exchange than the hexamer with ATPγS (Tables 2-6). These findings indicate that the hexamer with ADP is more solvated and has less secondary structure than the hexamer with ATPγS. It would appear that ATP binding induces global increases in secondary structure and

protection from solvent. This protection from solvent is likely due to decreases in local and global dynamics as increases in secondary structure rigidify the hexamer. This increase in rigidity can be thought of as a pre-payment of the entropic cost of substrate binding. This may have important implications for discrimination between soluble and aggregate substrates. When binding a large, stable aggregate, the main entropic penalty would come from decreases in mobility of the Hsp104 hexamer. Conversely, when binding soluble, potentially properly folded substrates, the main entropic penalty would come from the substrate. This mechanism of rigidifying the hexamer in preparation for substrate binding could contribute to discriminating between aggregated substrates, and soluble proteins that could, but should not, be remodeled. We have shown through our XF data as well as FITC-casein binding assays that substrate binds in the NTD and NBD1 domains. In the rigid, low entropy state the NTD and NBD1 are poised for substrate binding and the MD is in a configuration where motif 2 is making interactions with the NTD and NBD1 while motif 1 is making repressive contacts with NBD2 [222]. As substrate binding occurs at the NTD and NBD1, and/or Hsp70 binds at the MD/NTD interface, a cascade of events is triggered which relieves inhibition and allows substrate remodeling to commence. Substrate binding may trigger ATP hydrolysis in NBD1, as is seen in ClpB [232], or it may occur randomly. Whichever the case, hydrolysis of ATP results in a loss of rigidity of helix 2 of the MD, which results in loss of the repressive MD-NBD2 contact [222]. This allows signal transmission between NTD/NBD1 and NBD2 and may coordinate cooperativity. Our XF data shows us that the nucleotide-binding sites in NBD2 are only partially filled in the hexamer with ATPγS, and some may be open and unoccupied (in contrast to the nucleotide binding sites in NBD1 which are either all full or closed in the hexamer with ADP). Upon initial ATP hydrolysis at NBD1 and relief of the MD-NBD2 repression, nucleotide binding may occur more robustly in NBD2. Nucleotide binding at NBD2 stimulates hydrolysis in NBD1 [140], and therefore fully activates the Hsp104 hexamer. As ATP is hydrolyzed, the secondary substrate-binding loop, which we identified in our XF study, becomes positioned to engage substrate, potentially to prevent diffusion. The channel of the Hsp104 hexamer collapses, making a peristaltic pump motion N- C-terminally (Chapter 2).

Substrate can be engaged in NBD2 as channel collapse and NBD1 loop movements pull substrate C-terminally. NBD1 exchanges ADP for ATP while the secondary substrate-binding loop prevents substrate diffusion, and the NTD and NBD1 reengage the substrate higher up. Once the hexamer has been engaged, iterative rounds of these actions results in remodeled substrates.

3.3 Conclusions

In this chapter we have identified, from XF oxidative modification data, 1) Regions in the NTD likely to be involved in substrate and Hsp70 binding, 2) Novel sites of NTD:NBD1:MD interaction which may mediate cooperativity of the hexamer for which the NTD is essential, 3) A loop in NBD1 that may engage substrate in the ADP bound state to prevent substrate diffusion as ADP is exchanged for ATP, 4) The region of the MD (helix 2) responsible and the mechanism of signal transmission between NBD1 and NBD2, 5) Confirmed the validity of a hexameric model of the NBD2 domain, 6) Proposed a comprehensive model for the mechanism of Hsp104 substrate remodeling, and 7) Identified regions and specific residues in all of the Hsp104 domains which may play important roles for the hexamer, allowing the field to make directed changes in Hsp104 sequence rather than rely solely on random mutagenesis for the production of Hsp104 variants with altered activities. Our XF findings were supported using HD exchange (Alec Ricciuti, Englander lab), biochemical assays to confirm the importance of the NTD for substrate binding and productive Hsp70 interaction, *in vivo* and *in vitro* assays to confirm the importance of the novel NBD1 loop in substrate processing, and crosslinking studies to determine the MD:NBD2 interaction[222] and the importance of hydrophobic residues in the hexamer interface.

Chapter 4: Conclusions and future directions

4.1 Conclusions

We have used a hybrid approach, applying several structural and biochemical techniques, to elucidate novel details of the structure of the Hsp104 hexamer and its mechanism of substrate remodeling. In Chapter 2, we set out to determine the role of the Hsp104 N-terminal domain (NTD) and to visualize large conformational changes of the hexamer using small and wide-angle x-ray scattering (SAXS/WAXS). In Chapter 3, we used an in solution technique, x-ray footprinting (XF), that directly probes the solvation state of the Hsp104 hexamer in the presence of different nucleotides. The changes in solvation allowed us to make predictions about what these conformational changes mean for the individual domains, the Hsp104 hexamer as a whole, and the mechanism of substrate remodeling. We complemented the XF data with biochemical techniques, and were able to elucidate novel insights into substrate binding and processing, interaction with Hsp70, movements of the coiled-coil middle domain, and the subunit:subunit interface. By combining data from throughout the thesis we were able to propose a model of how Hsp104 is activated and remodels substrate.

In Chapter 2 we found that the Hsp104 NTD is necessary for nucleotide-dependent conformational changes that allow productive hexamer cooperativity. Cooperativity is dispensable for disordered aggregate dissolution, but necessary for robust and adaptable hexamer function [132]. This deficiency in hexamer cooperativity results in a deregulated ATPase rate, diminished unfoldase and tranlocase activity, and an inability to remodel exceptionally stable substrates such as amyloid, even in the presence of potentiating mutations. By examining the role of the N-terminal domain, we also discovered details about the WT Hsp104 hexamer. From our SAXS/WAXS studies in Chapter 2 we found that the Hsp104 channel undergoes peristaltic pump-like motions, which would facilitate directional movement of substrate through the central channel.

We have also discovered that partial unfolding of substrate can be sufficient for aggregate dissolution.

In Chapter 3 we used XF data to determine changes in solvation between Hsp104 hexamers bound to different nucleotides, and complemented our XF findings with biochemical assays. We found regions in the NTD likely to be involved in substrate and Hsp70 binding, and identified novel sites of NTD:NBD1:MD interaction, which may mediate cooperativity of the hexamer. We discovered a loop in NBD1 that may engage substrate in the ADP bound state to prevent substrate diffusion as ADP is exchanged for ATP. We determined the region of the MD (residues ~455-475 in helix 2) likely to be responsible for signal transmission between NBD1 and NBD2, and proposed a mechanism of transmission. We confirmed the validity of a hexameric model of the NBD2 domain we proposed based on published Hsp100 hexameric crystal structures. We proposed a comprehensive model for the mechanism of Hsp104 substrate remodeling and finally, we identified regions and specific residues in all of the Hsp104 domains that may play important roles for the hexamer. Identification of these regions will allow us to make directed changes in Hsp104 sequence rather than rely solely on random mutagenesis for production of Hsp104 variants with altered activities.

By combining our findings we propose a comprehensive model of the mechanism of Hsp104 substrate remodeling (Figure 1). Our findings indicate that ATP binding induces global increases in secondary structure and protection from solvent. This protection from solvent is likely due to decreases in local and global dynamics as increases in secondary structure rigidify the hexamer. Since Hsp104 engages substrate in the ATP-bound state, the rigidity of the hexamer with ATP can be thought of as a pre-payment of the entropic cost of substrate binding, especially since the entropic cost of binding to a large, insoluble aggregate would be paid primarily by the Hsp104 hexamer. In the rigid, low entropy state the NTD and NBD1 are poised for substrate binding and the MD is in a configuration where motif 2 is making interactions with the NTD and NBD1 while motif 1 is making repressive contacts with NBD2. As substrate binding occurs at the

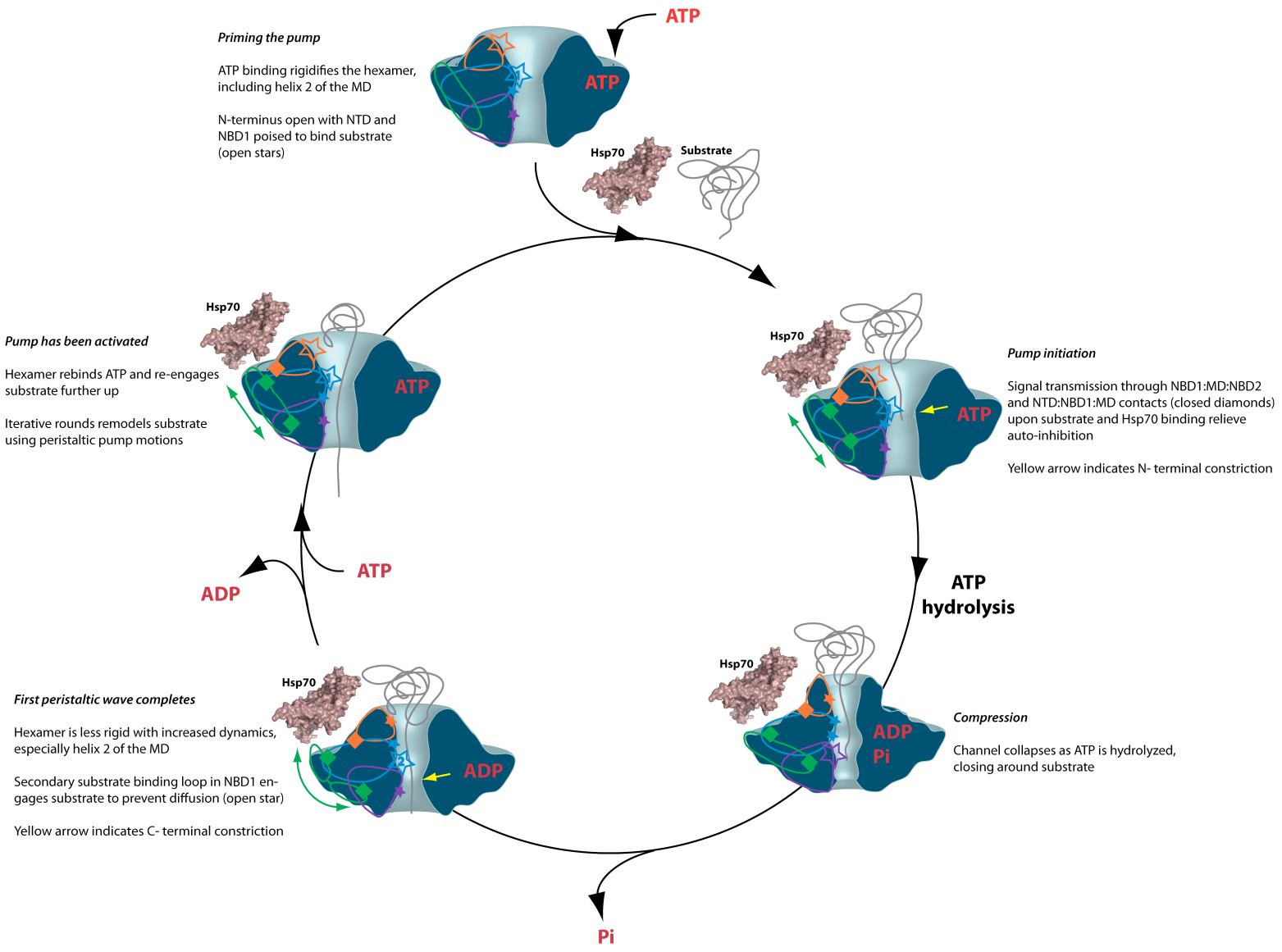
ATP
Priming the pump
ATP binding rigidifies the hexamer, including helix 2 of the MD
N-terminus open with NTD and NBD1 poised to bind substrate (open stars)
ATP
Hsp70
Substrate
Pump initiation
Signal transmission through NBD1:MD:NBD2 and NTD:NBD1:MD contacts (closed diamonds) upon substrate and Hsp70 binding relieve auto-inhibition
Yellow arrow indicates N- terminal constriction
Hsp70
ATP
ATP hydrolysis
Compression
Channel collapses as ATP is hydrolyzed, closing around substrate
Hsp70
ADP
Pi
Pi
First peristaltic wave completes
Hexamer is less rigid with increased dynamics, especially helix 2 of the MD
Secondary substrate binding loop in NBD1 engages substrate to prevent diffusion (open star)
Yellow arrow indicates C- terminal constriction
Hsp70
ADP
ATP
ADP
Pump has been activated
Hexamer rebinds ATP and re-engages substrate further up
Iterative rounds remodels substrate using peristaltic pump motions
Hsp70
ATP

Figure 1. Model of Hsp104 mechanism. ATP binding causes rigidification of the Hsp104 hexamer. The N-terminus of the channel is open in preparation for substrate binding in the NTD and the canonical NBD1 loop (open stars), and there is an N-terminal point of channel constriction. Substrate and Hsp70 binding initiates signal transmission through interdomain contacts (shown as closed diamonds). As the gamma-phosphate of ATP is cleaved, the channel closes around substrate. Upon release of the gamma-phosphate the hexamer, now bound to ADP, is less rigid, including helix 2 of the MD. The newly identified NBD1 loop, SBL2, engages substrate to prevent diffusion, and the point of constriction has shifted C-terminally. Once ADP is exchanged for ATP, the NTD and canonical NBD1 loop can reengage substrate further up. Iterative rounds of ATP hydrolysis and subsequent conformational changes remodels substrate.

NTD and NBD1, or Hsp70 binds at the MD/NTD interface, or both, a cascade of events is triggered which relieves inhibition and allows substrate remodeling to commence. This step can be thought of as 'priming the pump', or allowing the hexamer to unleash its auto-inhibited remodeling activity. Substrate binding may trigger ATP hydrolysis in NBD1, as is seen in ClpB [232], or it may occur randomly. Whichever the case, hydrolysis of ATP results in a loss of rigidity of helix 2 of the MD, which results in loss of the repressive MD-NBD2 contact [222]. This allows signal transmission between NTD/NBD1 and NBD2 and may coordinate cooperativity. Our XF data shows us that the nucleotide-binding sites in NBD2 are only partially filled in the hexamer with ATPγS, and some may be open and unoccupied (in contrast to the nucleotide binding sites in NBD1 which are either all full or closed in the hexamer with ATPγS). Upon initial ATP hydrolysis at NBD1 and relief of the MD-NBD2 repression, nucleotide binding may occur more robustly in NBD2. Nucleotide binding at NBD2 stimulates hydrolysis in NBD1 [140], and therefore fully activates the Hsp104 hexamer. This positive feedback loop allows the hexamer to transition from a repressed state to an active state. As ATP is hydrolyzed, the secondary substrate-binding loop, which we identified in our XF study, becomes positioned to engage substrate, potentially to prevent diffusion. The channel of the Hsp104 hexamer collapses, further preventing substrate diffusion, and makes a peristaltic pump motion with a wave of constriction moving N- C-terminally. Substrate can be engaged in NBD2 as channel collapse and NBD1 loop movements pull substrate C-terminally. NBD1 exchanges ADP for ATP and the NTD and NBD1 reengage the

substrate higher up. Once the hexamer has been engaged, iterative rounds of these actions results in remodeled substrates.

4.2 Future directions

Our XF studies have identified a number of regions that may be involved in substrate binding, Hsp70 interaction, hexamer cooperativity and signal transmission between domains. The next steps would be to test these areas to confirm or identify their role, and to make mutations to tailor Hsp104 to novel functions. In the NTD these regions include residues within the hydrophobic patch, which we believe may bind substrate, as well as regions that may be involved in Hsp70 interaction and an interface between the NTD, NBD1 and MD. Specifically, these residues include A91, L92, V95, and L96 (for the hydrophobic patch), T87, Y90, K94, S124, and S125 (for potential Hsp70 interaction site A) I102, Q103, K107 and S109 (for potential Hsp70 interaction site C) and residues that may be involved in the NTD:NBD1:MD interface, 8-15 (NTD), 39-52 (NTD), 148-166 (NTD-NBD1 linker), 230-240 (NBD1) and 496-498 (MD). Using mutagenesis and biochemical assays (substrate binding, aggregate reactivation, etc.) we can test whether these regions are involved in the activities we propose. The hydrophobic patch, if confirmed to be involved in substrate binding, could be mutated to develop Hsp104 variants with altered substrate specificities. Additionally, we have already identified potentiating mutations in the proposed NTD:NBD1:MD interface (D498V [179], T499D and I230N [Amber Tariq, Shorter lab unpublished data]), and therefore further mutations directed to these regions may reveal more potentiated Hsp104 variants with altered behaviors. We would also like to be able to test whether our proposed mechanism for the NBD1 291-GNGKD-295 loop, preventing substrate diffusion as subunits rebind ATP, is correct. We would like to measure release of substrate due to ATP hydrolysis after initial binding events, to confirm whether mutations in the loop result in more, or faster release of substrate. To do this we would incubate Hsp104 variants with ATPγS and FITC-casein. Once the fluorescence polarization (FP) signal reaches equilibrium, we can add a large

excess of ADP. As ATPγS is exchanged for ADP, some amount of substrate will be released. By comparing the change in FP signal between WT Hsp104 and our loop variants, we will be able to determine if the loop plays a role in preventing substrate diffusion.

Crosslinking studies and functional assays would further confirm the NBD2 hexameric model. If the model is sound, it can be used as a template for creation of a full hexameric model, with modifications to the original model based on the XF solvation data, particularly in the placement of the coiled-coil MD. This starting model can be used to generate ensembles of Hsp104 hexamers that can be filtered based on SAXS and XF constraints. These ensembles will allow us to visualize different possible orientations of highly mobile domains such as the MD and NTD.

Chapter 5: Methods

5.1 Protein expression and purification

Hsp104 variants were generated using QuikChange lightning mutagenesis (Agilent). Hsp104 variants were expressed and purified as N-terminally His_6-tagged constructs in a modified pPROEX HTb vector as described [233] or as untagged constructs in a pNOTAG vector from the Lindquist lab. Briefly, expression of Hsp104 variants in BL21 RIL (His_6-tagged constructs) or BL21 DE3 RIL (untagged constructs) was induced with 1 mM IPTG overnight at 15°C once cells reached log phase. Cells were harvested via centrifugation (4,000 rpm, 4°C, 20 min), resuspended in lysis buffer – 40 mM HEPES-KOH pH 7.4, 500 mM KCl, 20 mM $MgCl_2$, 2.5% (w/v) glycerol, 20 mM imidazole, 5 µM pepstatin A, complete protease inhibitor cocktail (1 EDTA-free tablet/50 mL), and 2 mM β-mercaptoethanol for His_6-tagged constructs or 50 mM Tris, pH 8, 10 mM $MgCl_2$, 2.5% glycerol (w/v), 5 µM pepstatin A, complete protease inhibitor cocktail (1 EDTA-free tablet/50 mL) (Roche), 2 mM β-mercaptoethanol for untagged constructs. Cells were lysed using a French press (Emulsiflex) homogenizer and cell debris removed via centrifugation (16,000 rpm, 4°C, 20 min). A 50% slurry of lysis buffer equilibrated Ni-Sepharose beads (GE) (for His_6-tagged constructs, 2 mL beads per 1 L of cells) or Affi-Gel Blue Media resin (Bio-Rad) (for untagged constructs, 3 mL resin per 1 L of cells) was added to the supernatant. Samples were rotated at 20 rpm, 4°C for 3 hours (His_6-tagged constructs) or 5 hours (untagged constructs). After incubation the beads/resin were washed three time, with 1) wash buffer – 40 mM HEPES-KOH pH 7.4, 140 mM KCl, 10 mM $MgCl_2$, 2.5% (w/v) glycerol, 20 mM imidazole, 2 mM β-mercaptoethanol), 2) wash buffer with 1 M KCl, and 3) wash buffer (His_6-tagged constructs), or 4 times with 50 mM Tris, pH 8, 10 mM $MgCl_2$, 100 mM KCl, 2.5% glycerol (w/v), 2 mM β-mercaptoethanol (for untagged constructs). The beads/resin were collected after each wash by centrifugation at 2,000 rpm for 2 min at 4°C (Eppendorf 5810R centrifuge) and the supernatant discarded. After washing the protein was eluted with wash buffer with 350 mM imidazole (for His_6-

tagged constructs) or wash buffer with 1 M KCl (for untagged constructs). After elution His_6-tagged and untagged constructs were buffer exchanged into buffer Q (20 mM Tris-HCl pH 8, 0.5 mM EDTA, 5 mM $MgCl_2$, 50 mM NaCl) and purified via anion exchange using a Resource Q column (GE) and a gradient of buffer Q+ (20 mM Tris-HCl pH 8, 0.5 mM EDTA, 5 mM $MgCl_2$, 1 M NaCl) Hsp104 typically elutes off the column at ~34% buffer Q+ (~31 mS/cm). All His_6-tagged constructs contain a TEV protease cleavage site. Prior to use, the His_6-tag was cleaved off with proTEV protease (Promega) or AcTEV protease (Invitrogen) according to manufacturer's instructions. His_6-tagged Sup35 was purified as described from BL21 (DE3) pLysS cells [20, 81].

ClpP was expressed and purified as a C-terminally His_6-tagged construct as described [179]. $RepA_{1-70}$-GFP and $GroEL^{TRAP}$ were purified as described [113]. Firefly luciferase was from Sigma. Hsc70, Hdj2, Hsp72 and Hsp40 were from Enzo Life Sciences, FITC-casein was from Sigma, and creatine kinase was from Roche. Unless otherwise stated Hsp104 concentrations refer to the hexamer.

5.2 Sup35 fiber inhibition assay

Amyloid fiber assembly of full length Sup35 was tracked by monitoring the change in fluorescence of the amyloid binding dye thioflavin T (excitation at 450 nm, emission 482 nm) on a Tecan Infinite M1000 [20, 81]. The assembly reactions were carried out in buffer alone (40 mM HEPES 7.4, 15 0mM KCl, 20 mM $MgCl_2$, 10% w/v glycerol, 1 mM GTP, 1 mM DTT, 5.1 mM ATP and an ATP regenerating system (1 mM creatine phosphate, 0.25 μM creatine kinase) or buffer with an Hsp104 variant. Reaction endpoints were also visualized by negative stain electron microscopy [20, 81].

5.3 Luciferase reactivation

Luciferase aggregation and reactivation were performed as described [132]. Briefly, firefly

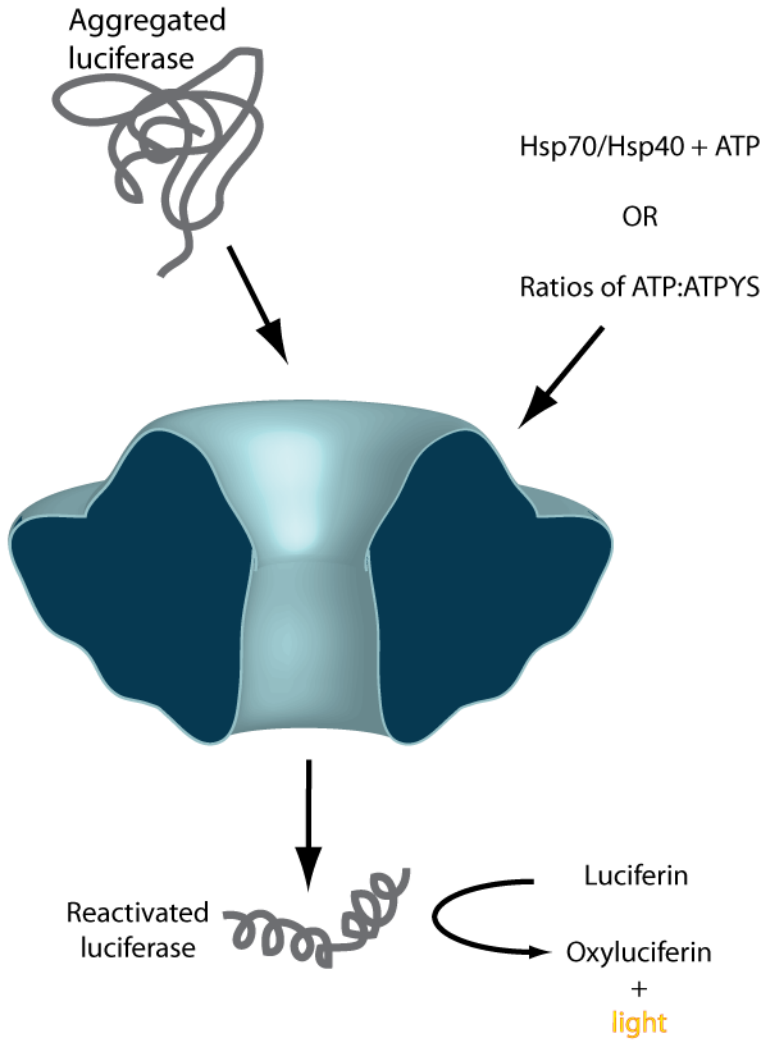

Figure 1. Luciferase reactivation. Aggregated luciferase is incubated with Hsp104 and Hsp70, Hsp40, and ATP, or different ratios of ATP:ATPγS. The amount of reactivated luciferase is determined by measuring luminescence, a product of the conversion of luciferin to oxyluciferin, the reaction catalyzed by active luciferase.

luciferase (50 μM) was incubated in LRB (25 mM HEPES-KOH pH 7.4, 150 mM KOAc, 10 mM MgOAc, 10 mM DTT) with 8 M urea at 30°C for 30 min to form aggregates. After a rapid 100-fold dilution in LRB, the aggregates were flash frozen and stored at -80°C until use. Reactivation assays were carried out with Hsp104 (1 μM), Hsp70 (Hsc70 or Hsp72 at 1 μM), Hsp40 (Hdj2, 1 μM), 5.1mM ATP, and an ATP regenerating system (1mM creatine phosphate, 0.25 μM creatine

kinase) for 90 min at 25°C. Alternatively, Hsp70, Hsp40 and 5.1 mM ATP were replaced with 5.1 mM nucleotide of different ratios of ATP:ATPγS. Luciferase activity was assessed using a luciferase assay system from Promega. Luminescence was measured on a Tecan Infinite M1000 or Safire^2 plate reader.

5.4 In vivo thermotolerance assay (Michelle Go, Shorter lab)

Yeast thermotolerance assays were performed as described [179]. Briefly, W303 Δ*hsp104* (*MATa, can1-100, his3-11,15, leu2-3,112, trp1-1, ura3-1, ade2-1, hsp104:kanMX4*) yeast was transformed with a centromeric pHSE plasmid encoding an Hsp104 variant [106]. The strains were grown in SD-ura media to an OD_{600} of 0.5, and incubated at 37°C for 30 min to induce Hsp104 expression. Cells were then heat shocked for 0-20 min at 50°C, immediately transferred to ice for 2 min, and then spotted on SD-ura plates in a 5–fold dilution series. After a two-day incubation at 30°C, plates were imaged for analysis. Alternatively, the thermotolerance products were plated on SD-ura plates, and after a 2-day incubation at 30°C colonies were counted using an acolyte automated colony counter (Synbiosis). Immunoblotting was used to confirm expressions levels of Hsp104 and disease proteins (when applicable).

5.5 Testing toxicity suppression of human disease proteins (Dr. Meredith Jackrel, Shorter lab)

Full length or NTD deletion Hsp104 variants harboring known potentiating mutations were transformed into yeast with pAG303GAL-TDP-43, pAG303GAL-FUS, or pAG303GAL-α-syn. The strains were then spotted in 5-fold dilution series on glucose (off) or galactose (on) media to test for toxicity suppression [179].

5.6 ATPase assay

Hsp104 variants (0.25 μM monomer) were incubated for 5 min at 25°C with ATP (1 mM). ATPase activity was assessed using a malachite green phosphate detection kit (Innova).

5.7 Fluorescence polarization

Fluorescent polarization experiments with Hsp104 variants and FITC-casein were performed as described [179]. Briefly, Hsp104 variants in increasing concentrations (10 nM-4 μM) were added to FITC-casein (6 nM), and ATPγS (2 mM) in LRB. After a 20 min incubation fluorescent polarization of the FITC-casein was measured using a Tecan Infinite M1000 plate reader. For binding in the presence of ADP, ATPγS was replaced with 2 mM ADP, FITC-casein was 100 nM and Hsp104 concentrations varied from 0.5-15 μM.

5.8 Casein degradation

FITC-casein degradation assays were performed as described [179]. Briefly, FITC-casein (100 nM-60 μM) was incubated with HAP variants (1 μM), ClpP (21 μM monomer), 5.1 mM ATP and an ATP regenerating system. Degradation of FITC-casein was monitored by measuring fluorescence of free FITC (excitation 490 nm, emission 520 nm) using a Tecan Infinite M1000 or Safire^2 plate reader.

5.9 $RepA_{1-70}$-GFP unfolding

$RepA_{1-70}$-GFP assays were performed as described [179]. Briefly, $RepA_{1-70}$-GFP (0.7 μM) was added to $GroEL^{TRAP}$ (1.5 μM), WT or ΔN Hsp104 (1 μM), either 2.6 mM ATP and 2.5 mM ATPγS (1:1) or 3.43 mM ATP and 1.67 mM ATPγS (2:1), BSA (0.02 mg/mL), Triton (0.005%) and an ATP regenerating system (1 mM creatine phosphate, 0.25 μM creatine kinase). The decrease

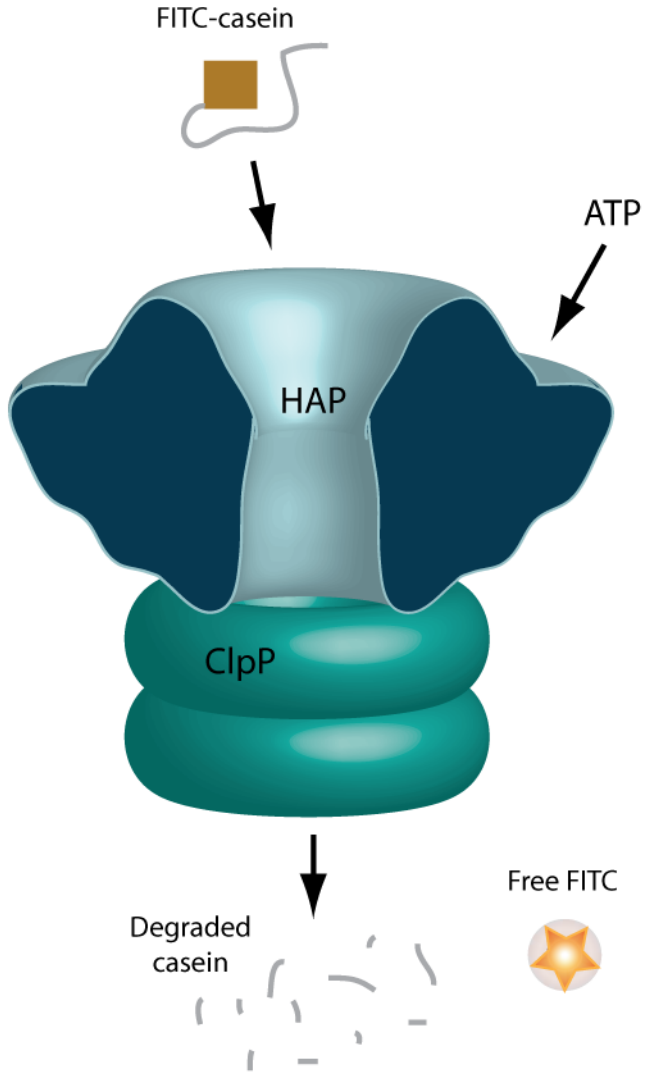

Figure 2. Casein degradation. FITC-casein is incubated with the Hsp104 variant HAP, the proteolytic chamber ClpP and ATP. When FITC is attached to casein its fluorescence is quenched. FITC-casein is translocated through HAP into ClpP. Casein is degraded and free FITC is released. FITC fluorescence is measured to indicate the amount of casein translocation and degradation.

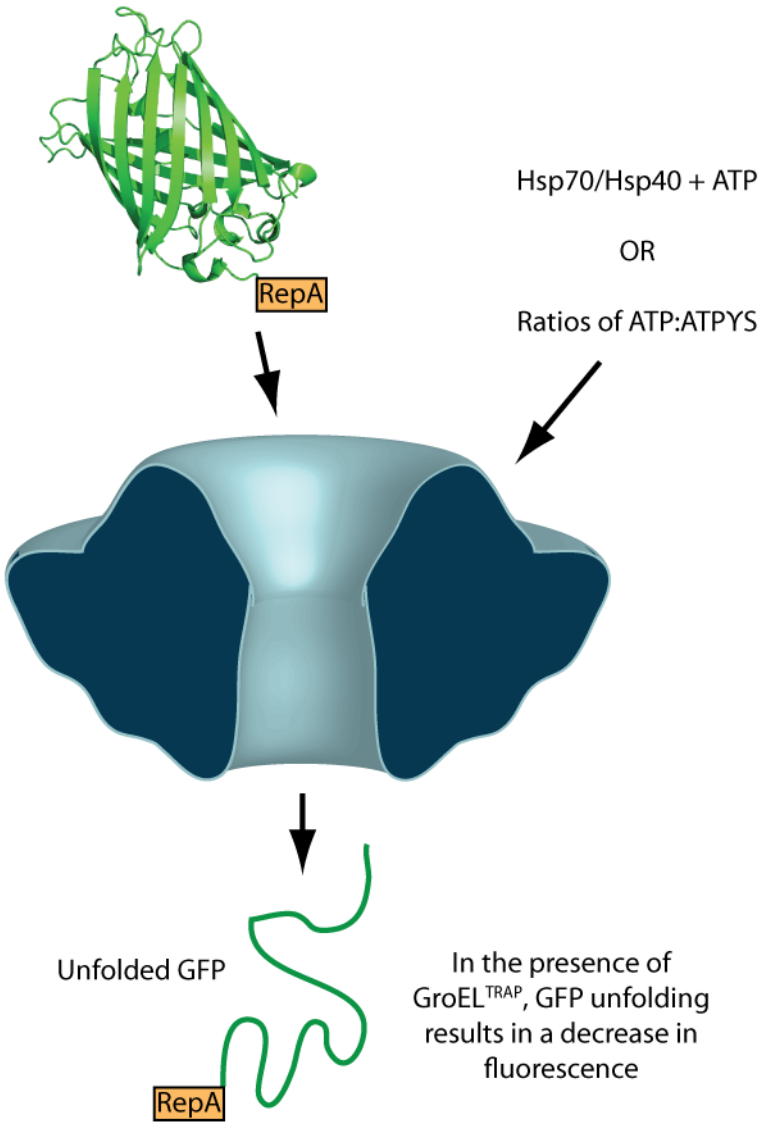

Figure 3. GFP unfolding. RepA tagged GFP is incubated with Hsp104, GroEL^{TRAP}, and Hsp70, Hsp40, and ATP, or different ratios of ATP:ATPγS. The decrease in fluorescence is used as a measure of GFP unfolding.

in fluorescence (excitation at 395 nm, emission 510 nm) over time was monitored using a Tecan Infinite M1000.

5.10 Mutant subunit doping

Luciferase aggregation and reactivation were performed as described [132] (see above). Reactivation assays were carried out with Hsp104 (1 μM), Hsp72 (1 μM), Hdj2 (1 μM), 5.1 mM ATP, and an ATP regenerating system (1 mM creatine phosphate, 0.25 mM creatine kinase) for 90 min at 25°C. Prior to addition, WT (or ΔN) Hsp104 and mutant were mixed in the following ratios: 6:0, 5:1, 4:2, 3:3, 2:4, 1:5, 0:6 and incubated for 30 min on ice. Luciferase activity was assessed using a luciferase assay system from Promega. Luminescence was measured on a Tecan Infinite M1000.

5.11 Glutaraldehyde crosslinking

Glutaraldehyde crosslinking experiments were carried out as described [139]. Briefly, Hsp104 variants were diluted to 0.04 mg/mL in 40 mM Hepes-KOH pH 7.4, 140 mM KCl, 10 mM $MgCl_2$, 1 mM DTT plus either 20 mM EDTA or 5 mM ATP. The samples were incubated with glutaraldehyde (0.1%) for 12 min. The crosslinking reaction was quenched by addition of 1 M glycine pH 6, and the proteins were precipitated using trichloroacetic acid. After two washes with chilled acetone the samples were run on an SDS-PAGE gel and reactions products visualized using a silver stain kit (Invitrogen).

5.12 Synchrotron hydroxyl radical footprinting (XF)

5.12.1 Sample irradiation

WT Hsp104 was purified as in [233], with a final step of gel filtration using a Superdex 200 column (GE) equilibrated in 50 mM Cacodylate pH 7.0, 140 mM KCl, 10 mM $MgCl_2$, (for the hexamer) or 50 mM Cacodylate pH 7.0, 500 mM KCl, and 20 mM $MgCl_2$ (for the monomer, as confirmed by Size Exclusion Chromatography followed by Multi Angle Light Scattering, SEC-MALS (Wyatt)). Samples were kept on ice and transported to Brookhaven National Laboratory

(Upton, NY). All samples were kept on ice and diluted at the beamline 10 min prior to use to 10 μM Hsp104 in 50 mM Cacodylate pH 7.0, 140 mM KCl, 10 mM $MgCl_2$, and 1 mM ADP or ATPγS (for the hexamer) or 50 mM Cacodylate pH 7.0, 500 mM KCl, and 20 mM $MgCl_2$ (for the monomer). X-ray dose- dependent oxidation of Alexa488 (Invitrogen) in the three buffer conditions was used to determine optimal exposure times and provide normalization constants. The samples were exposed to a mirror-focused synchrotron x-ray beam (5.5 mrad angle, focus value of 6 mm) at the X28C beamline of the National Synchrotron Light Source at Brookhaven National Laboratory for 0-20 ms. The exposure time of the samples was controlled by flow rate through the flow cell of a KinTek (Austin, TX) stopped flow apparatus [218]. Oxidation was immediately quenched by the addition of 10 mM methioninamide, and samples were frozen with dry ice, transported to the University of Pennsylvania and stored at -80°C.

5.12.2 Mass spectrometry on the XF samples

The irradiated samples were thawed on ice and diluted to 1 μM in 5mM HEPES NaOH pH 7.0, 140 mM KCl, 10 mM $MgCl_2$, 1 mM DTT, 1% TFA and immediately injected onto an in-line fragmentation-separation/MS analysis system. Samples first passed through an immobilized pepsin column onto a C8 trap column and washed for 3 min (2% acetonitrile, 1% formic acid, pH 2, 0°C). Samples then flowed onto an analytical C18 column, were eluted using a gradient optimized for the highly charged Hsp104 peptides (6 μL/min non-linear 2-50% acetonitrile gradient, 0.1% formic acid, pH 2 and 0°C), and injected by electron spray ionization into an LTQ Orbitrap XL mass spectrometer (Thermo Scientific). The four most abundant peptides from each scan was selected for fragmentation by CID and measured in the LTQ stage.

5.12.3 Identification of oxidatively modified peptides using ExMS-CL (Dr. Zhong-yuan Kan, Englander lab)

A modified version of the ExMS program, called ExMS-CL (which stands for "covalent labeling"), was used to process/analyze the x-ray footprinting MS/MS data to identifying oxidative modifications on the protein samples. Its workflow can be briefly described as follows. First, ExMS-CL makes a peptide list of the target protein including unmodified and modified peptides. The unmodified peptides are obtained from searching MS/MS runs (similar to SEQUEST), with a user-set score threshold (in this case a p score cut-off of 0.01) to build a "peptide pool". Based on the sequence of the unmodified "peptide pool" and the table of amino acid specific potential oxidative modifications (see Table 1 in ref [213]), ExMS-CL enumerates a full list of peptides with all potential modifications. For each peptide in the list, its theoretical monoisotopic m/z and isotopic peak intensity distribution (the envelope shape) are calculated. The reference retention time (RT) of unmodified peptides is directly copied from the MS/MS search result, and ExMS-CL uses a user-set shift (e.g., -3 minutes to +5 minutes) to create and use a specific RT search window for modified version of peptides. All of this information is saved together in the peptide list.

By using the above compiled list, ExMS-CL searches each peptide in the MS1 data, within each specific RT window for modified versions of peptides (see Figure 4 for an example of unmodified and modified versions of a peptide identified by ExMS-CL). ExMS-CL matches peptide theoretical masses and envelope shapes to the experimental data, and performs multiple tests and checks as in the original ExMS (algorithm details described in ref [220]) to ensure the identification is correct. At the end of this step, normal ExMS outputs are saved, including every identified peptides RT range, summed isotopic peak mass spectrum and centroid. Next, ExMS-CL confirms the modified peptides and locates the modification sites at MS1 and MS2 levels. From the MS1 ExMS output, peptide ("goodModPepSet") and protein sequence ("proModTable") tables are compiled to list all the modifications found with their individual position on the peptide, the peptide intensity quantification, and the number of modification possibilities ("sharing times").

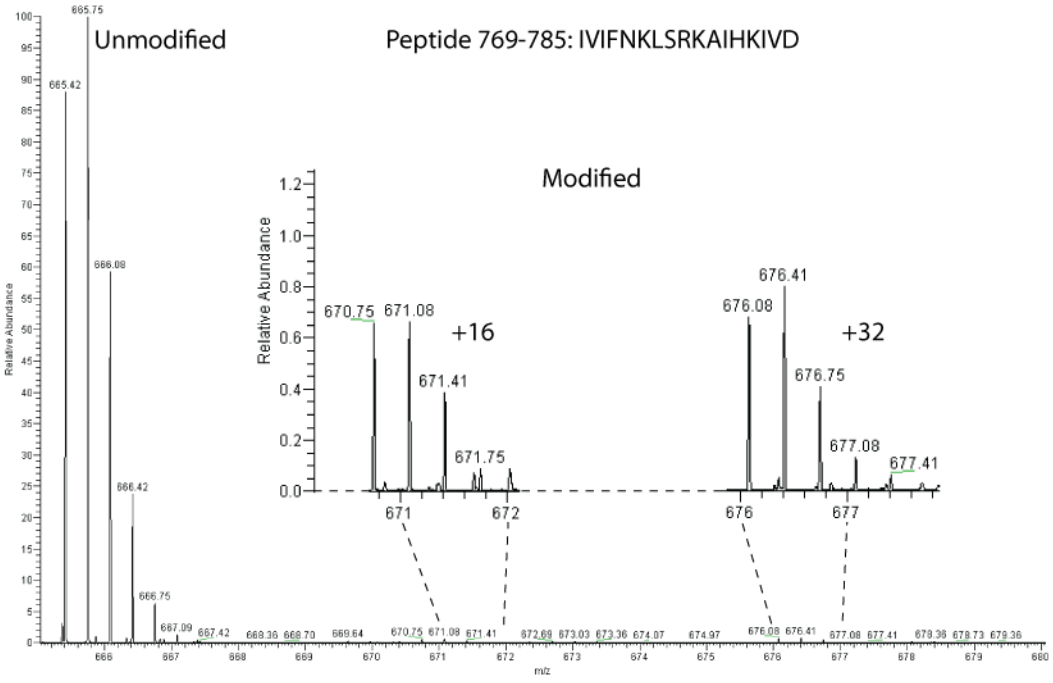

Figure 4. Mass spectra of a modified peptide. Modified and unmodified mass spectra for the monomer peptide 769-785 from a 2.5 ms timepoint are shown. All peptides are charge state 3.

The latter information can be used to judge if the modification can be uniquely assigned to an amino acid location. Further, ExMS-CL looks into the MS2 data by matching the parent ions to the mass of found modified peptides, then extracting the matched experimental CID spectra and comparing with the peptide's predicted CID spectra. A MS2 score is calculated to help confirm the identity of that modified peptide. Finally, ExMS-CL reports the analysis results of identified peptides in both modified and unmodified forms.

5.12.4 Analysis of modification rate of identified peptides using Matlab (Dr. Matthew Sochor, Lewis lab)

Output of ExMS-CL was read into Matlab (Mathworks) and analyzed using custom scripts. Modified and unmodified versions of peptides and their intensities were read from the

ExMS-CL output files and matched up. Fraction unmodified was calculated for each MS/MS sample using the peptide intensities (the sum of unmodified versions of the peptide divided by the sum of all modified and unmodified versions of the peptide). For each timepoint, the MS/MS run outputs were averaged together and standard deviation calculated. For each peptide, the average fraction unmodified was reported for each timepoint. Once time-dependent modification was calculated, each peptide was binned into one of three categories by the Matlab program, no time-dependent modification (0-1 timepoints after time 0 were modified with respect to time 0), sporadic modification (2 timepoints after time 0 were modified with respect to time 0), and time-dependent modification (greater than 2 timepoints after time 0 were modified with respect to time 0). For the peptides that displayed time-dependent modification, the program used the first four timepoints (0, 2.5, 5, and 7.5 ms) to determine the rate of modification by fitting to a first order exponential decay. The earliest timepoints were used due to evidence of over-oxidation in many of the 10 and 20 ms timepoints. Each of the fits was visually checked and manually refitting using Origin 8.1 was used when the Matlab program failed to converge onto a visually accurate fit to the data.

5.13 Small and wide angle x-ray scattering (SAXS/WAXS)

5.13.1 SAXS methods overview

X-ray scattering data were collected at beamline 4-2 at the Stanford Synchrotron Radiation Laboratory (SSRL, Menlo Park, CA), and beamline X9 at the National Synchrotron Light Source (NSLS, Upton, NY) (details specific to each beamline below). Data were collected at multiple concentrations between 1.5 mg/mL and 6.0 mg/mL. The two-dimensional scattering images were collected on CCD detectors, and circularly averaged using software developed at the individual beamlines to yield one-dimensional scattering profiles as a function of momentum transfer q ($q=4\pi\sin(\theta)/\lambda$, where 2π is the scattering angle and λ is the wavelength. The raw scattering data were scaled and buffer subtracted using the program PRIMUS [234]. Each

individual scattering curve was visually inspected for radiation damage and aggregation prior to averaging, including Guinier and Kratky plot analysis. For data collected at NSLS, where both SAXS and WAXS data are collected on separate detectors simultaneously, averaged scattering curves from the SAXS and WAXS detectors were scaled and merged in PRIMUS to yield a low-noise composite curve. The radii of gyration (R_g) were initially calculated using Guinier plots [235]. Distance distribution functions P(r) were calculated by the program GNOM [236] using an indirect Fourier transform. The maximum dimension of the particle (D_{max}) was determined by examining the quality of fit to the experimental data for a D_{max} range of 180 Å to 280 Å, varied in 5 Å. Fits were assessed by maximizing the Total Estimate figure, minimizing the discrepancy between calculated and experimental profiles, and optimizing the visual properties of the shape distribution function. Values for R_g were computed from the second moment of the P(r) and compared favorably to those calculated using Guinier plot analysis. The Porod volume and P value were calculated by the java-based program ScÅtter: http://www.bioisis.net/tutorial/9. The mass of the particle was calculated from Qr as described [237].

5.13.2 Small-Angle X-ray Scattering at SSRL Beamline 4-2

SAXS data were collected at beamline 4-2 at the Stanford Synchrotron Radiation Laboratory (SSRL, Menlo Park, CA) at room temperature with a sample to detector distance of 1600 mm. Using software developed at the beamline, two-dimensional scattering profiles collected using a Rayonix MX225-HE detector were converted into one-dimensional intensity profiles. The x-ray wavelength was 1.2 Å and the angular range was $0.0140 \leq q \geq 0.4435$ $Å^{-1}$. The protein samples and matching buffer solutions, 30 μL for each measurement, were exposed for ten 10 s exposures in a 1.2 mm path capillary with thin mica windows sealed across the evacuated flight path. Each exposure was checked for radiation damage by the automated software prior to averaging. After each measurement the capillary was washed thoroughly and purged with compressed nitrogen.

5.13.3 Small and Wide-Angle X-ray Scattering at NSLS Beamline X9

SAXS and WAXS data were collected simultaneously at beamline X9 at the National Synchrotron Light Source (NSLS, Upton, NY) at 10°C, or 25°C for the ADP-AlF_x state, by two overlapping detectors, a Mar 165 CCD SAXS detector 3.4 m from the sample, and a custom built Photonic Science CCD WAXS detector. The two-dimensional images were converted into one-dimensional scattering profiles using software developed at the beamline. The x-ray wavelength was 0.855 Å and the angular range collected was $0.00550 \leq q \geq 1.0060$; an angular range of $0.0100 \leq q \geq 0.7950$ was used for data analysis and reconstructions; reconstructions were also carried out with q=0.4950, which compared favorably to the reconstructions to q=0.7950. The sample cell contained a glass capillary sealed across the evacuated chamber. The protein samples and matching buffer solutions were flowed through the capillary and oscillated during exposure to reduce radiation damage. For data collection 30 μL of the protein sample or matching buffer solution was exposed for 180 s, subdivided into 3 60 s exposures of 10 μL.

5.13.4 Shape reconstructions from SAXS/WAXS data

Shape reconstructions of the hexamer were generated using the program GASBOR [201]. Information required for GASBOR modeling is the x-ray scattering profile, the number of residues to be modeled (GASBOR assigns a dummy reside to represent each residue), and the D_{max}. Six-fold symmetry was imposed. Since each inverse scattering has no one unique solution, ten independent *ab initio* reconstructions were performed for each state. Regions that are flexible are assigned different positions in individual simulations. The ten independent dummy residue reconstructions were aligned and scored based on the normalized spatial discrepancy (NSD) [238]. The individual reconstructions were only included if their NSD < mean NSD + 2 * variation. The included reconstructions were averaged and filtered to yield a final most-probable model using the DAMAVER suite of programs [202]. The individual bead models were visualized in

PyMOL (DeLano, W.L. The PyMOL Molecular Graphics System (2002) on World Wide Web http://www.pymol.org). The filtered and unfiltered average models were converted to volume envelopes using SITUS [239] and visualized using Chimera [240].

5.13.5 Channel calculations (Dr. Matthew Sochor, Lewis lab)

5.13.5.1 Volume measurement

The situs maps were converted to mrc maps using map2map, part of the SITUS suite of programs [239]. The three-dimensional electron density file in the .mrc format was imported into Matlab (Mathworks) using a custom script which parses the file into a three dimensional matrix of electron density. The read function also extracts the voxel dimensions in order to scale the measurement. The built in Matlab function “edge” was used to find the edges of two-dimensional slices of the electron density using the Sobel method. The Sobel method finds the edges by approximating the first derivative over the image; maxima of the first derivative are edges.

A custom script was then used to find edges for each two-dimensional slice of the density matrix. The x, y, and z coordinates of each edge point were stored in an array and the array scaled by the voxel dimensions. This array is a list of all three-dimensional vectors; each vector points to a unique edge point. The built in Matlab function “convhulln” was then used to convert this vector array into a convex hull and it measured the volume of the hull. The convex hull is the shell of the channel and the volume is the volume of the Hsp104 hexamer channel.

5.13.5.2 Distance measurement

Distance was measured for each slice of the channel. First, edges were found for each slice using the Matlab function “edge”. A horizontal mid-line of the channel was extracted and the distance from edge to edge was measured, scaled by the horizontal voxel dimension. The vertical

mid-line of the channel was then extracted and the edge-to-edge scaled distance was measured. Both distances were stored in an array. Then the slice was rotated 5 degrees and the algorithm was repeated to measure horizontal and vertical edge-to-edge, scaled distances. When the image had been rotated 45 degrees, every distance across the channel had been measured for a total of 18 distance measurements. The algorithm was then iterated over every slice of the density to measure the channel widths for each slice. The final array of distances was then output for further processing.

5.14 Hydrogen – deuterium exchange (Alec Ricciuti, Englander lab)

Hydrogen-deuterium exchange was carried out as described [220, 241] on the monomer, apo hexamer, hexamer with ADP and hexamer with ATPγS at several deuterium exchange timepoints. Curves showing deuterium incorporation versus time for peptides from different samples allowed for the determination of protection factors for the hexameric states when compared to the monomer.

5.15 Homology modeling

Hsp104 was homology modeled domain by domain using SWISS-MODEL [242-244] based on the ClpB crystal structures 1khy (N terminal domain) [142] and 1qvr (NBD1, MD, NBD2) [102]. Hydrogen-exchange (HD) experiments have revealed that the Hsp104 monomer homology modeled off the tClpB structure has accurately placed loops and stable secondary structure (data not shown, Alec Ricciuti and Walter Englander, manuscript in preparation), suggesting that the homology model is reasonably accurate. The separate domains were then rigid body fit into the volume envelope for the hexamer with ATP generated by the SAXS analysis using Chimera [240].

Bibliography

1. Dobson CM: **Principles of protein folding, misfolding and aggregation**. *Seminars in cell & developmental biology* 2004, **15**(1):3-16.
2. Stefani M, Dobson CM: **Protein aggregation and aggregate toxicity: new insights into protein folding, misfolding diseases and biological evolution**. *Journal of molecular medicine* 2003, **81**(11):678-699.
3. Thomas PJ, Qu BH, Pedersen PL: **Defective protein folding as a basis of human disease**. *Trends in biochemical sciences* 1995, **20**(11):456-459.
4. Dobson CM: **Protein folding and misfolding**. *Nature* 2003, **426**(6968):884-890.
5. Dobson CM: **Protein misfolding, evolution and disease**. *Trends in biochemical sciences* 1999, **24**(9):329-332.
6. Bucciantini M, Giannoni E, Chiti F, Baroni F, Formigli L, Zurdo J, Taddei N, Ramponi G, Dobson CM, Stefani M: **Inherent toxicity of aggregates implies a common mechanism for protein misfolding diseases**. *Nature* 2002, **416**(6880):507-511.
7. Chiti F, Dobson CM: **Protein misfolding, functional amyloid, and human disease**. *Annual review of biochemistry* 2006, **75**:333-366.
8. Anfinsen CB: **Principles that govern the folding of protein chains**. *Science* 1973, **181**(4096):223-230.
9. Jeffery CJ: **Moonlighting proteins**. *Trends in biochemical sciences* 1999, **24**(1):8-11.
10. Pettersson-Kastberg J, Aits S, Gustafsson L, Mossberg A, Storm P, Trulsson M, Persson F, Mok KH, Svanborg C: **Can misfolded proteins be beneficial? The HAMLET case**. *Annals of medicine* 2009, **41**(3):162-176.
11. Baldwin RL: **The nature of protein folding pathways: the classical versus the new view**. *Journal of biomolecular NMR* 1995, **5**(2):103-109.
12. Dill KA, Chan HS: **From Levinthal to pathways to funnels**. *Nature structural biology* 1997, **4**(1):10-19.
13. Walsh CT, Garneau-Tsodikova S, Gatto GJ: **Protein Posttranslational Modifications: The Chemistry of Proteome Diversifications**. *Angewandte Chemie International Edition* 2005, **44**(45):7342-7372.
14. Hashimoto K, Nishi H, Bryant S, Panchenko AR: **Caught in self-interaction: evolutionary and functional mechanisms of protein homooligomerization**. *Physical biology* 2011, **8**(3):035007.
15. Wright PE, Dyson HJ: **Intrinsically unstructured proteins: re-assessing the protein structure-function paradigm**. *Journal of molecular biology* 1999, **293**(2):321-331.
16. Dyson HJ, Wright PE: **Coupling of folding and binding for unstructured proteins**. *Current opinion in structural biology* 2002, **12**(1):54-60.
17. Hartl FU, Bracher A, Hayer-Hartl M: **Molecular chaperones in protein folding and proteostasis**. *Nature* 2011, **475**(7356):324-332.
18. Chi EY, Krishnan S, Randolph TW, Carpenter JF: **Physical stability of proteins in aqueous solution: mechanism and driving forces in nonnative protein aggregation**. *Pharmaceutical research* 2003, **20**(9):1325-1336.
19. Uversky VN: **A decade and a half of protein intrinsic disorder: biology still waits for physics**. *Protein science : a publication of the Protein Society* 2013, **22**(6):693-724.
20. Shorter J, Lindquist S: **Hsp104 catalyzes formation and elimination of self-replicating Sup35 prion conformers**. *Science* 2004, **304**(5678):1793-1797.
21. Zimmerman SB, Trach SO: **Estimation of macromolecule concentrations and excluded volume effects for the cytoplasm of Escherichia coli**. *Journal of molecular biology* 1991, **222**(3):599-620.
22. Hartl FU: **Molecular Chaperones in the Cytosol: from Nascent Chain to Folded Protein**. *Science* 2002, **295**(5561):1852-1858.
23. Ozcan U, Yilmaz E, Ozcan L, Furuhashi M, Vaillancourt E, Smith RO, Gorgun CZ, Hotamisligil GS: **Chemical chaperones reduce ER stress and restore glucose**

homeostasis in a mouse model of type 2 diabetes. *Science* 2006, **313**(5790):1137-1140.
24. Glover JR, Lindquist S: **Hsp104, Hsp70, and Hsp40: a novel chaperone system that rescues previously aggregated proteins**. *Cell* 1998, **94**(1):73-82.
25. Motohashi K, Watanabe Y, Yohda M, Yoshida M: **Heat-inactivated proteins are rescued by the DnaK.J-GrpE set and ClpB chaperones**. *Proceedings of the National Academy of Sciences of the United States of America* 1999, **96**(13):7184-7189.
26. Baumeister W, Walz J, Zuhl F, Seemuller E: **The proteasome: paradigm of a self-compartmentalizing protease**. *Cell* 1998, **92**(3):367-380.
27. Baker TA, Sauer RT: **ClpXP, an ATP-powered unfolding and protein-degradation machine**. *Biochimica et biophysica acta* 2012, **1823**(1):15-28.
28. Buchan JR, Parker R: **Eukaryotic stress granules: the ins and outs of translation**. *Molecular cell* 2009, **36**(6):932-941.
29. Kedersha N, Ivanov P, Anderson P: **Stress granules and cell signaling: more than just a passing phase?** *Trends in biochemical sciences* 2013, **38**(10):494-506.
30. Shorter J, Lindquist S: **Prions as adaptive conduits of memory and inheritance**. *Nature reviews Genetics* 2005, **6**(6):435-450.
31. Si K, Lindquist S, Kandel ER: **A neuronal isoform of the aplysia CPEB has prion-like properties**. *Cell* 2003, **115**(7):879-891.
32. Heinrich SU, Lindquist S: **Protein-only mechanism induces self-perpetuating changes in the activity of neuronal Aplysia cytoplasmic polyadenylation element binding protein (CPEB)**. *Proceedings of the National Academy of Sciences of the United States of America* 2011, **108**(7):2999-3004.
33. Fowler DM, Koulov AV, Balch WE, Kelly JW: **Functional amyloid--from bacteria to humans**. *Trends in biochemical sciences* 2007, **32**(5):217-224.
34. Watt B, van Niel G, Raposo G, Marks MS: **PMEL: a pigment cell-specific model for functional amyloid formation**. *Pigment cell & melanoma research* 2013, **26**(3):300-315.
35. Wang L, Schubert D, Sawaya MR, Eisenberg D, Riek R: **Multidimensional structure-activity relationship of a protein in its aggregated states**. *Angewandte Chemie* 2010, **49**(23):3904-3908.
36. Guijarro JI, Sunde M, Jones JA, Campbell ID, Dobson CM: **Amyloid fibril formation by an SH3 domain**. *Proceedings of the National Academy of Sciences of the United States of America* 1998, **95**(8):4224-4228.
37. Kim HJ, Kim NC, Wang YD, Scarborough EA, Moore J, Diaz Z, MacLea KS, Freibaum B, Li S, Molliex A *et al*: **Mutations in prion-like domains in hnRNPA2B1 and hnRNPA1 cause multisystem proteinopathy and ALS**. *Nature* 2013, **495**(7442):467-473.
38. Johnson BS, Snead D, Lee JJ, McCaffery JM, Shorter J, Gitler AD: **TDP-43 is intrinsically aggregation-prone, and amyotrophic lateral sclerosis-linked mutations accelerate aggregation and increase toxicity**. *The Journal of biological chemistry* 2009, **284**(30):20329-20339.
39. Xu J, Reumers J, Couceiro JR, De Smet F, Gallardo R, Rudyak S, Cornelis A, Rozenski J, Zwolinska A, Marine JC *et al*: **Gain of function of mutant p53 by coaggregation with multiple tumor suppressors**. *Nature chemical biology* 2011, **7**(5):285-295.
40. Powell K, Zeitlin PL: **Therapeutic approaches to repair defects in deltaF508 CFTR folding and cellular targeting**. *Advanced drug delivery reviews* 2002, **54**(11):1395-1408.
41. Eanes ED, Glenner GG: **X-Ray Diffraction Studies on Amyloid Filaments**. *Journal of Histochemistry & Cytochemistry* 1968, **16**(11):673-677.
42. Sunde M, Serpell LC, Bartlam M, Fraser PE, Pepys MB, Blake CC: **Common core structure of amyloid fibrils by synchrotron X-ray diffraction**. *Journal of molecular biology* 1997, **273**(3):729-739.
43. Jahn TR, Makin OS, Morris KL, Marshall KE, Tian P, Sikorski P, Serpell LC: **The common architecture of cross-beta amyloid**. *Journal of molecular biology* 2010, **395**(4):717-727.

44. Nelson R, Sawaya MR, Balbirnie M, Madsen AO, Riekel C, Grothe R, Eisenberg D: **Structure of the cross-beta spine of amyloid-like fibrils**. *Nature* 2005, **435**(7043):773-778.
45. Jarrett JT, Lansbury PT, Jr.: **Seeding "one-dimensional crystallization" of amyloid: a pathogenic mechanism in Alzheimer's disease and scrapie?** *Cell* 1993, **73**(6):1055-1058.
46. Klunk WE, Pettegrew JW, Abraham DJ: **Quantitative evaluation of congo red binding to amyloid-like proteins with a beta-pleated sheet conformation**. *Journal of Histochemistry & Cytochemistry* 1989, **37**(8):1273-1281.
47. Sabate R, Rodriguez-Santiago L, Sodupe M, Saupe SJ, Ventura S: **Thioflavin-T excimer formation upon interaction with amyloid fibers**. *Chemical communications* 2013, **49**(51):5745-5747.
48. Nilsson MR: **Techniques to study amyloid fibril formation in vitro**. *Methods* 2004, **34**(1):151-160.
49. Golabek AA, Kida E, Walus M, Perez C, Wisniewski T, Soto C: **Sodium dodecyl sulfate-resistant complexes of Alzheimer's amyloid beta-peptide with the N-terminal, receptor binding domain of apolipoprotein E**. *Biophysical journal* 2000, **79**(2):1008-1015.
50. Coalier KA, Paranjape GS, Karki S, Nichols MR: **Stability of early-stage amyloid-beta(1-42) aggregation species**. *Biochimica et biophysica acta* 2013, **1834**(1):65-70.
51. Surmacz-Chwedoruk W, Malka I, Bozycki L, Nieznanska H, Dzwolak W: **On the heat stability of amyloid-based biological activity: insights from thermal degradation of insulin fibrils**. *PloS one* 2014, **9**(1):e86320.
52. Concha-Marambio L, Diaz-Espinoza R, Soto C: **The extent of protease resistance of misfolded prion protein is highly dependent on the salt concentration**. *The Journal of biological chemistry* 2014, **289**(5):3073-3079.
53. True HL, Lindquist SL: **A yeast prion provides a mechanism for genetic variation and phenotypic diversity**. *Nature* 2000, **407**(6803):477-483.
54. Soto C, Saborio GP: **Prions: disease propagation and disease therapy by conformational transmission**. *Trends in molecular medicine* 2001, **7**(3):109-114.
55. Buxbaum JN: **The systemic amyloidoses**. *Current opinion in rheumatology* 2004, **16**(1):67-75.
56. Prusiner SB: **Shattuck lecture--neurodegenerative diseases and prions**. *The New England journal of medicine* 2001, **344**(20):1516-1526.
57. Kelly JW: **The alternative conformations of amyloidogenic proteins and their multi-step assembly pathways**. *Current opinion in structural biology* 1998, **8**(1):101-106.
58. Serio TR, Cashikar AG, Kowal AS, Sawicki GJ, Moslehi JJ, Serpell L, Arnsdorf MF, Lindquist SL: **Nucleated conformational conversion and the replication of conformational information by a prion determinant**. *Science* 2000, **289**(5483):1317-1321.
59. Lim KH, Dyson HJ, Kelly JW, Wright PE: **Localized structural fluctuations promote amyloidogenic conformations in transthyretin**. *Journal of molecular biology* 2013, **425**(6):977-988.
60. Lue L-F, Kuo Y-M, Roher AE, Brachova L, Shen Y, Sue L, Beach T, Kurth JH, Rydel RE, Rogers J: **Soluble Amyloid β Peptide Concentration as a Predictor of Synaptic Change in Alzheimer's Disease**. *The American Journal of Pathology* 1999, **155**(3):853-862.
61. McLean CA, Cherny RA, Fraser FW, Fuller SJ, Smith MJ, Beyreuther K, Bush AI, Masters CL: **Soluble pool of Abeta amyloid as a determinant of severity of neurodegeneration in Alzheimer's disease**. *Annals of neurology* 1999, **46**(6):860-866.
62. Wang J, Dickson DW, Trojanowski JQ, Lee VM: **The levels of soluble versus insoluble brain Abeta distinguish Alzheimer's disease from normal and pathologic aging**. *Experimental neurology* 1999, **158**(2):328-337.

63. Kayed R, Head E, Thompson JL, McIntire TM, Milton SC, Cotman CW, Glabe CG: **Common structure of soluble amyloid oligomers implies common mechanism of pathogenesis**. *Science* 2003, **300**(5618):486-489.
64. Harper JD, Lansbury PT, Jr.: **Models of amyloid seeding in Alzheimer's disease and scrapie: mechanistic truths and physiological consequences of the time-dependent solubility of amyloid proteins**. *Annual review of biochemistry* 1997, **66**:385-407.
65. Morales R, Moreno-Gonzalez I, Soto C: **Cross-seeding of misfolded proteins: implications for etiology and pathogenesis of protein misfolding diseases**. *PLoS pathogens* 2013, **9**(9):e1003537.
66. Ono K, Takahashi R, Ikeda T, Mizuguchi M, Hamaguchi T, Yamada M: **Exogenous amyloidogenic proteins function as seeds in amyloid beta-protein aggregation**. *Biochimica et biophysica acta* 2014, **1842**(4):646-653.
67. Vitrenko YA, Gracheva EO, Richmond JE, Liebman SW: **Visualization of aggregation of the Rnq1 prion domain and cross-seeding interactions with Sup35NM**. *The Journal of biological chemistry* 2007, **282**(3):1779-1787.
68. Derkatch IL, Bradley ME, Hong JY, Liebman SW: **Prions affect the appearance of other prions: the story of [PIN(+)]**. *Cell* 2001, **106**(2):171-182.
69. Lacroute F: **Non-Mendelian mutation allowing ureidosuccinic acid uptake in yeast**. *Journal of bacteriology* 1971, **106**(2):519-522.
70. Cox BS: **PSI, A Cytoplasmic Suppressor of Super-Suppressor in Yeast**. *Heredity* 1965, **20**:505-521.
71. Wickner RB: **[URE3] as an altered URE2 protein: evidence for a prion analog in Saccharomyces cerevisiae**. *Science* 1994, **264**(5158):566-569.
72. Aigle M, Lacroute F: **Genetical aspects of [URE3], a non-mitochondrial, cytoplasmically inherited mutation in yeast**. *Molecular & general genetics : MGG* 1975, **136**(4):327-335.
73. Tuite MF, Mundy CR, Cox BS: **Agents that cause a high frequency of genetic change from [psi+] to [psi-] in Saccharomyces cerevisiae**. *Genetics* 1981, **98**(4):691-711.
74. Newby GA, Lindquist S: **Blessings in disguise: biological benefits of prion-like mechanisms**. *Trends in cell biology* 2013, **23**(6):251-259.
75. Liebman SW, Sherman F: **Extrachromosomal psi+ determinant suppresses nonsense mutations in yeast**. *Journal of bacteriology* 1979, **139**(3):1068-1071.
76. Rogoza T, Goginashvili A, Rodionova S, Ivanov M, Viktorovskaya O, Rubel A, Volkov K, Mironova L: **Non-Mendelian determinant [ISP+] in yeast is a nuclear-residing prion form of the global transcriptional regulator Sfp1**. *Proceedings of the National Academy of Sciences of the United States of America* 2010, **107**(23):10573-10577.
77. Suzuki G, Shimazu N, Tanaka M: **A yeast prion, Mod5, promotes acquired drug resistance and cell survival under environmental stress**. *Science* 2012, **336**(6079):355-359.
78. Paushkin SV, Kushnirov VV, Smirnov VN, Ter-Avanesyan MD: **Propagation of the yeast prion-like [psi+] determinant is mediated by oligomerization of the SUP35-encoded polypeptide chain release factor**. *The EMBO journal* 1996, **15**(12):3127-3134.
79. Patino MM, Liu JJ, Glover JR, Lindquist S: **Support for the prion hypothesis for inheritance of a phenotypic trait in yeast**. *Science* 1996, **273**(5275):622-626.
80. True HL, Berlin I, Lindquist SL: **Epigenetic regulation of translation reveals hidden genetic variation to produce complex traits**. *Nature* 2004, **431**(7005):184-187.
81. Shorter J, Lindquist S: **Destruction or potentiation of different prions catalyzed by similar Hsp104 remodeling activities**. *Molecular cell* 2006, **23**(3):425-438.
82. Chernoff YO, Lindquist SL, Ono B, Inge-Vechtomov SG, Liebman SW: **Role of the chaperone protein Hsp104 in propagation of the yeast prion-like factor [psi+]**. *Science* 1995, **268**(5212):880-884.

83. Moriyama H, Edskes HK, Wickner RB: **[URE3] prion propagation in Saccharomyces cerevisiae: requirement for chaperone Hsp104 and curing by overexpressed chaperone Ydj1p**. *Molecular and cellular biology* 2000, **20**(23):8916-8922.
84. Sondheimer N, Lindquist S: **Rnq1: an epigenetic modifier of protein function in yeast**. *Molecular cell* 2000, **5**(1):163-172.
85. Halfmann R, Jarosz DF, Jones SK, Chang A, Lancaster AK, Lindquist S: **Prions are a common mechanism for phenotypic inheritance in wild yeasts**. *Nature* 2012, **482**(7385):363-368.
86. Alberti S, Halfmann R, King O, Kapila A, Lindquist S: **A systematic survey identifies prions and illuminates sequence features of prionogenic proteins**. *Cell* 2009, **137**(1):146-158.
87. Edskes HK, Gray VT, Wickner RB: **The [URE3] prion is an aggregated form of Ure2p that can be cured by overexpression of Ure2p fragments**. *Proceedings of the National Academy of Sciences of the United States of America* 1999, **96**(4):1498-1503.
88. Li L, Lindquist S: **Creating a protein-based element of inheritance**. *Science* 2000, **287**(5453):661-664.
89. Santoso A, Chien P, Osherovich LZ, Weissman JS: **Molecular basis of a yeast prion species barrier**. *Cell* 2000, **100**(2):277-288.
90. DePace AH, Santoso A, Hillner P, Weissman JS: **A critical role for amino-terminal glutamine/asparagine repeats in the formation and propagation of a yeast prion**. *Cell* 1998, **93**(7):1241-1252.
91. King OD, Gitler AD, Shorter J: **The tip of the iceberg: RNA-binding proteins with prion-like domains in neurodegenerative disease**. *Brain research* 2012, **1462**:61-80.
92. Li YR, King OD, Shorter J, Gitler AD: **Stress granules as crucibles of ALS pathogenesis**. *The Journal of cell biology* 2013, **201**(3):361-372.
93. Vishveshwara N, Bradley ME, Liebman SW: **Sequestration of essential proteins causes prion associated toxicity in yeast**. *Molecular microbiology* 2009, **73**(6):1101-1114.
94. Holmes DL, Lancaster AK, Lindquist S, Halfmann R: **Heritable remodeling of yeast multicellularity by an environmentally responsive prion**. *Cell* 2013, **153**(1):153-165.
95. Sweeny EA, Shorter J: **Prion proteostasis: Hsp104 meets its supporting cast**. *Prion* 2008, **2**(4):135-140.
96. Schirmer EC, Glover JR, Singer MA, Lindquist S: **HSP100/Clp proteins: a common mechanism explains diverse functions**. *Trends in biochemical sciences* 1996, **21**(8):289-296.
97. Neuwald AF, Aravind L, Spouge JL, Koonin EV: **AAA+: A class of chaperone-like ATPases associated with the assembly, operation, and disassembly of protein complexes**. *Genome research* 1999, **9**(1):27-43.
98. Glover JR, Tkach JM: **Crowbars and ratchets: hsp100 chaperones as tools in reversing protein aggregation**. *Biochemistry and cell biology = Biochimie et biologie cellulaire* 2001, **79**(5):557-568.
99. Martin A, Baker TA, Sauer RT: **Rebuilt AAA + motors reveal operating principles for ATP-fuelled machines**. *Nature* 2005, **437**(7062):1115-1120.
100. Davies JM, Tsuruta H, May AP, Weis WI: **Conformational changes of p97 during nucleotide hydrolysis determined by small-angle X-Ray scattering**. *Structure* 2005, **13**(2):183-195.
101. Enemark EJ, Joshua-Tor L: **Mechanism of DNA translocation in a replicative hexameric helicase**. *Nature* 2006, **442**(7100):270-275.
102. Lee S, Sowa ME, Watanabe YH, Sigler PB, Chiu W, Yoshida M, Tsai FT: **The structure of ClpB: a molecular chaperone that rescues proteins from an aggregated state**. *Cell* 2003, **115**(2):229-240.
103. Winkler J, Tyedmers J, Bukau B, Mogk A: **Chaperone networks in protein disaggregation and prion propagation**. *Journal of structural biology* 2012, **179**(2):152-160.

104. Erjavec N, Larsson L, Grantham J, Nystrom T: **Accelerated aging and failure to segregate damaged proteins in Sir2 mutants can be suppressed by overproducing the protein aggregation-remodeling factor Hsp104p**. *Genes & development* 2007, **21**(19):2410-2421.
105. Tessarz P, Schwarz M, Mogk A, Bukau B: **The yeast AAA+ chaperone Hsp104 is part of a network that links the actin cytoskeleton with the inheritance of damaged proteins**. *Molecular and cellular biology* 2009, **29**(13):3738-3745.
106. Sanchez Y, Lindquist SL: **HSP104 required for induced thermotolerance**. *Science* 1990, **248**(4959):1112-1115.
107. Sanchez Y, Taulien J, Borkovich KA, Lindquist S: **Hsp104 is required for tolerance to many forms of stress**. *The EMBO journal* 1992, **11**(6):2357-2364.
108. Parsell DA, Sanchez Y, Stitzel JD, Lindquist S: **Hsp104 is a highly conserved protein with two essential nucleotide-binding sites**. *Nature* 1991, **353**(6341):270-273.
109. Reid BG, Fenton WA, Horwich AL, Weber-Ban EU: **ClpA mediates directional translocation of substrate proteins into the ClpP protease**. *Proceedings of the National Academy of Sciences of the United States of America* 2001, **98**(7):3768-3772.
110. Parsell DA, Kowal AS, Singer MA, Lindquist S: **Protein disaggregation mediated by heat-shock protein Hsp104**. *Nature* 1994, **372**(6505):475-478.
111. Tessarz P, Mogk A, Bukau B: **Substrate threading through the central pore of the Hsp104 chaperone as a common mechanism for protein disaggregation and prion propagation**. *Molecular microbiology* 2008, **68**(1):87-97.
112. Wickner RB, Edskes HK, Shewmaker F, Nakayashiki T: **Prions of fungi: inherited structures and biological roles**. *Nature reviews Microbiology* 2007, **5**(8):611-618.
113. Doyle SM, Shorter J, Zolkiewski M, Hoskins JR, Lindquist S, Wickner S: **Asymmetric deceleration of ClpB or Hsp104 ATPase activity unleashes protein-remodeling activity**. *Nature structural & molecular biology* 2007, **14**(2):114-122.
114. Shorter J, Lindquist S: **Hsp104, Hsp70 and Hsp40 interplay regulates formation, growth and elimination of Sup35 prions**. *The EMBO journal* 2008, **27**(20):2712-2724.
115. Huh WK, Falvo JV, Gerke LC, Carroll AS, Howson RW, Weissman JS, O'Shea EK: **Global analysis of protein localization in budding yeast**. *Nature* 2003, **425**(6959):686-691.
116. Nelson RJ, Ziegelhoffer T, Nicolet C, Werner-Washburne M, Craig EA: **The translation machinery and 70 kd heat shock protein cooperate in protein synthesis**. *Cell* 1992, **71**(1):97-105.
117. Allen KD, Wegrzyn RD, Chernova TA, Muller S, Newnam GP, Winslett PA, Wittich KB, Wilkinson KD, Chernoff YO: **Hsp70 chaperones as modulators of prion life cycle: novel effects of Ssa and Ssb on the Saccharomyces cerevisiae prion [PSI+]**. *Genetics* 2005, **169**(3):1227-1242.
118. Kushnirov VV, Kryndushkin DS, Boguta M, Smirnov VN, Ter-Avanesyan MD: **Chaperones that cure yeast artificial [PSI+] and their prion-specific effects**. *Current biology : CB* 2000, **10**(22):1443-1446.
119. Chernoff YO, Newnam GP, Kumar J, Allen K, Zink AD: **Evidence for a protein mutator in yeast: role of the Hsp70-related chaperone ssb in formation, stability, and toxicity of the [PSI] prion**. *Molecular and cellular biology* 1999, **19**(12):8103-8112.
120. Jung G, Jones G, Wegrzyn RD, Masison DC: **A role for cytosolic hsp70 in yeast [PSI(+)] prion propagation and [PSI(+)] as a cellular stress**. *Genetics* 2000, **156**(2):559-570.
121. Jones G, Song Y, Chung S, Masison DC: **Propagation of Saccharomyces cerevisiae [PSI+] Prion Is Impaired by Factors That Regulate Hsp70 Substrate Binding**. *Molecular and cellular biology* 2004, **24**(9):3928-3937.
122. Newnam GP, Wegrzyn RD, Lindquist SL, Chernoff YO: **Antagonistic interactions between yeast chaperones Hsp104 and Hsp70 in prion curing**. *Molecular and cellular biology* 1999, **19**(2):1325-1333.

123. Sadlish H, Rampelt H, Shorter J, Wegrzyn RD, Andreasson C, Lindquist S, Bukau B: **Hsp110 chaperones regulate prion formation and propagation in S. cerevisiae by two discrete activities**. *PloS one* 2008, **3**(3):e1763.
124. Kryndushkin DS, Smirnov VN, Ter-Avanesyan MD, Kushnirov VV: **Increased expression of Hsp40 chaperones, transcriptional factors, and ribosomal protein Rpp0 can cure yeast prions**. *The Journal of biological chemistry* 2002, **277**(26):23702-23708.
125. Lu Z, Cyr DM: **Protein folding activity of Hsp70 is modified differentially by the hsp40 co-chaperones Sis1 and Ydj1**. *The Journal of biological chemistry* 1998, **273**(43):27824-27830.
126. Huang P, Gautschi M, Walter W, Rospert S, Craig EA: **The Hsp70 Ssz1 modulates the function of the ribosome-associated J-protein Zuo1**. *Nature structural & molecular biology* 2005, **12**(6):497-504.
127. Dragovic Z, Broadley SA, Shomura Y, Bracher A, Hartl FU: **Molecular chaperones of the Hsp110 family act as nucleotide exchange factors of Hsp70s**. *The EMBO journal* 2006, **25**(11):2519-2528.
128. Dragovic Z, Shomura Y, Tzvetkov N, Hartl FU, Bracher A: **Fes1p acts as a nucleotide exchange factor for the ribosome-associated molecular chaperone Ssb1p**. *Biological chemistry* 2006, **387**(12):1593-1600.
129. Kabani M, Beckerich JM, Brodsky JL: **Nucleotide Exchange Factor for the Yeast Hsp70 Molecular Chaperone Ssa1p**. *Molecular and cellular biology* 2002, **22**(13):4677-4689.
130. Raviol H, Sadlish H, Rodriguez F, Mayer MP, Bukau B: **Chaperone network in the yeast cytosol: Hsp110 is revealed as an Hsp70 nucleotide exchange factor**. *The EMBO journal* 2006, **25**(11):2510-2518.
131. Bagriantsev SN, Gracheva EO, Richmond JE, Liebman SW: **Variant-specific [PSI+] infection is transmitted by Sup35 polymers within [PSI+] aggregates with heterogeneous protein composition**. *Molecular biology of the cell* 2008, **19**(6):2433-2443.
132. DeSantis ME, Leung EH, Sweeny EA, Jackrel ME, Cushman-Nick M, Neuhaus-Follini A, Vashist S, Sochor MA, Knight MN, Shorter J: **Operational plasticity enables hsp104 to disaggregate diverse amyloid and nonamyloid clients**. *Cell* 2012, **151**(4):778-793.
133. Coelho M, Dereli A, Haese A, Kühn S, Malinovska L, DeSantis Morgan E, Shorter J, Alberti S, Gross T, Tolić-Nørrelykke Iva M: **Fission Yeast Does Not Age under Favorable Conditions, but Does So after Stress**. *Current Biology* 2013, **23**(19):1844-1852.
134. Spokoini R, Moldavski O, Nahmias Y, England JL, Schuldiner M, Kaganovich D: **Confinement to organelle-associated inclusion structures mediates asymmetric inheritance of aggregated protein in budding yeast**. *Cell reports* 2012, **2**(4):738-747.
135. DeSantis ME, Shorter J: **The elusive middle domain of Hsp104 and ClpB: Location and function**. *Biochimica et Biophysica Acta (BBA) - Molecular Cell Research* 2012, **1823**(1):29-39.
136. Wendler P, Shorter J, Plisson C, Cashikar AG, Lindquist S, Saibil HR: **Atypical AAA+ subunit packing creates an expanded cavity for disaggregation by the protein-remodeling factor Hsp104**. *Cell* 2007, **131**(7):1366-1377.
137. Wendler P, Shorter J, Snead D, Plisson C, Clare DK, Lindquist S, Saibil HR: **Motor mechanism for protein threading through Hsp104**. *Molecular cell* 2009, **34**(1):81-92.
138. Grimminger-Marquardt V, Lashuel HA: **Structure and function of the molecular chaperone Hsp104 from yeast**. *Biopolymers* 2010, **93**(3):252-276.
139. Parsell DA, Kowal AS, Lindquist S: **Saccharomyces cerevisiae Hsp104 protein. Purification and characterization of ATP-induced structural changes**. *The Journal of biological chemistry* 1994, **269**(6):4480-4487.

140. Hattendorf DA, Lindquist SL: **Cooperative kinetics of both Hsp104 ATPase domains and interdomain communication revealed by AAA sensor-1 mutants**. *The EMBO journal* 2002, **21**(1-2):12-21.
141. Xia D, Esser L, Singh SK, Guo F, Maurizi MR: **Crystallographic investigation of peptide binding sites in the N-domain of the ClpA chaperone**. *Journal of structural biology* 2004, **146**(1-2):166-179.
142. Li J, Sha B: **Crystal structure of the E. coli Hsp100 ClpB N-terminal domain**. *Structure* 2003, **11**(3):323-328.
143. Wang F, Mei Z, Qi Y, Yan C, Hu Q, Wang J, Shi Y: **Structure and mechanism of the hexameric MecA-ClpC molecular machine**. *Nature* 2011, **471**(7338):331-335.
144. Lo JH, Baker TA, Sauer RT: **Characterization of the N-terminal repeat domain of Escherichia coli ClpA-A class I Clp/HSP100 ATPase**. *Protein science : a publication of the Protein Society* 2001, **10**(3):551-559.
145. Mogk A, Schlieker C, Strub C, Rist W, Weibezahn J, Bukau B: **Roles of individual domains and conserved motifs of the AAA+ chaperone ClpB in oligomerization, ATP hydrolysis, and chaperone activity**. *The Journal of biological chemistry* 2003, **278**(20):17615-17624.
146. Ishikawa T, Maurizi MR, Steven AC: **The N-terminal substrate-binding domain of ClpA unfoldase is highly mobile and extends axially from the distal surface of ClpAP protease**. *Journal of structural biology* 2004, **146**(1-2):180-188.
147. Lee S, Choi JM, Tsai FT: **Visualizing the ATPase cycle in a protein disaggregating machine: structural basis for substrate binding by ClpB**. *Molecular cell* 2007, **25**(2):261-271.
148. Park SK, Kim KI, Woo KM, Seol JH, Tanaka K, Ichihara A, Ha DB, Chung CH: **Site-directed mutagenesis of the dual translational initiation sites of the clpB gene of Escherichia coli and characterization of its gene products**. *The Journal of biological chemistry* 1993, **268**(27):20170-20174.
149. Beinker P, Schlee S, Groemping Y, Seidel R, Reinstein J: **The N terminus of ClpB from Thermus thermophilus is not essential for the chaperone activity**. *The Journal of biological chemistry* 2002, **277**(49):47160-47166.
150. Barnett ME, Nagy M, Kedzierska S, Zolkiewski M: **The amino-terminal domain of ClpB supports binding to strongly aggregated proteins**. *The Journal of biological chemistry* 2005, **280**(41):34940-34945.
151. Tanaka N, Tani Y, Hattori H, Tada T, Kunugi S: **Interaction of the N-terminal domain of Escherichia coli heat-shock protein ClpB and protein aggregates during chaperone activity**. *Protein science : a publication of the Protein Society* 2004, **13**(12):3214-3221.
152. Mizuno S, Nakazaki Y, Yoshida M, Watanabe YH: **Orientation of the amino-terminal domain of ClpB affects the disaggregation of the protein**. *The FEBS journal* 2012, **279**(8):1474-1484.
153. Zhang T, Ploetz EA, Nagy M, Doyle SM, Wickner S, Smith PE, Zolkiewski M: **Flexible connection of the N-terminal domain in ClpB modulates substrate binding and the aggregate reactivation efficiency**. *Proteins* 2012, **80**(12):2758-2768.
154. Hung GC, Masison DC: **N-terminal domain of yeast Hsp104 chaperone is dispensable for thermotolerance and prion propagation but necessary for curing prions by Hsp104 overexpression**. *Genetics* 2006, **173**(2):611-620.
155. Erzberger JP, Berger JM: **Evolutionary relationships and structural mechanisms of AAA+ proteins**. *Annual review of biophysics and biomolecular structure* 2006, **35**:93-114.
156. Iyer LM, Leipe DD, Koonin EV, Aravind L: **Evolutionary history and higher order classification of AAA+ ATPases**. *Journal of structural biology* 2004, **146**(1-2):11-31.
157. Tkach JM, Glover JR: **Nucleocytoplasmic trafficking of the molecular chaperone Hsp104 in unstressed and heat-shocked cells**. *Traffic* 2008, **9**(1):39-56.
158. Walker JE, Saraste M, Runswick MJ, Gay NJ: **Distantly related sequences in the alpha- and beta-subunits of ATP synthase, myosin, kinases and other ATP-**

requiring enzymes and a common nucleotide binding fold. *The EMBO journal* 1982, **1**(8):945-951.
159. Saraste M, Sibbald PR, Wittinghofer A: **The P-loop--a common motif in ATP- and GTP-binding proteins**. *Trends in biochemical sciences* 1990, **15**(11):430-434.
160. Schirmer EC, Queitsch C, Kowal AS, Parsell DA, Lindquist S: **The ATPase activity of Hsp104, effects of environmental conditions and mutations**. *The Journal of biological chemistry* 1998, **273**(25):15546-15552.
161. Weibezahn J, Schlieker C, Bukau B, Mogk A: **Characterization of a trap mutant of the AAA+ chaperone ClpB**. *The Journal of biological chemistry* 2003, **278**(35):32608-32617.
162. Guenther B, Onrust R, Sali A, O'Donnell M, Kuriyan J: **Crystal structure of the delta' subunit of the clamp-loader complex of E. coli DNA polymerase III**. *Cell* 1997, **91**(3):335-345.
163. Hanson PI, Whiteheart SW: **AAA+ proteins: have engine, will work**. *Nature reviews Molecular cell biology* 2005, **6**(7):519-529.
164. Hattendorf DA, Lindquist SL: **Analysis of the AAA sensor-2 motif in the C-terminal ATPase domain of Hsp104 with a site-specific fluorescent probe of nucleotide binding**. *Proceedings of the National Academy of Sciences of the United States of America* 2002, **99**(5):2732-2737.
165. Ogura T, Whiteheart SW, Wilkinson AJ: **Conserved arginine residues implicated in ATP hydrolysis, nucleotide-sensing, and inter-subunit interactions in AAA and AAA+ ATPases**. *Journal of structural biology* 2004, **146**(1-2):106-112.
166. Simonetta KR, Kazmirski SL, Goedken ER, Cantor AJ, Kelch BA, McNally R, Seyedin SN, Makino DL, O'Donnell M, Kuriyan J: **The mechanism of ATP-dependent primer-template recognition by a clamp loader complex**. *Cell* 2009, **137**(4):659-671.
167. Lum R, Tkach JM, Vierling E, Glover JR: **Evidence for an unfolding/threading mechanism for protein disaggregation by Saccharomyces cerevisiae Hsp104**. *The Journal of biological chemistry* 2004, **279**(28):29139-29146.
168. Hinnerwisch J, Fenton WA, Furtak KJ, Farr GW, Horwich AL: **Loops in the central channel of ClpA chaperone mediate protein binding, unfolding, and translocation**. *Cell* 2005, **121**(7):1029-1041.
169. Schlieker C, Weibezahn J, Patzelt H, Tessarz P, Strub C, Zeth K, Erbse A, Schneider-Mergener J, Chin JW, Schultz PG *et al*: **Substrate recognition by the AAA+ chaperone ClpB**. *Nature structural & molecular biology* 2004, **11**(7):607-615.
170. Weibezahn J, Tessarz P, Schlieker C, Zahn R, Maglica Z, Lee S, Zentgraf H, Weber-Ban EU, Dougan DA, Tsai FT *et al*: **Thermotolerance requires refolding of aggregated proteins by substrate translocation through the central pore of ClpB**. *Cell* 2004, **119**(5):653-665.
171. Lee S, Sielaff B, Lee J, Tsai FT: **CryoEM structure of Hsp104 and its mechanistic implication for protein disaggregation**. *Proceedings of the National Academy of Sciences of the United States of America* 2010, **107**(18):8135-8140.
172. Haslberger T, Weibezahn J, Zahn R, Lee S, Tsai FT, Bukau B, Mogk A: **M domains couple the ClpB threading motor with the DnaK chaperone activity**. *Molecular cell* 2007, **25**(2):247-260.
173. Sielaff B, Tsai FT: **The M-domain controls Hsp104 protein remodeling activity in an Hsp70/Hsp40-dependent manner**. *Journal of molecular biology* 2010, **402**(1):30-37.
174. Miot M, Reidy M, Doyle SM, Hoskins JR, Johnston DM, Genest O, Vitery MC, Masison DC, Wickner S: **Species-specific collaboration of heat shock proteins (Hsp) 70 and 100 in thermotolerance and protein disaggregation**. *Proceedings of the National Academy of Sciences of the United States of America* 2011, **108**(17):6915-6920.
175. Seyffer F, Kummer E, Oguchi Y, Winkler J, Kumar M, Zahn R, Sourjik V, Bukau B, Mogk A: **Hsp70 proteins bind Hsp100 regulatory M domains to activate AAA+ disaggregase at aggregate surfaces**. *Nature structural & molecular biology* 2012, **19**(12):1347-1355.

176. Oguchi Y, Kummer E, Seyffer F, Berynskyy M, Anstett B, Zahn R, Wade RC, Mogk A, Bukau B: **A tightly regulated molecular toggle controls AAA+ disaggregase**. *Nature structural & molecular biology* 2012, **19**(12):1338-1346.
177. Dulle JE, Stein KC, True HL: **Regulation of the hsp104 middle domain activity is critical for yeast prion propagation**. *PloS one* 2014, **9**(1):e87521.
178. Lee J, Kim JH, Biter AB, Sielaff B, Lee S, Tsai FT: **Heat shock protein (Hsp) 70 is an activator of the Hsp104 motor**. *Proceedings of the National Academy of Sciences of the United States of America* 2013, **110**(21):8513-8518.
179. Jackrel ME, Desantis ME, Martinez BA, Castellano LM, Stewart RM, Caldwell KA, Caldwell GA, Shorter J: **Potentiated hsp104 variants antagonize diverse proteotoxic misfolding events**. *Cell* 2014, **156**(1-2):170-182.
180. Mackay RG, Helsen CW, Tkach JM, Glover JR: **The C-terminal extension of Saccharomyces cerevisiae Hsp104 plays a role in oligomer assembly**. *Biochemistry* 2008, **47**(7):1918-1927.
181. Cashikar AG, Schirmer EC, Hattendorf DA, Glover JR, Ramakrishnan MS, Ware DM, Lindquist SL: **Defining a pathway of communication from the C-terminal peptide binding domain to the N-terminal ATPase domain in a AAA protein**. *Molecular cell* 2002, **9**(4):751-760.
182. Tkach JM, Glover JR: **Amino acid substitutions in the C-terminal AAA+ module of Hsp104 prevent substrate recognition by disrupting oligomerization and cause high temperature inactivation**. *The Journal of biological chemistry* 2004, **279**(34):35692-35701.
183. Seol JH, Yoo SJ, Kim KI, Kang MS, Ha DB, Chung CH: **The 65-kDa protein derived from the internal translational initiation site of the clpA gene inhibits the ATP-dependent protease Ti in Escherichia coli**. *The Journal of biological chemistry* 1994, **269**(47):29468-29473.
184. Singh SK, Rozycki J, Ortega J, Ishikawa T, Lo J, Steven AC, Maurizi MR: **Functional domains of the ClpA and ClpX molecular chaperones identified by limited proteolysis and deletion analysis**. *The Journal of biological chemistry* 2001, **276**(31):29420-29429.
185. Brunger AT, DeLaBarre B: **NSF and p97/VCP: similar at first, different at last**. *FEBS letters* 2003, **555**(1):126-133.
186. Rouiller I, Butel VM, Latterich M, Milligan RA, Wilson-Kubalek EM: **A major conformational change in p97 AAA ATPase upon ATP binding**. *Molecular cell* 2000, **6**(6):1485-1490.
187. Tang WK, Xia D: **Structural and functional deviations in disease-associated p97 mutants**. *Journal of structural biology* 2012, **179**(2):83-92.
188. Dreveny I, Kondo H, Uchiyama K, Shaw A, Zhang X, Freemont PS: **Structural basis of the interaction between the AAA ATPase p97/VCP and its adaptor protein p47**. *The EMBO journal* 2004, **23**(5):1030-1039.
189. Madsen L, Seeger M, Semple CA, Hartmann-Petersen R: **New ATPase regulators--p97 goes to the PUB**. *The international journal of biochemistry & cell biology* 2009, **41**(12):2380-2388.
190. Schuberth C, Buchberger A: **UBX domain proteins: major regulators of the AAA ATPase Cdc48/p97**. *Cellular and molecular life sciences : CMLS* 2008, **65**(15):2360-2371.
191. Dougan DA, Reid BG, Horwich AL, Bukau B: **ClpS, a substrate modulator of the ClpAP machine**. *Molecular cell* 2002, **9**(3):673-683.
192. Chow IT, Barnett ME, Zolkiewski M, Baneyx F: **The N-terminal domain of Escherichia coli ClpB enhances chaperone function**. *FEBS letters* 2005, **579**(20):4242-4248.
193. Mei Z, Wang F, Qi Y, Zhou Z, Hu Q, Li H, Wu J, Shi Y: **Molecular determinants of MecA as a degradation tag for the ClpCP protease**. *The Journal of biological chemistry* 2009, **284**(49):34366-34375.

194. Zolkiewski M: **ClpB Cooperates with DnaK, DnaJ, and GrpE in Suppressing Protein Aggregation. A NOVEL MULTI-CHAPERONE SYSTEM FROM ESCHERICHIA COLI**. *Journal of Biological Chemistry* 1999, **274**(40):28083-28086.
195. Goloubinoff P, Mogk A, Zvi AP, Tomoyasu T, Bukau B: **Sequential mechanism of solubilization and refolding of stable protein aggregates by a bichaperone network**. *Proceedings of the National Academy of Sciences of the United States of America* 1999, **96**(24):13732-13737.
196. Rosenzweig R, Moradi S, Zarrine-Afsar A, Glover JR, Kay LE: **Unraveling the mechanism of protein disaggregation through a ClpB-DnaK interaction**. *Science* 2013, **339**(6123):1080-1083.
197. Tipton KA, Verges KJ, Weissman JS: **In vivo monitoring of the prion replication cycle reveals a critical role for Sis1 in delivering substrates to Hsp104**. *Molecular cell* 2008, **32**(4):584-591.
198. DeSantis ME, Shorter J: **Hsp104 drives "protein-only" positive selection of Sup35 prion strains encoding strong [PSI(+)]**. *Chemistry & biology* 2012, **19**(11):1400-1410.
199. Konarev PV, Volkov VV, Sokolova AV, Koch MHJ, Svergun DI: **PRIMUS: a Windows PC-based system for small-angle scattering data analysis**. *J Appl Crystallogr* 2003, **36**:1277-1282.
200. Svergun DI: **Determination of the Regularization Parameter in Indirect-Transform Methods Using Perceptual Criteria**. *J Appl Crystallogr* 1992, **25**:495-503.
201. Svergun DI, Petoukhov MV, Koch MH: **Determination of domain structure of proteins from X-ray solution scattering**. *Biophysical journal* 2001, **80**(6):2946-2953.
202. Volkov VV, Svergun DI: **Uniqueness of ab initio shape determination in small-angle scattering**. *J Appl Crystallogr* 2003, **36**:860-864.
203. Weber-Ban EU, Reid BG, Miranker AD, Horwich AL: **Global unfolding of a substrate protein by the Hsp100 chaperone ClpA**. *Nature* 1999, **401**(6748):90-93.
204. Lum R, Niggemann M, Glover JR: **Peptide and protein binding in the axial channel of Hsp104. Insights into the mechanism of protein unfolding**. *The Journal of biological chemistry* 2008, **283**(44):30139-30150.
205. Robberecht W, Philips T: **The changing scene of amyotrophic lateral sclerosis**. *Nature reviews Neuroscience* 2013, **14**(4):248-264.
206. Cushman M, Johnson BS, King OD, Gitler AD, Shorter J: **Prion-like disorders: blurring the divide between transmissibility and infectivity**. *Journal of cell science* 2010, **123**(Pt 8):1191-1201.
207. Takamoto K, Chance MR: **Radiolytic protein footprinting with mass spectrometry to probe the structure of macromolecular complexes**. *Annual review of biophysics and biomolecular structure* 2006, **35**:251-276.
208. Kiselar JG, Maleknia SD, Sullivan M, Downard KM, Chance MR: **Hydroxyl radical probe of protein surfaces using synchrotron X-ray radiolysis and mass spectrometry**. *International journal of radiation biology* 2002, **78**(2):101-114.
209. Maleknia SD, Kiselar JG, Downard KM: **Hydroxyl radical probe of the surface of lysozyme by synchrotron radiolysis and mass spectrometry**. *Rapid communications in mass spectrometry : RCM* 2002, **16**(1):53-61.
210. Sclavi B, Sullivan M, Chance MR, Brenowitz M, Woodson SA: **RNA folding at millisecond intervals by synchrotron hydroxyl radical footprinting**. *Science* 1998, **279**(5358):1940-1943.
211. Xu G, Chance MR: **Hydroxyl radical-mediated modification of proteins as probes for structural proteomics**. *Chemical reviews* 2007, **107**(8):3514-3543.
212. Xu G, Chance MR: **Radiolytic modification and reactivity of amino acid residues serving as structural probes for protein footprinting**. *Analytical chemistry* 2005, **77**(14):4549-4555.
213. Kaur P, Kiselar JG, Chance MR: **Integrated algorithms for high-throughput examination of covalently labeled biomolecules by structural mass spectrometry**. *Analytical chemistry* 2009, **81**(19):8141-8149.

214. Hoofnagle AN, Resing KA, Ahn NG: **Protein analysis by hydrogen exchange mass spectrometry**. *Annual review of biophysics and biomolecular structure* 2003, **32**:1-25.
215. Katta V, Chait BT: **Conformational changes in proteins probed by hydrogen-exchange electrospray-ionization mass spectrometry**. *Rapid communications in mass spectrometry : RCM* 1991, **5**(4):214-217.
216. Maleknia SD, Brenowitz M, Chance MR: **Millisecond radiolytic modification of peptides by synchrotron X-rays identified by mass spectrometry**. *Analytical chemistry* 1999, **71**(18):3965-3973.
217. Xu G, Kiselar J, He Q, Chance MR: **Secondary reactions and strategies to improve quantitative protein footprinting**. *Analytical chemistry* 2005, **77**(10):3029-3037.
218. Gupta S, Sullivan M, Toomey J, Kiselar J, Chance MR: **The Beamline X28C of the Center for Synchrotron Biosciences: a national resource for biomolecular structure and dynamics experiments using synchrotron footprinting**. *Journal of synchrotron radiation* 2007, **14**(Pt 3):233-243.
219. Bohon J, Jennings LD, Phillips CM, Licht S, Chance MR: **Synchrotron protein footprinting supports substrate translocation by ClpA via ATP-induced movements of the D2 loop**. *Structure* 2008, **16**(8):1157-1165.
220. Kan ZY, Mayne L, Chetty PS, Englander SW: **ExMS: data analysis for HX-MS experiments**. *Journal of the American Society for Mass Spectrometry* 2011, **22**(11):1906-1915.
221. Wojtyra UA, Thibault G, Tuite A, Houry WA: **The N-terminal zinc binding domain of ClpX is a dimerization domain that modulates the chaperone function**. *The Journal of biological chemistry* 2003, **278**(49):48981-48990.
222. Desantis ME, Sweeny EA, Snead D, Leung EH, Go MS, Gupta K, Wendler P, Shorter J: **Conserved distal loop residues in the Hsp104 and ClpB middle domain contact nucleotide-binding domain 2 and enable Hsp70-dependent protein disaggregation**. *The Journal of biological chemistry* 2013.
223. Liu T, Daniels CK, Cao S: **Comprehensive review on the HSC70 functions, interactions with related molecules and involvement in clinical diseases and therapeutic potential**. *Pharmacology & therapeutics* 2012, **136**(3):354-374.
224. Kregel KC: **Heat shock proteins: modifying factors in physiological stress responses and acquired thermotolerance**. *Journal of applied physiology* 2002, **92**(5):2177-2186.
225. Biter AB, Lee S, Sung N, Tsai FT: **Structural basis for intersubunit signaling in a protein disaggregating machine**. *Proceedings of the National Academy of Sciences of the United States of America* 2012, **109**(31):12515-12520.
226. Glynn SE, Martin A, Nager AR, Baker TA, Sauer RT: **Structures of asymmetric ClpX hexamers reveal nucleotide-dependent motions in a AAA+ protein-unfolding machine**. *Cell* 2009, **139**(4):744-756.
227. Bosl B, Grimminger V, Walter S: **Substrate binding to the molecular chaperone Hsp104 and its regulation by nucleotides**. *The Journal of biological chemistry* 2005, **280**(46):38170-38176.
228. Watanabe YH, Nakazaki Y, Suno R, Yoshida M: **Stability of the two wings of the coiled-coil domain of ClpB chaperone is critical for its disaggregation activity**. *The Biochemical journal* 2009, **421**(1):71-77.
229. Watanabe YH, Takano M, Yoshida M: **ATP binding to nucleotide binding domain (NBD)1 of the ClpB chaperone induces motion of the long coiled-coil, stabilizes the hexamer, and activates NBD2**. *The Journal of biological chemistry* 2005, **280**(26):24562-24567.
230. Schirmer EC, Homann OR, Kowal AS, Lindquist S: **Dominant gain-of-function mutations in Hsp104p reveal crucial roles for the middle region**. *Molecular biology of the cell* 2004, **15**(5):2061-2072.
231. Lipinska N, Zietkiewicz S, Sobczak A, Jurczyk A, Potocki W, Morawiec E, Wawrzycka A, Gumowski K, Slusarz M, Rodziewicz-Motowidlo S *et al*: **Disruption of ionic interactions**

between the nucleotide binding domain 1 (NBD1) and middle (M) domain in Hsp100 disaggregase unleashes toxic hyperactivity and partial independence from Hsp70. *The Journal of biological chemistry* 2013, **288**(4):2857-2869.
232. Liu Z, Tek V, Akoev V, Zolkiewski M: **Conserved Amino Acid Residues within the Amino-terminal Domain of ClpB are Essential for the Chaperone Activity**. *Journal of molecular biology* 2002, **321**(1):111-120.
233. Sweeny EA, DeSantis ME, Shorter J: **Purification of hsp104, a protein disaggregase**. *Journal of visualized experiments : JoVE* 2011(55).
234. Konarev PV, Volkov VV, Sokolova AV, Koch MHJ, Svergun DI: **PRIMUS: a Windows PC-based system for small-angle scattering data analysis**. *J Appl Cryst* 2003, **36**(5):1277-1282.
235. Rice SA: **Small angle scattering of X-rays. A. Guinier and G. Fournet. Translated by C. B. Wilson and with a bibliographical appendix by K. L. Yudowitch. Wiley, New York, 1955.** *Journal of Polymer Science* 1956, **19**(93):594-594.
236. Svergun D: **Determination of the regularization parameter in indirect-transform methods using perceptual criteria**. *J Appl Cryst* 1992, **25**(4):495-503.
237. Rambo RP, Tainer JA: **Accurate assessment of mass, models and resolution by small-angle scattering**. *Nature* 2013, **496**(7446):477-481.
238. Kozin MB, Svergun DI: **Automated matching of high- and low-resolution structural models**. *J Appl Crystallogr* 2001, **34**:33-41.
239. Wriggers W, Milligan RA, McCammon JA: **Situs: A package for docking crystal structures into low-resolution maps from electron microscopy**. *Journal of structural biology* 1999, **125**(2-3):185-195.
240. Pettersen EF, Goddard TD, Huang CC, Couch GS, Greenblatt DM, Meng EC, Ferrin TE: **UCSF Chimera--a visualization system for exploratory research and analysis**. *Journal of computational chemistry* 2004, **25**(13):1605-1612.
241. Mayne L, Kan ZY, Chetty PS, Ricciuti A, Walters BT, Englander SW: **Many overlapping peptides for protein hydrogen exchange experiments by the fragment separation-mass spectrometry method**. *Journal of the American Society for Mass Spectrometry* 2011, **22**(11):1898-1905.
242. Arnold K, Bordoli L, Kopp J, Schwede T: **The SWISS-MODEL workspace: a web-based environment for protein structure homology modelling**. *Bioinformatics* 2006, **22**(2):195-201.
243. Kiefer F, Arnold K, Kunzli M, Bordoli L, Schwede T: **The SWISS-MODEL Repository and associated resources**. *Nucleic acids research* 2009, **37**(Database issue):D387-392.
244. Peitsch MC: **Protein Modeling by E-Mail**. *Bio-Technol* 1995, **13**(7):658-660.